The Institute of Paper Chemistry

Appleton, Wisconsin

Doctor's Dissertation

An Investigation of the Elastic and Dielectric Anisotropy of Paper

Elmer H. Fleischman, Jr.

June, 1981

AN INVESTIGATION OF THE ELASTIC AND DIELECTRIC ANISOTROPY OF PAPER

A thesis submitted by

Elmer H. Fleischman, Jr.

B. S. 1976, University of Wisconsin, Stevens Point

M. S. 1978, Lawrence University

in partial fulfillment of the requirements
of The Institute of Paper Chemistry
for the degree of Doctor of Philosophy
from Lawrence University,
Appleton, Wisconsin

June, 1981

TABLE OF CONTENTS

SUMMARY

This investigation was undertaken to learn more about the way in which fiber orientation and drying restraint affect the elastic and dielectric properties in all three principal directions of paper.

It was found that both variables affect the in-plane elastic anisotropy by similar magnitudes. What was surprising, however, was that wet straining had the greatest effect in the z-direction. The z-direction stiffness was reduced 50% as a result of only a moderate 2.4% wet strain in the plane of the sheet.

On the other hand, the dielectric anisotropy was affected very little by wet straining. In fact, the dielectric results could be explained in terms of mixture theories. The anisotropy in the dielectric constant when measured at microwave frequencies could largely be explained as being the result of fiber orientation alone without having to assume that the fiber has an anisotropic dielectric constant.

From comparison of the elastic and dielectric results, it may be concluded that the mechanism by which wet straining enhances the elastic anisotropy does not involve a large fiber orientation in the direction of wet straining.

From a practical standpoint, one could use the dielectric anisotropy measured at microwave frequencies as a measure of the fiber orientation distribution in the sheet. On the basis of the results presented here, this measurement should be quite insensitive to any stresses imposed on the sheet as it dries.

INTRODUCTION

In general, a material is said to be anisotropic if it exhibits properties that have different values when measured in different directions. If the material has three mutually perpendicular planes of symmetry, it is said to be orthotropic. In an idealized sense machine-made paper is an orthotropic material with the principal axes (x, y, and z) corresponding to the machine, cross-machine, and thickness directions, respectively. Indeed, it has been found that when wave theories derived for orthotropic platelike materials were applied to paper, satisfactory agreement was obtained between the theoretically predicted and the experimentally measured wave velocities (1). In this study, paper is regarded as an orthotropic material, although in a strict sense this is only an approximation.

The anisotropy between the z-direction and either the x- or y-directions could be entirely the result of fiber orientation. In the making of paper, fibers are filtered from a dilute suspension onto a screen. The sheet thus formed will be layered in appearance with flattened, ribbonlike fibers lying almost exclusively in the plane of the sheet (2). As a result of this fiber orientation alone, one would expect that a large anisotropy would exist between the z-direction and the plane of the sheet. An additional anisotropy would be expected, however, if the fibers were also anisotropic. For example, if a property measured in the radial direction of the fiber had a lower value than that measured in the axial direction, this would be reflected in the anisotropy of the sheet. No matter how dense the sheet could be made, the property measured in the z-direction of the sheet could never be greater than the value measured in the radial direction of the fiber. The elastic modulus measured in the z-direction can be as much as two orders of magnitude less than that measured in the plane of the sheet (1).

The anisotropy between the x- and y-directions of a sheet of machine-made paper is not quite as pronounced as that in the z-direction; however, it is still very significant. Although there may be many effects occurring during the making of paper that contribute to the anisotropy in the plane of the sheet, two of these effects are by far the most important. The first is the result of the flow dynamics during sheet formation. These flow patterns normally tend to preferentially align fibers in the machine direction of paper. The second effect occurs during drying. The moist paper web is stretched and exposed to a greater tension in the machine direction than in the cross direction during drying. Both of these effects tend to increase the elastic modulus measured in the x-direction over that measured in the y-direction. The ratio of the elastic modulus in the x-direction to that in the y-direction is about 2:1 for typical machine-made papers (3).

The dielectric anisotropy of paper has not been investigated to the same extent as has the elastic anisotropy. It was originally suspected that when measured at microwave frequencies, the dielectric constant could depend only on fiber orientation and not be significantly affected by the conditions under which the sheet is dried (4).

This investigation explores the elastic and dielectric anisotropy of paper by specifically addressing two questions. First, is the observed dielectric anisotropy due to fiber orientation only or also affected by stretching and applying greater drying tension in one in-plane direction of the sheet? Second, what effect does the drying tension applied in the plane of the sheet have on the elastic properties measured in the z-direction of the sheet?

BACKGROUND

Throughout this report the structure and properties of a sheet of paper will be discussed in terms of a rectangular Cartesian coordinate system. The sheet of paper is taken to lie in the x, y plane with the x-direction corresponding to the direction of preferred fiber orientation and/or the direction of induced wet strain or enhanced drying stress. The z coordinate represents the thickness direction of the sheet.

ELASTIC ANISOTROPY

MECHANICAL ANISOTROPY IN THE PLANE OF THE SHEET

To completely explain the elastic response of an orthotropic material, nine elastic constants are required (see Appendix I for a brief discussion of these constants). For the most part, however, investigations have been primarily concerned with the in-plane constants of paper. In particular, the anisotropy observed between the two in-plane Young's moduli, E_x and E_y, and the anisotropy in the strength of paper measured in the x- and y-directions have both been extensively investigated.

At first it was believed that the preferred orientation of fibers was the primary cause of the in-plane anisotropy. But as early as 1945, Edge (5) demonstrated that the tension in the web during drying had a significant effect on the tensile strength anisotropy. In fact, from his results one would conclude that the amount of tension applied in the plane of the sheet has a much greater effect on the development of tensile strength anisotropy than does fiber orientation alone.

In discussing tension applied to the sheet during drying, one must clarify the terminology used. When dried in an uninhibited manner, paper will shrink. The paper shrinkage is the direct result of the shrinkage that occurs in each fiber as the

sheet dries (6). The transverse shrinkage of fibers can be very high, even in the range of 20-30%. The longitudinal shrinkage is very small, on the order of 1-2%. At fiber crossings, the lateral contraction of one fiber will tend to shorten the other fiber crossing it in the axial direction. The net result is that the entire sheet would, if unrestrained, shrink about 10% in both in-plane directions.

If the sheet is restrained, somehow, and prevented from shrinking, it is said that a certain degree of "drying restraint" has been imposed. Conceivably, this could be accomplished by either applying a constant stress to the sheet, or by imposing a constant strain as the sheet dries. If a constant stress is applied, the sheet will initially be stretched. Then as shrinkage forces increase during drying, the sheet will contract, but not to the same value as if no stress had been applied. If a constant strain is imposed, usually the sheet is stretched when wet to the desired strain level and kept at that level throughout the drying process. Both of these methods induce a certain degree of drying restraint; the first applies a known drying stress and the latter a known degree of strain. The two methods are not independent, however. An increase in the strain imposed on a wet sheet will result in an increase in the stress induced by the sheet as it dries and vice versa. Usually the degree of drying restraint is varied by straining the wet sheet to different levels and keeping the strain constant as the sheet is dried. Sometimes the stress imposed by the sheet is measured as it dries under these conditions.

In a detailed study, Schulz (7) investigated the effect of wet straining on the mechanical properties measured in the x-direction of sheets of random fiber orientation. He found that wet straining had a marked effect on the tensile strength and apparent Young's modulus of the sheets. In the range of wet strains investigated (from 0 to about 6%) these properties increased to a maximum at about 3-4% strain and then decreased with increasing strain. At the maximum, for a well-beaten pulp, the elastic modulus and tensile strength values were almost 40% higher than those

measured for sheets with zero wet strain. No change in the zero span breaking stress of the sheets was observed as a result of wet straining. On the basis of these and other results, Schulz concluded that the effect of increased strain during drying was to alter slightly the internal structure of the sheet in such a way that upon later application of a load, the stress would be more evenly distributed among the fibers. Using the zero span test results as evidence, Schulz concluded that the fibers themselves did not strengthen as a result of wet straining. Also, it was not likely that gross fiber realignment or fibril orientation was related to the wet straining effect.

Setterholm (8,9) has presented many data on the effects of drying restraint on the mechanical properties of paper. He found that for sheets with random fiber orientation the primary factors that determine the measured value of Young's modulus in the direction of applied restraint were the final apparent density of the sheet, the degree of drying restraint, and the drying temperature. When measuring the tensile strength in the x-direction, he found that in addition to apparent density and the degree of drying restraint, the type of pulp did have an effect. Setterholm investigated the effect of drying restraint by straining wet sheets and then drying them under uniaxial restraint as did Schulz. In addition, some sheets were made in which the sheet was allowed to shrink to a given negative strain value at which time it was restrained from further shrinkage. Over the entire range of wet strain investigated, from the completely unrestrained sheet (which probably had about a -6% strain, although the exact value was not reported) to the highest strain level of 3%, both the elastic modulus and tensile strength measured in the x-direction increased with increasing wet strain at a given apparent density.

Other similar studies of the effect of drying restraint on handsheets of random fiber orientation have been reported. Meyers (10) employed varying degrees of

biaxial restraint in the plane of the sheet and investigated the effect of drying restraint on the mechanical properties of the sheets under a compressive load. He found that the in-plane modulus of elasticity measured in compression varied with the amount of induced strain in the sheet in a manner similar to the modulus of elasticity measured in a tensile test. At a given wet strain induced in the x-direction, the compression modulus measured in the y-direction did not vary even if different strain levels were induced in this direction. The compressive strength measured in the x-direction was found to increase with increasing degree of drying restraint.

In another investigation, Parsons (11) found that the zero span tensile strength increased with increasing degree of drying restraint, a finding quite contrary to that observed by Schulz. Otherwise Parsons's results were similar, in that wet straining tended to increase the modulus and strength properties in the direction of applied restraint. Matolesy (12) also reported that an increase in the degree of drying restraint resulted in an increase in the zero span test result. These results were interpreted as evidence that the individual fiber strength increased as the degree of drying restraint was increased. This conclusion is not without question, however. It has been suggested that the zero span test result may be a linear function of the normal tensile strength even at a constant individual fiber strength (13).

The other cause for in-plane elastic anisotropy is the preferential alignment of fibers in one direction. It is easy to visualize that as more load-supporting members become oriented in one direction, the modulus and strength of the network would increase in that direction while being reduced in the other perpendicular direction.

Prud'homme and Robertson (14) produced highly oriented sheets on a special laboratory apparatus. They could make paper that had a 15:1 ratio of Young's modulus in the x-direction to that in the y-direction.

Several researchers have investigated the effect of both fiber orientation and drying restraint on the mechanical properties of paper (15-20). By and large, all of the researchers found that both fiber orientation and drying restraint increased the modulus, increased the tensile strength, and decreased the strain at rupture. Whereas both fiber orientation and drying restraint generally had a large effect on the measured modulus of the sheet, fiber orientation usually was the dominating effect controlling the tensile strength. In particular, Setterholm (20) found that for a softwood, bleached, kraft pulp beaten to 580 mL CSF, the elastic modulus increased about 50% with increasing fiber orientation in the range studied and about 30% with wet straining in the range from zero to 3% strain. In these same ranges, the tensile strength increased about 80% with increasing fiber orientation and about 10% with increasing wet strain.

THE EFFECT OF DRYING RESTRAINT ON INDIVIDUAL FIBER PROPERTIES

In an effort to elucidate the mechanism by which the elastic properties are enhanced by drying restraint, Jentzen (21) investigated the effects of stress applied during drying on individual holocellulose fibers. He found that for fibers dried under a small load, the measured modulus was about 100-200% greater than for fibers dried under no load. The tensile strength of the fibers dried under stress was about 40-90% greater than the fibers dried under no load. The springwood fibers showed more of an effect due to drying restraint that did the summerwood fibers. From X-ray diffraction data it was observed that crystallite orientation increased in the fibers dried under load, but that the degree of crystallinity remained constant.

Working with holocellulose fibers, Spiegelberg (22) extracted various amounts of the hemicellulose carbohydrate fraction of the fibers and examined the effect of drying restraint on these fibers. Holocellulose fibers in which the hemicellulose fraction is extracted are more similar to fibers from a conventional kraft pulping

process than are unextracted holocellulose fibers. Spiegelberg found that the removal of hemicelluloses reduced the tensile strength and modulus of elasticity of the fibers. If dried under load, however, the strength and modulus of the extracted fibers increased, approaching the values measured for unextracted fibers dried under load. Thus, the percent increase in modulus or tensile strength due to drying restraint was greater for the extracted fibers than that observed by Jentzen for the unextracted fibers. Indeed, the modulus for some extracted fibers increased over 600% when dried under load.

Both Jentzen and Spiegelberg studied the effect of drying restraint on fibers that had never been dried previously. Kim (23) investigated the effect of drying restraint on once-dried fibers. He observed that for once-dried kraft fibers, the tensile strength did not increase when the fibers were dried under stress, even when stresses much higher than those used by Jentzen and Spiegelberg were applied.

THE MECHANICAL PROPERTIES OF PAPER IN THE Z-DIRECTION

Since the z-direction of paper is very thin, measurements of elasticity in that direction are exceedingly hard to make with conventional load-elongation test equipment. Van Liew (24) did, however, obtain some data. The measured stress-strain curves were nonlinear, however, and the results were complicated because of non-parallel separation of the surfaces, indicating that a nonuniform strain existed over the specimen area. Correcting for the latter effect and taking the slope at zero strain from a polynomial regression of the data, Van Liew obtained values for the z-direction modulus ranging from 0.2 to 0.5 GPa.

Using ultrasonic pulse propagation techniques, Mann (1) obtained a value for the z-direction modulus of a machine-made milk carton board and two samples of linerboard. His measured values were 0.023 GPa and 0.032 GPa for the linerboard samples and 0.041 GPa for the milk carton board sample.

These values of the z-direction modulus may be compared with a "typical" value for the modulus in the plane of the sheet of about 5 GPa. Thus, an extreme anisotropy exists between the modulus determined in the plane of the sheet and that measured in the z-direction.

The z-direction strength of paper has been investigated more than the modulus. For the most part, the studies have been concerned with trying to determine the bonding strength between fibers. Schulz (7), in the course of his investigation of the effects of drying restraint on the x-direction mechanical properties of paper, also measured the z-direction tensile strength of the sheets. Wet straining the sheet resulted in a decrease in the z-direction tensile strength. This was interpreted as evidence that wet straining reduces the bonding strength of paper.

Using the Scott Bond test as one measure of interfiber bonding, Parsons (11) also noted that wet straining in the plane of the sheet results in a reduction in the strength measured in the z-direction.

SUMMARY

The elastic anisotropy in the plane of the sheet is due to two effects - fiber orientation and drying restraint. Both fiber orientation and drying restraint increase the modulus measured in the x-direction by similar magnitudes. The tensile strength in the plane of the sheet, however, is determined more by the fiber orientation than by the imposed drying restraints. Wet straining decreases the z-direction strength of the sheet, but the effect of wet straining on the z-direction modulus is unknown.

The observed increase in modulus and tensile strength in the plane of the sheet with increasing drying restraint is usually explained as being the result of an equalization of stress among the load-bearing elements. Although it has been shown

that drying individual fibers under stress will result in an increase in the strength and modulus of never-dried holocellulose fibers, no increase in these properties is observed for once-dried kraft fibers.

DIELECTRIC ANISOTROPY

Paper also exhibits anisotropy with respect to the measured dielectric constant (4,25-27). The reader is referred to Appendix II for a brief discussion describing the meaning of the dielectric constant of a material. For paper the measured dielectric constant is hardly constant at all. In addition to depending on the orientation of the sample, the dielectric constant is a function of the frequency of the applied field, the temperature of the sample, the amount of moisture present in the sample, and the apparent density of the sheet.

Although in general the dielectric properties of polymers are very complex, the combined effects of frequency and temperature are often discussed as being the result of actions occurring on a simplified molecular level (28). Permanent molecular dipoles in the material rotate with the applied field to contribute to the polarization of the material. The dipoles are described by a certain relaxation frequency, f_r, above which they can no longer keep up with the field and thus no longer contribute to the polarization of the material. By assuming that the orientation of the dipoles can be represented by two states separated by a potential barrier, application of simple reaction rate theory leads to an equation of the form

$$f_r = B \exp(-\Delta H/RT) \qquad (1)$$

where ΔH is an activation energy per mole, R is the ideal gas constant, and T is the absolute temperature (29). The symbol B is actually a function of temperature but is often assumed to be constant as is the activation energy ΔH. Thus a plot of $\log_{10} f_r$ vs. 1/T will produce a line more or less straight depending on the validity

of the assumptions. For polymers, there are usually more than one line in these plots, indicating more than one type of molecular relaxation process.

The dielectric properties of dry cellulose have recently been reviewed (30). Dry cellulose has been observed to exhibit four different relaxations. The highest frequency relaxation occurs at about 10^7 Hz at 20°C. Relaxations have been observed in paper, wood, cotton, cellophane, and rayon, which all fall along approximately the same line, suggesting that the molecular relaxation processes are similar for these cellulosic substances at high frequencies. This high-frequency relaxation has been associated with two different mechanisms that may occur in the amorphous regions of cellulose. The CH_2OH group on the cellulose molecule may rotate with the applied field (30), or the relaxation may be associated with changes in the conformation of the pyranose rings (31).

The presence of water in these cellulosic materials tends to increase the magnitude of the measured dielectric constant by two mechanisms. Water acts as a plasticizer and shifts the relaxation processes to higher frequencies. Also, because water has a permanent dipole moment, it will contribute to the measured dielectric constant by rotating with the field. Indeed, free water has a very large dielectric constant, being about 60 at 10^{10} Hz and 20°C. The dielectric constant of dry cellulose is about 4 at this frequency and temperature; thus, water would be expected to make a significant contribution to the measured dielectric constant even if only a small amount is present. A discussion of the dielectric properties of materials containing water has been given by Hasted (32).

When measuring the dielectric constant of paper, one other complication is that paper is not a homogeneous cellulosic substance, but is composed of cellulosic fibers and air voids. Working with wood pulp fibers, it is very difficult to measure a value for the dielectric constant of the cell wall substance. What is typically measured is the dielectric constant for the mixture of fiber and air. The measured

value would thus depend on the apparent density of the sample, or alternatively on the void volume of the material. For studies solely concerned with the measurement of the relaxation frequency as a function of temperature and moisture content, the presence of air in the sample is probably not important. However, if one wishes to obtain an estimate of the magnitude of the dielectric constant of the cellulosic material, then the presence of air must be accounted for.

As previously mentioned, it has been observed that paper exhibits dielectric anisotropy. Assuming paper to be an orthotropic material, there are three independent dielectric constants corresponding to situations in which the applied electric field is oriented in each of the three principal directions of the material.

The dielectric anisotropy observed in paper could be associated with the anisotropy of the structure of paper on two different levels. On a molecular level, because of the arrangement of atoms and bonds, the cellulose molecule itself would be expected to exhibit anisotropy. If the cellulose molecules are preferentially oriented in one of the principal directions of the fiber, then the fiber itself would exhibit anisotropy. Indeed, there is considerable evidence that the molecules are oriented in wood pulp fibers. [See, for example, Ref. (33) and (34).] Then any difference in the alignment of the fibers will result in a difference in the alignment of the cellulose molecules with respect to the sheet directions. Also, it is conceivable that any process that results in an alteration of the alignment of the cellulose molecules within a fiber could affect the measured anisotropy of the sheet. Specifically, it is possible that increasing the degree of drying restraint applied to the sheet could conceivably affect the measured dielectric anisotropy of the sheet by alignment of the cellulose molecules either through alignment of the fibers or fibrils.

On the other hand, because fibers are long and slender and because paper is an assemblage of fiber and air, anisotropy could be exhibited in paper even if the

fibers themselves were completely isotropic. In this case, wet straining would have no effect on the dielectric anisotropy of the sheet unless a significant reorientation of the fibers occurred during wet straining.

EFFECTIVE CONSTANTS OF HETEROGENEOUS MIXTURES

In the discussion of the elastic and dielectric constants of paper it was tacitly assumed that these constants could be measured as if paper were a continuous homogeneous material. Paper, of course, is not homogeneous but is composed of fiber and air in comparable proportions by volume. The presence of air has a marked effect on paper properties. Indeed, significant anisotropy can be predicted for paper as a consequence of its structure even if one would assume the constituent fibers to be completely isotropic. When discussing the elastic or dielectric constants of paper, one must be aware that the constants measured are actually "effective constants" for the fiber-air mixture.

If a material is homogeneous, consisting of just one material or phase, constants for the material may be defined unambiguously. Suppose, for example, that one wished to determine a value for Young's modulus, E. One would simply subject the material of sample length L and cross-sectional area A to a tensile force F. By measuring the change in length, ΔL, one can calculate E from the formula

$$E = \frac{F/A}{\Delta L/L} \tag{2}$$

If the material is heterogeneous, i.e., if the modulus varies from point to point in the material, the value calculated for E from an experiment as described above will vary depending on the particular area and sample length chosen for the test. In such situations the concept of the heterogeneous material having a unique modulus is not valid at all. However, it is common to define an effective modulus

in which the test is performed exactly as described above except that a restriction is imposed that the specimen dimensions be very large in comparison with the local spacial variation in modulus.

A heterogeneous material is often composed of a finite number of constituents, each having a single valued property constant. In such situations it is often desired to predict the effective constant of the mixture knowing the constants for the constituents and the amount of each present in the mixture. Unfortunately, this information alone is not enough to uniquely determine an effective constant. Consider, for example, a heterogeneous mixture of rubber and steel. Assume that there are equal quantities of rubber and steel and that one wished to calculate the effective modulus knowing the modulus of the rubber and steel. One cannot determine a unique value for the effective modulus on the basis of this information alone since a situation could exist in which the rubber is present as isolated inclusions in a continuous steel matrix or vice versa, as indicated in Fig. 1. It is intuitively obvious that the effective Young's modulus for the case of rubber inclusions in a steel matrix is much greater than the case of steel inclusions in a rubber matrix even though there is the same quantity of each material in both cases.

The difference between the effective Young's modulus for the two different geometries described above is intuitively obvious. However, the mathematics is such that the conclusion is the same if one were determining the effective stiffness, dielectric constant, thermal conductivity, or magnetic permeability. In each case, the effective constant for the mixture is greater whenever the geometry allows a more continuous path through the component having the highest value for the constant.

BOUNDS FOR THE EFFECTIVE DIELECTRIC CONSTANT OF PAPER

As a first approximation, paper may be considered to be a two-component mixture of moist cellulose fiber and air each having an isotropic dielectric constant.

These two components, fiber and air, are assumed to completely fill the "volume" of paper. Furthermore, it is assumed that there are no synergistic effects. That is, the individual dielectric constants of the moist fiber and air are constant and independent of how they are mixed.

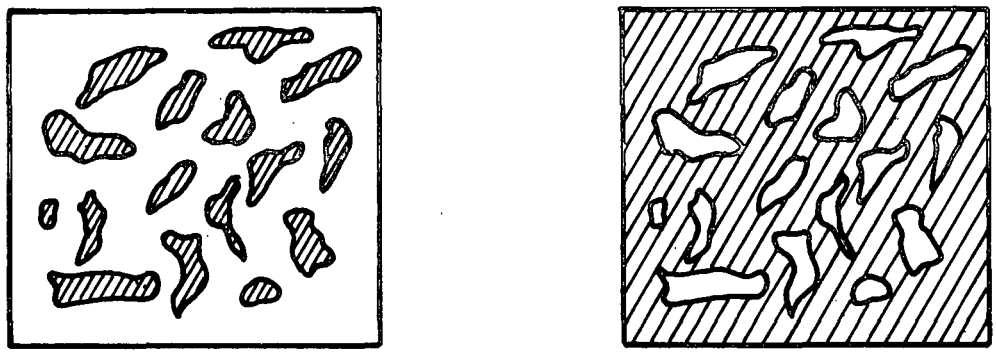

Figure 1. Two limiting types of inclusions: (a) where the rubber phase exists as isolated inclusions in a continuous steel phase, and (b) where the steel phase exists as isolated inclusions in a continuous rubber matrix.

Although it is not possible to determine a unique value for the effective dielectric constant of paper knowing only the dielectric constants, ε_f and ε_a, and the volume fraction of the fiber, P, it is possible to establish bounds for the constant. It can be shown that the effective dielectric constant in any one direction of a mixture of isotropic components is bounded by the following relationship (35).

$$\langle \varepsilon^{-1} \rangle^{-1} \leq \varepsilon^* \leq \langle \varepsilon \rangle \tag{3}$$

where ε^* is the effective dielectric constant of the mixture in any one direction and symbols $\langle\ \rangle$ represent averages over the volume of the sample. Thus, for paper, the effective dielectric constant is bounded by

$$\left[\frac{P}{\varepsilon_f} + \frac{(1-P)}{\varepsilon_a} \right]^{-1} \leq \varepsilon^* \leq P\ \varepsilon_f + (1-P)\ \varepsilon_a \tag{4}$$

The lower bound corresponds to a series combination of fiber and air, whereas the upper bound corresponds to a parallel combination as illustrated in Fig. 2.

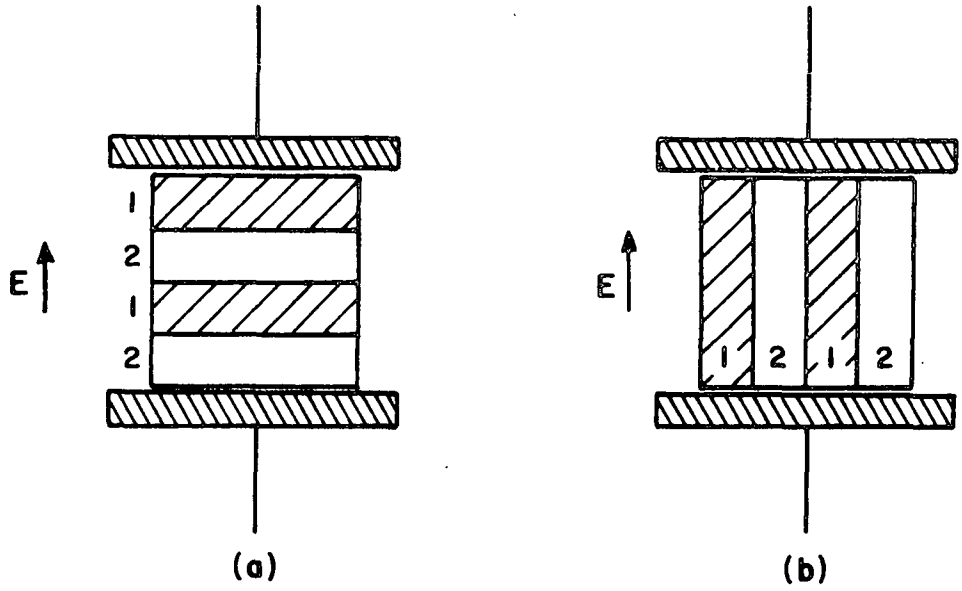

Figure 2. Series (a) and parallel (b) combinations of fiber and air representing the bounds for the effective dielectric constant of paper.

In the figure the number of layers, and thus the thickness of each layer, does not affect the calculation of the dielectric constant of the mixture as long as the volume fractions of the components are not changed. The bounds for the effective dielectric constant as given by Eq. (4) are plotted in Fig. 3 as a function of the volume fraction of fiber, P.

The anisotropy indicated in Fig. 3 is the maximum possible that could be observed in the dielectric constant of paper at any given apparent density assuming the fiber to be isotropic. Furthermore, unless something more is known about the fiber-air geometry, a better estimate of the effective dielectric constant of the mixture cannot be obtained.

CALCULATIONS BASED ON A SIMPLIFIED GEOMETRY FOR PAPER

In principle, if the geometry of the fiber-air mixture in paper could be described exactly, one could calculate an exact value for the effective dielectric constant.

In practice, however, even for fairly simple geometries, only approximate relationships are derived. One fairly common approach is to make what is called a "self-consistent" approximation. The procedure outlined here is taken directly from Ref. (35) for the special case of a two-component mixture.

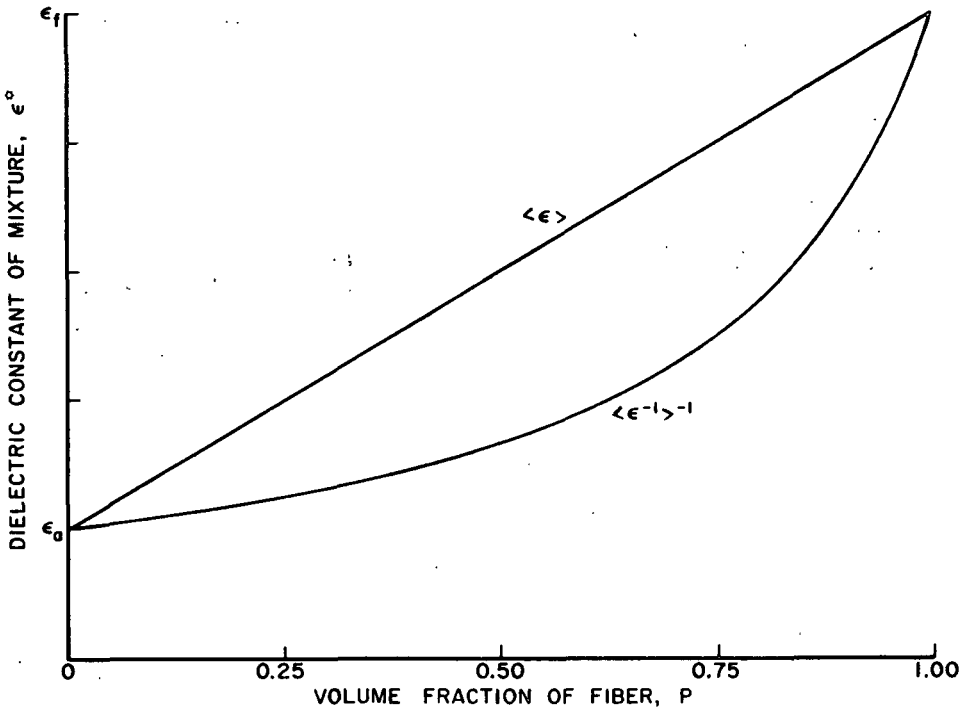

Figure 3. Bounds for the effective dielectric constant of paper.

One considers separately the cases in which the applied field, E, is oriented in each of the three principal directions of the sample. For the case in which the applied field is in the x-direction, one can define the effective dielectric constant in terms of the average displacement and electric fields $\langle D_x \rangle$ and $E_x\rangle$ by

$$\langle D_x \rangle = \varepsilon_x^* \langle E_x \rangle \tag{5}$$

where the symbols $\langle\ \rangle$ again denote volume averages. One can also write

$$U = \frac{1}{2}\ \varepsilon_x^*\ \langle E_x \rangle^2 = \frac{1}{2}\ \langle D_x \rangle\ \langle E_x \rangle \tag{6}$$

where U is the energy/unit volume of the sample. One may rewrite Eq. (6) by adding and subtracting at every point in the mixture the quantity $\langle E_x \rangle \varepsilon_a E_x$ where ε_a is the dielectric constant of the air. Equation (6) then becomes

$$U = \frac{1}{2V} \int_V \langle E_x \rangle \varepsilon_a E_x dV + \frac{1}{2V} \int_V \langle E_x \rangle (\langle D_x \rangle - \varepsilon_a E_x) dV \tag{7}$$

where V is the volume of the entire sample. Noting that

$$\langle E_x \rangle = P\langle E_x \rangle_f + (1-P) \langle E_x \rangle_a \tag{8}$$

and similarly

$$\langle D_x \rangle = P \varepsilon_f \langle E_x \rangle_f + (1-P) \varepsilon_a \langle E_x \rangle_a \tag{9}$$

Equation (7) becomes

$$U = \frac{1}{2} \varepsilon_x^* \langle E_x \rangle^2 = \frac{\langle E_x \rangle^2}{2} \left\{ \varepsilon_a + P(\varepsilon_f - \varepsilon_a) \frac{\langle E_x \rangle_f}{\langle E_a \rangle} \right\} \tag{10}$$

where the symbols $\langle \rangle_f$ and $\langle \rangle_a$ represent averages over the fiber and air volumes, respectively. From Eq. (10) it follows directly that

$$\varepsilon_x^* = \varepsilon_a + P(\varepsilon_f - \varepsilon_a) \langle E_x \rangle_f / \langle E_x \rangle \tag{11}$$

Similar equations can be derived for ε_y^* and ε_z^*.

Equation (11) is exact and contains only the term $\langle E_x \rangle_f$ which must be evaluated. The self-consistency approximation evaluates $\langle E_x \rangle_f$ by calculating the average electric field in an "average" fiber segment that is embedded in a continuous medium of dielectric constant ε_x^*. This is no trivial task. Davies (36) has done this for a two-component mixture of long, thin fiberlike inclusions embedded in a continuous medium.[1]

[1]Although not explicitly stated by Davies (36), considering how the equations were derived, the fibers apparently have a cross-sectional shape that depends on the anisotropy of the dielectric constant of the mixture (37).

Equations were given by Davies for the special case in which the fibers are all aligned in the x-y plane and have a random distribution in that plane. For this case

$$\varepsilon_x^* = \varepsilon_y^* = \varepsilon_a + \frac{P(\varepsilon_f - \varepsilon_a)\ (\varepsilon_f + 3\ \varepsilon_x^*)}{2(\varepsilon_x^* + \varepsilon_f)} \tag{12}$$

and

$$\varepsilon_z^* = \varepsilon_a + \frac{2P\ \varepsilon_z^*\ (\varepsilon_f - \varepsilon_a)}{\varepsilon_z^* + \varepsilon_f} \tag{13}$$

For comparison, these equations are plotted together with the bounds given earlier for the effective dielectric constant of paper in Fig. 4.

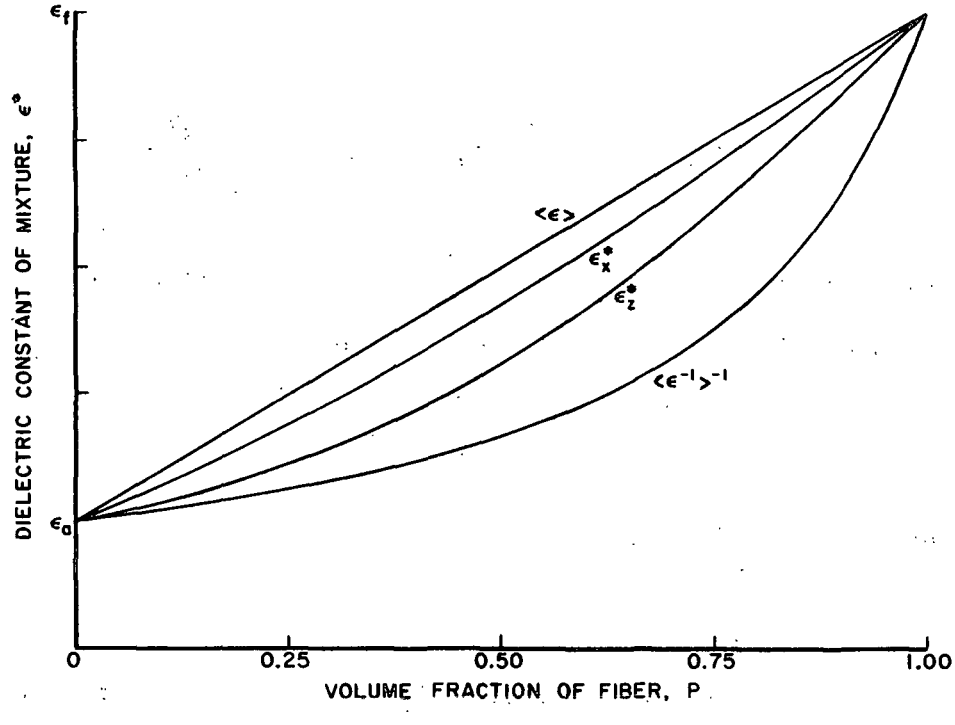

Figure 4. Davies (36) approximate relations for ε_x^* [Eq. (12)] and ε_z^* [Eq. (13)] together with the bounds for ε^* given earlier.

THE EFFECTIVE ELASTIC MODULUS OF PAPER AS A MIXTURE

It was noted earlier that due to the mathematical similarity of the problems the same mixture analysis used to calculate the effective dielectric constant may be

applied to calculate the effective elastic modulus of heterogeneous media. This is true; however, in the case of paper there is a major problem. Paper is composed of a mixture of two materials - fiber with a finite, large modulus, and air with a modulus of zero. The bounds given by Eq. (4) are not very helpful. The lower bound is zero over the entire apparent density range except at $P = 1.0$ where the modulus is equal to the modulus of the fiber. The upper bound is simply the modulus of the fiber times P over the entire range.

In short, an accurate description of the geometry of the fiber-air mixture is much more important in calculating the effective modulus of paper than it is in calculating the effective dielectric constant. The analysis of paper as a mixture, however, suggests why it is found that the elastic properties of paper are such strong functions of the apparent density of the sheet and also perhaps why the z-direction stiffness is so low.

EXPERIMENTAL PROGRAM

STATEMENT OF OBJECTIVE

The objective of this study was to investigate the effects of fiber orientation and drying restraint applied in the plane of the sheet on the dielectric constants and elastic moduli measured in all three principal directions of paper. It was well known that fiber orientation and drying restraint both affect the in-plane moduli considerably. The effect of these variables on the modulus in the z-direction was to be determined. The observed in-plane dielectric anisotropy when measured at microwave frequencies was believed to be due to fiber orientation only. It was desired to determine if the drying restraint had any effect on this anisotropy. By analyzing the elastic data together with the dielectric data, it was hoped that additional information would be obtained that would help explain the underlying mechanism for the effects of drying paper under restraint.

OUTLINE OF THE EXPERIMENTAL PROGRAM

The detailed procedures used to form and test the sheets are given in Appendixes III-V. Only a brief outline will be given here.

Four sets of sheets were prepared - one set of sheets with random fiber orientation in the plane of the sheet and three sets of sheets with fibers preferentially oriented in the x-direction. All of the sheets were made from a bleached western softwood kraft pulp, obtained in dry-lap form. This probably eliminated one possible mechanism for the effect of drying restraint on the sheet properties, because for once-dried kraft fibers no increase in the individual fiber strength is expected as a result of drying under stress (23).

The pulp was soaked, defibered, and beaten in a laboratory Valley beater to a freeness of approximately 500 mL CSF. The effect of varying the degree of beating or the method of beating was not investigated.

The random sheets were formed on an eight-inch-square screen in a Noble and Wood sheet mold. The oriented sheets were formed using a "Formette Dynamique" sheet machine manufactured by Allimand. The device has been described in the literature (38,39). A schematic of the device is presented in Fig. 5.

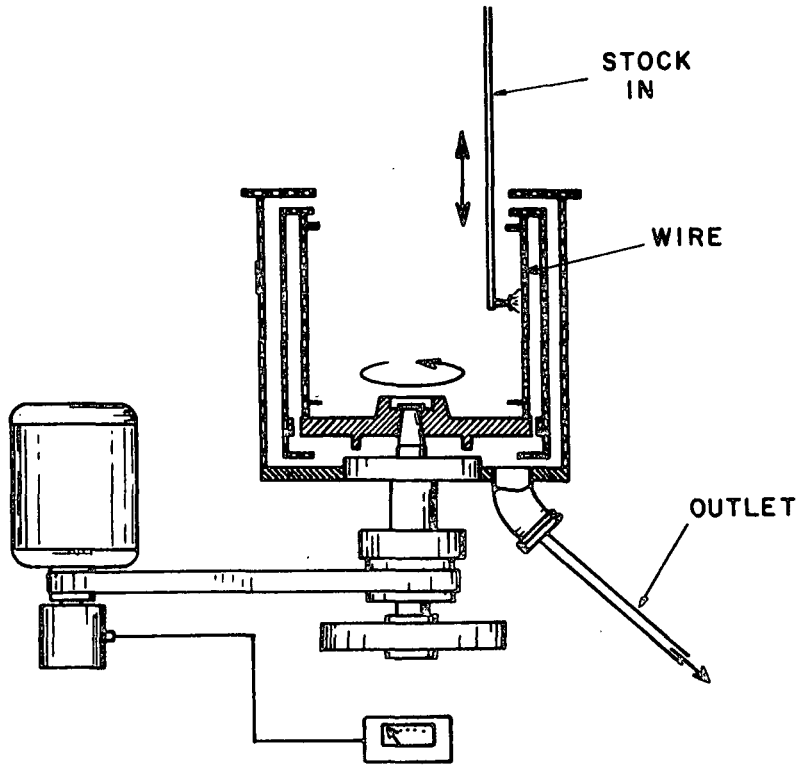

Figure 5. A schematic drawing of the Formette Dynamique sheet machine.

The machine essentially consists of a rotating perforated drum with a forming wire placed on the inside of the drum wall. Stock is sprayed onto the wire as the drum rotates. Due to the velocity difference between the stock at the nozzle and the rotating drum wall, shear forces tend to align the fibers in the direction of drum rotation. The Weyerhaeuser Company generously allowed the use of their machine

for making the oriented sheets. Three levels of fiber orientation designated "low," "medium," and "high" were achieved by appropriate adjustments of the stock jet velocity and wire speed on the Formette. The actual fiber orientation distribution corresponding to the three levels of fiber orientations studied was measured later. The details of the measuring technique are given in Appendix VII.

Since accurate z-direction measurements require thick sheets, all of the sheets were formed with a basis weight of about 0.40 a.d. kg/m^2. These heavy sheets were formed in a single layer on the Formette with little difficulty. The random sheets, however, were formed by wet pressing together six sheets, each with a basis weight of about 0.065 a.d. kg/m^2.

It is well known from a theoretical as well as a practical standpoint that paper properties vary considerably as a function of the final apparent density of the sheet. Since the process conditions adjusted to produce sheets with different fiber orientations and drying restraints resulted in changing the apparent density as well, it was necessary to include apparent density as a variable. The apparent density was varied by applying different wet pressing pressures with a platen type press.

After wet pressing, the sheets were dried under one of three levels of controlled restraint. The lowest level involved clamping the sheet biaxially using two pairs of line-type clamps and drying it without allowing any dimensional change. The edges of the sheet were not dried before clamping as some researchers have done (8,9,10,12, 20). For the medium and high levels of restraint, the sheet was clamped in the x-direction and then strained while still wet to about 1.2% or 2.4%, respectively, at a rate of about 0.8% per minute. When strained in the x-direction, the wet sheet contracted in the y-direction. After wet straining, the sheet was also clamped in the y-direction, allowing no further dimensional change during drying. The stress induced by the sheet in both the x- and y-directions as it dried was measured.

After drying, the sheets were tested. All tests were performed in a controlled environment of 23°C and 50% R.H. Ultrasonic pulse propagation techniques were used to obtain values for seven of the nine orthotropic elastic constants of each sheet. In the plane of the sheet, values for the two Young's moduli (E_x and E_y), the shear modulus (G_{xy}), and the Poisson ratios (υ_{xy} and υ_{yx}) were obtained. In the z-direction, a value for the longitudinal stiffness C_{33} was determined with good precision. Values were also obtained for the shear stiffnesses C_{44} and C_{55}; however, these values were considerably more scattered than those obtained for C_{33}.

Values for the in-plane Young's moduli were also obtained from tests performed on each sheet using the Instron Universal Testing Machine. In addition, the tensile strength in the x-, y-, and z-directions was measured. On the oriented sheets, the compressive strength in the x- and y-directions was determined using the STFI tester.

Finally, the complex dielectric constant was measured in each of the three principal directions of the sheet. The measurements were made at a single frequency of 9.6 GHz in the controlled environment at 23°C and 50% R.H.

RESULTS AND DISCUSSION

ELASTIC AND STRENGTH PROPERTIES

The results of the elastic and strength measurements made on the sheets are all expressed in stress units of force per unit area. (One Pascal is equivalent to one newton per meter^2.) The area referred to is the cross-sectional area of the paper sheet, not the solid fiber area. The thickness and apparent density of each sheet were determined using a standard Schopper caliper gage. This gage conforms to TAPPI standard methods, and the results are thus consistent with previously published literature.

For the dielectric constants, however, the thickness and apparent density of each sheet were determined using a different method. This method resulted in a slightly higher value for the apparent density of each sheet. The two methods for measuring the sheet thickness and apparent density are discussed in Appendix IV. It is believed that the method used to determine the apparent density for the dielectric measurements is more accurate than that used for the elastic measurements, although the precision is about equal. The use of either method, however, does not affect the conclusions reached in this investigation.

IN-PLANE ELASTIC PROPERTIES

The values of Young's modulus measured in the x-direction using ultrasonic pulse propagation techniques are illustrated in Fig. 6. The results are plotted as a function of apparent density with different symbols used to indicate the different levels of fiber orientation and wet straining. The fiber orientation levels designated as medium and high were almost identical. From the measured fiber segment distributions discussed in Appendix VII, it was found that the average difference between the two distributions was only about 7%. Thus in Fig. 6, as in all

the figures presented, results are only plotted for three levels of fiber orientation - the random sheets and the low and high levels of oriented sheets. These three levels of fiber orientation are represented in the figures as circles, triangles, and squares, respectively. For clarity, only the lowest and highest levels of wet straining are plotted. These are indicated by the open and filled symbols in the figure.

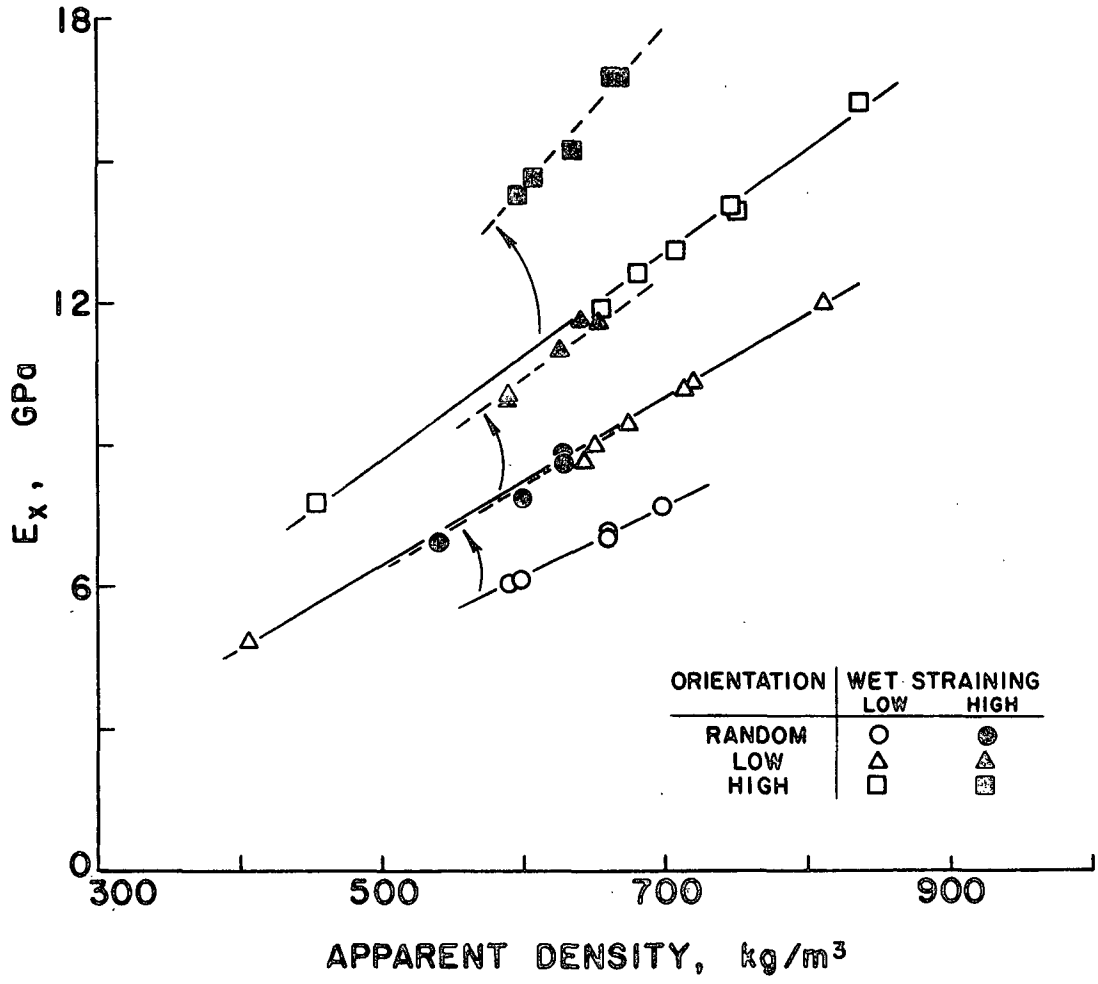

Figure 6. Young's modulus in the x-direction as determined using ultrasonic techniques.

As shown in the figure, Young's modulus depends strongly on all three variables - apparent density, fiber orientation, and wet straining. At the average apparent density of 650 kg/m^3, the modulus increased about 70% going from the randomly

oriented sheet to the most highly oriented. At each fiber orientation level, wet straining increased the modulus by an additional 30%.

The values measured for Young's modulus in the y-direction are presented in Fig. 7. As more fibers are oriented in the x-direction, the modulus in the y-direction decreases. The y-direction modulus is further decreased by wet straining in the x-direction.

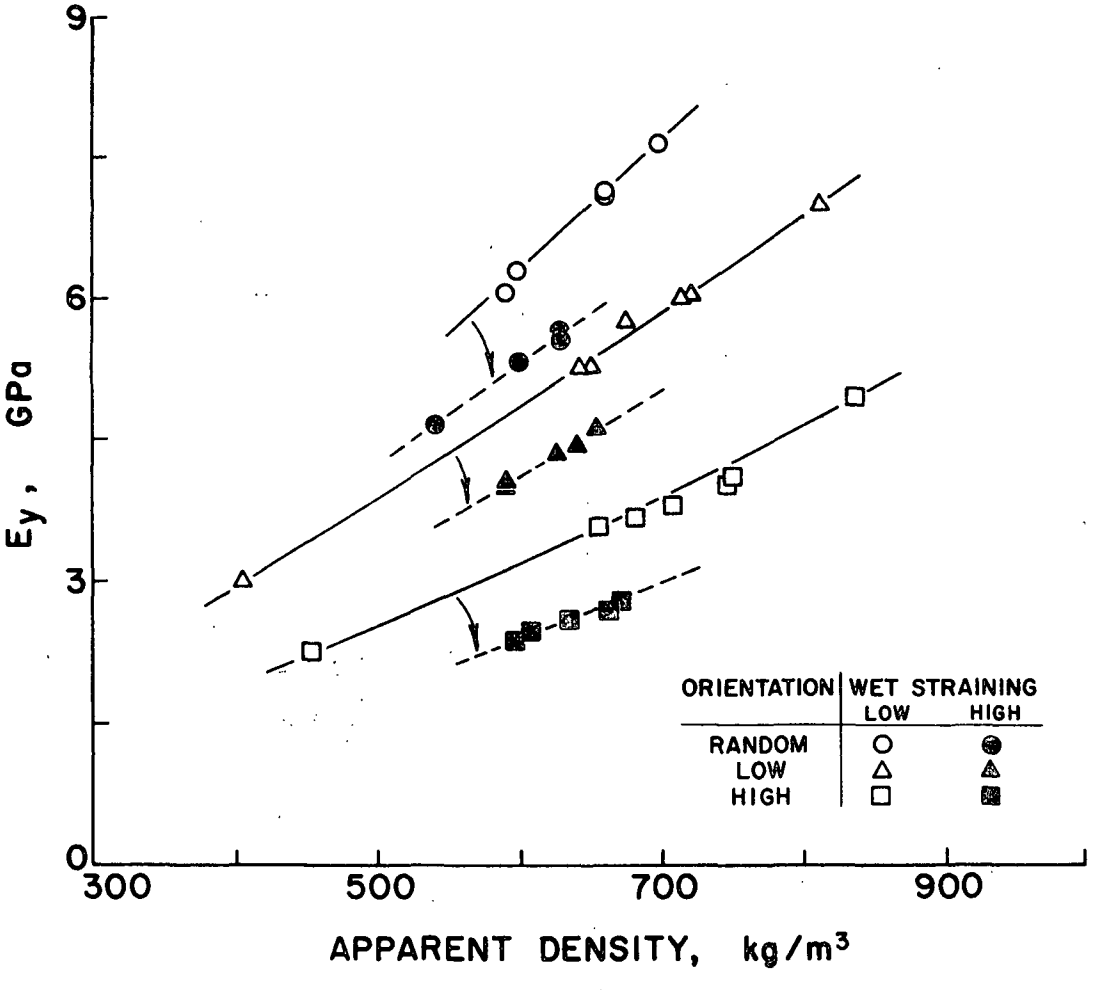

Figure 7. Young's modulus in the y-direction as determined using ultrasonic techniques.

It is interesting to examine the elastic anisotropy induced in the plane of the sheet by fiber orientation and wet straining. The elastic anisotropy may be defined

as E_x/E_y where E_x and E_y are the Young's moduli in the x- and y-directions, respectively. The effect of fiber orientation and wet straining on the in-plane elastic anisotropy, E_x/E_y, is given in Table I.

TABLE I

THE IN-PLANE ELASTIC ANISOTROPY RATIO E_x/E_y AS A FUNCTION OF FIBER ORIENTATION AND WET STRAINING

Wet Strain	Random	Fiber Orientation		
		Low	Medium	High
Low	1.00	1.67	3.20	3.41
Medium	1.24	2.09	4.30	4.55
High	1.51	2.55	6.03	5.98

In general, tables similar to Table I were prepared from a linear regression analysis of the data. This was done so the effect of fiber orientation and wet straining could be compared at a constant apparent density. There are actually only three independent variables - fiber orientation, apparent density, and wet straining. To adequately fit the data, however, six other "variables" were included in the regression analysis to account for nonlinear effects and first-order interactions. These six variables are simply the products and squares of the three independent variables mentioned previously.

The apparent density and induced strain in the x-direction were measured on each sheet, and these values were used in the regression analysis. The values for the fiber orientation level were assumed to be constant for each set of sheets - equal to 1.0 for the random sheets and 1.44, 2.10, and 2.18 for the low, medium, and high levels of oriented sheets, respectively. The numbers for the fiber orientation levels correspond to the number of fiber segments oriented $\pm$ 5 degrees from the x-direction relative to a randomly oriented sheet as obtained from the measured fiber orientation distributions discussed in Appendix VII.

The regression analyses were carried out by a forward elimination procedure using a computer program. The procedure sequentially chose from the nine total independent variables that variable which reduced the residual sum of the squares about the regression the most. Additional variables were introduced until the inclusion of another variable did not result in a statistically significant reduction in the error. For most of the regression analyses, there were about 50 observations. Accounting for the regressed variables, the remaining degrees of freedom were about 40. A value of $t = 2.02$, corresponding to a confidence level of 95% at 40 degrees of freedom, was used to determine the statistical significance of an introduced variable.

From the final regression equation the values of the dependent variable listed in the tables were calculated at a constant apparent density using $\rho = 650$ kg/m^3 for the elastic and strength results and $\rho = 700$ kg/m^3 for the dielectric results. The values of the dependent variable were calculated using 0.0, 1.4, and 2.8% for the low, medium, and high values of wet strain and 1.0, 1.44, and 2.18 for the random, low, and high levels of fiber orientation. By preparing the tables in this manner, the effects of fiber orientation and wet straining could be compared at a constant sheet apparent density. In addition, because the values presented in these tables were calculated from the regression equation, any changes in the values due to fiber orientation or wet straining are statistically significant at the 95% confidence level.

When the regression analysis was performed on the data presented in Table I, however, it was found that the elastic anisotropy ratio was not dependent on apparent density. For this table (and only this table) the values presented at each level of fiber orientation and wet strain are simply averages of all values within the set.

Examination of Table I reveals that both fiber orientation and wet straining affect the in-plane anisotropy by comparable magnitudes. With no wet straining, one can increase the anisotropy ratio from 1.0 to 3.4. At the highest fiber orientation level, one can increase the anisotropy ratio from 3.4 to 6.0 by wet straining the sheet.

The two in-plane Young's moduli were also determined "mechanically" using an Instron testing machine. Although there was more scatter in the data, the results were qualitatively the same. In fact, it was observed that generally there was a simple linear relationship between the moduli determined by these two methods. This relationship is illustrated in Fig. 8. In the figure are plotted values at all levels of fiber orientation in both the x- and y-directions of the sheet. Open symbols correspond to no wet straining, and the filled symbols correspond to sheets wet strained 2.4%. It can be seen that the modulus determined on the Instron is about 25% lower than that determined from ultrasonic wave velocity measurements. It is very interesting to find that this simple linear relationship does not appear to depend on fiber orientation, apparent density, or whether one measures the constants in the x- or y-direction of sheet. Wet straining does, however, appear to affect this relationship as indicated in the figure. Wet straining the sheets tended to decrease the measured difference between the moduli determined by these two methods in the x-direction. Unfortunately, without knowing the fundamental reason for the observed difference between the moduli determined by these two methods, it is not possible to use this observation as evidence for a mechanism by which wet straining alters sheet properties.

It has been suggested that the geometric mean of the Young's moduli, $(E_x * E_y)^{1/2}$, may be an invariant for paper independent of fiber orientation at constant drying conditions (40). For the sheets measured in this study, however, this quantity was only approximately constant. As indicated in Table II, the geometric mean

of the Young's moduli as determined from ultrasonic measurements depended on both the fiber orientation as well as the degree of wet straining. As noted earlier, this table was prepared from a multiple linear regression of the data and represents only effects that are statistically significant given the linear model assumed. Similar results are obtained if one examines the geometric mean of the stiffnesses, $(C_{11} * C_{22})^{1/2}$.

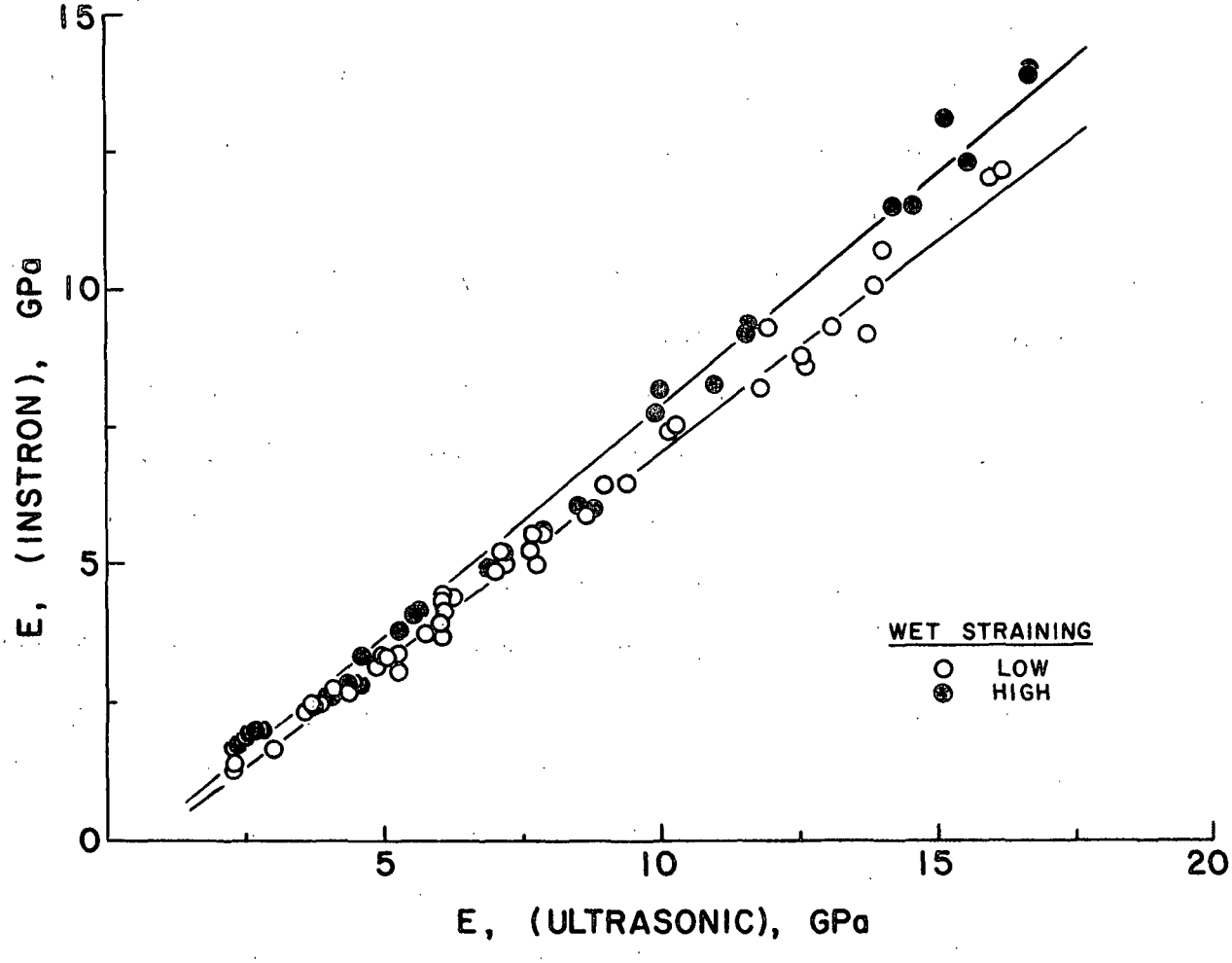

Figure 8. The relationship between Young's modulus determined mechanically and ultrasonically.

The geometric mean of the Young's moduli is considerably less sensitive to changes in the fiber orientation and degree of wet straining than is the arithmetic mean of these moduli. It thus is useful in comparing sheets with different degrees

of in-plane anisotropy. However, on the basis of these data, it does not appear that the quantity $(E_x * E_y)^{1/2}$ is an invariant for paper, in the strict sense of the term.

TABLE II

THE DEPENDENCE OF THE GEOMETRIC MEAN OF THE YOUNG'S MODULI, $(E_x * E_y)^{1/2}$[a], ON FIBER ORIENTATION AND WET STRAINING

Wet Strain	Fiber Orientation		
	Random	Low	High
Low	6.93	6.93	6.37
Medium	7.25	7.19	6.52
High	7.34	7.22	6.44

[a]Values have units of GPa.

The in-plane shear modulus (G_{xy}) was determined from ultrasonic wave velocity measurements. The dependence of G_{xy} on apparent density, fiber orientation, and wet straining is illustrated in Fig. 9. At both the random and low levels of fiber orientation, G_{xy} is approximately constant, depending mainly on the apparent density of the sheet. At the highest level of fiber orientation, however, G_{xy} is reduced and is further reduced by wet straining.

For an orthotropic material, there are four in-plane constants. The remaining engineering constant that has not been discussed yet is the Poisson ratio (υ_{xy}). It is more informative, however, to examine the stiffness coefficient (C_{12}). This stiffness coefficient for planar materials is related to υ_{xy} by $C_{12} = C_{11}\ \upsilon_{xy}$. In terms of both Poisson ratios, $C_{12} = (C_{11} * C_{22})^{1/2}\ (\upsilon_{xy} * \upsilon_{yx})^{1/2}$. C_{12} is the ratio of the stress induced in the x- or y-direction due to a strain induced in the other principal in-plane direction. The dimensions are force per unit area, and C_{12} is a function of apparent density as are the other moduli. At the average apparent density of 650 kg/m^3, Table III indicates the dependence of C_{12} on fiber orientation and wet straining.

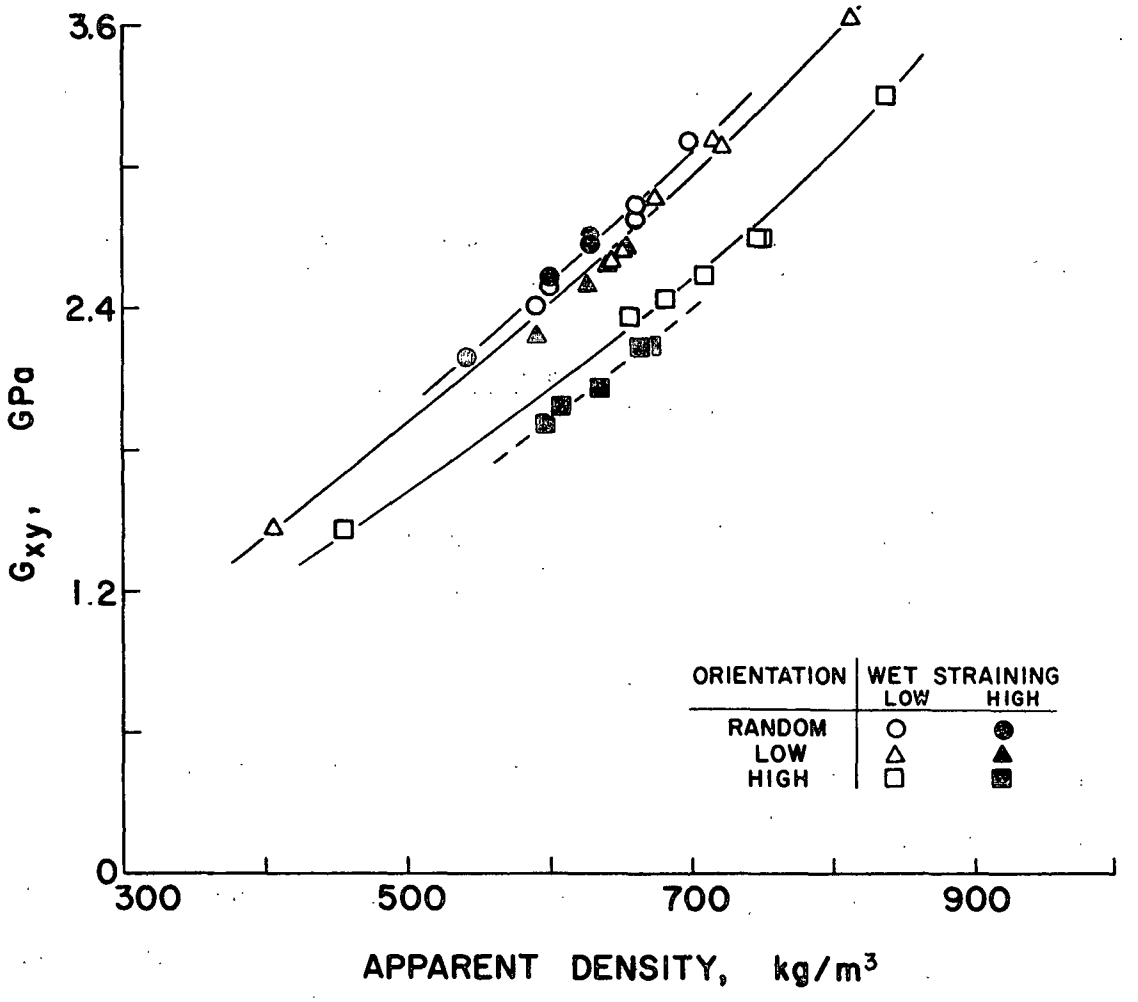

Figure 9. The in-plane shear modulus G_{xy} as determined using ultrasonic techniques.

TABLE III

THE DEPENDENCE OF C_{12}[a] ON FIBER ORIENTATION AND WET STRAINING

Wet Strain	Fiber Orientation		
	Random	Low	High
Low	1.74	2.03	1.33
Medium	1.93	2.00	0.92
High	2.11	1.96	0.51

[a]Values have units of GPa.

The stiffness C_{12} may be thought of as a measure of how "interrelated" the tensions applied in one principal in-plane direction are to the tension induced in the

other direction. As is indicated in Table III, this interrelationship is not a simple function of either fiber orientation or wet straining. For random sheets, wet straining tends to increase C_{12} slightly, whereas for the most highly oriented sheets C_{12} is dramatically reduced by wet straining.

IN-PLANE STRENGTH PROPERTIES

The values of the tensile strength measured in the x- and y-directions are plotted in Fig. 10 and 11. The dependence of the tensile strength on apparent density, fiber orientation, and wet straining is qualitatively the same as the dependence of the Young's modulus. Wet straining has less of an effect on the tensile strength than it does on the Young's modulus, however. At the average apparent density, in the range of variables investigated, fiber orientation increased the tensile strength about 80% in the x-direction, whereas wet straining increased it about 18%. In the y-direction, the tensile strength is reduced as the fibers become more aligned in the x-direction and is further reduced with wet straining in the x-direction.

The compressive strength was measured on only the oriented sheets (low, medium, and high levels). An STFI compressive strength tester was used (41). The results of these measurements made in the x- and y-directions are illustrated for the low and high levels of fiber orientation in Fig. 12 and 13. The effect of wet straining on the compressive strength is somewhat smaller than the effect of wet straining on the tensile strength. In going from zero to the highest level of wet straining, the compressive strength increased only about 12% in the x-direction. Fiber orientation also had a lesser effect. In the x-direction the tensile strength increased about 40% in going from the low to high levels of fiber orientation. In the same range, the compressive strength increases only about 20%. In the y-direction the compressive strength decreases with increasing fiber orientation and wet straining in the x-direction.

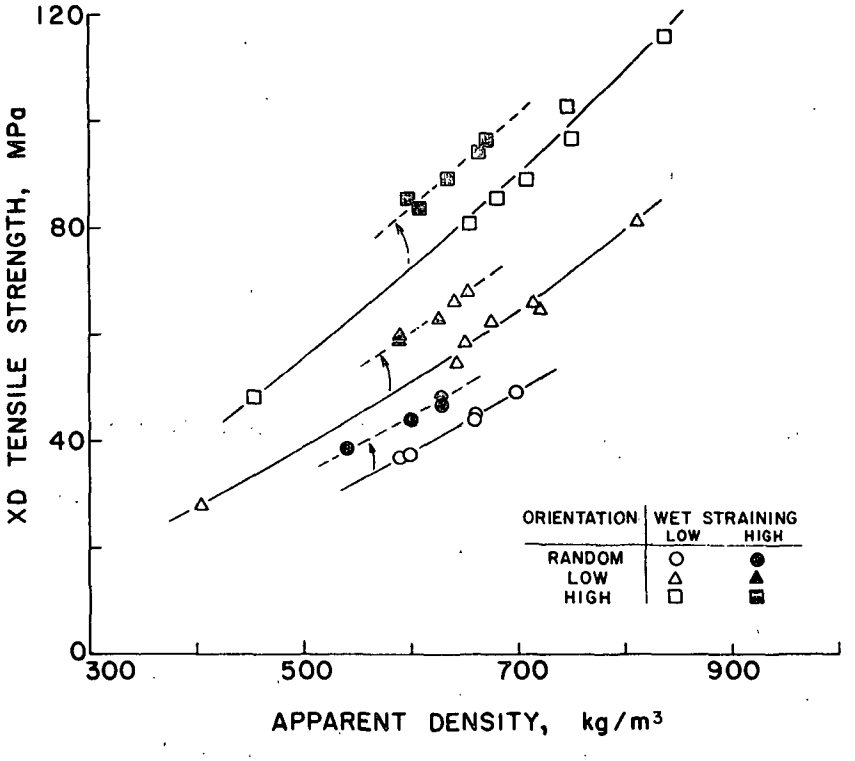

Figure 10. The tensile strength measured in the x-direction.

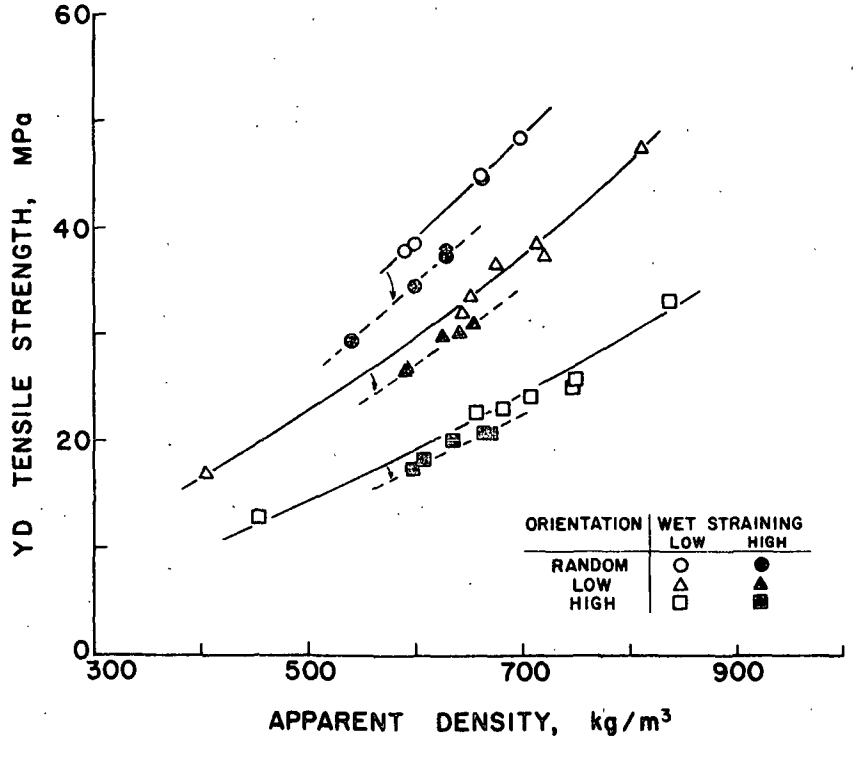

Figure 11. The tensile strength measured in the y-direction.

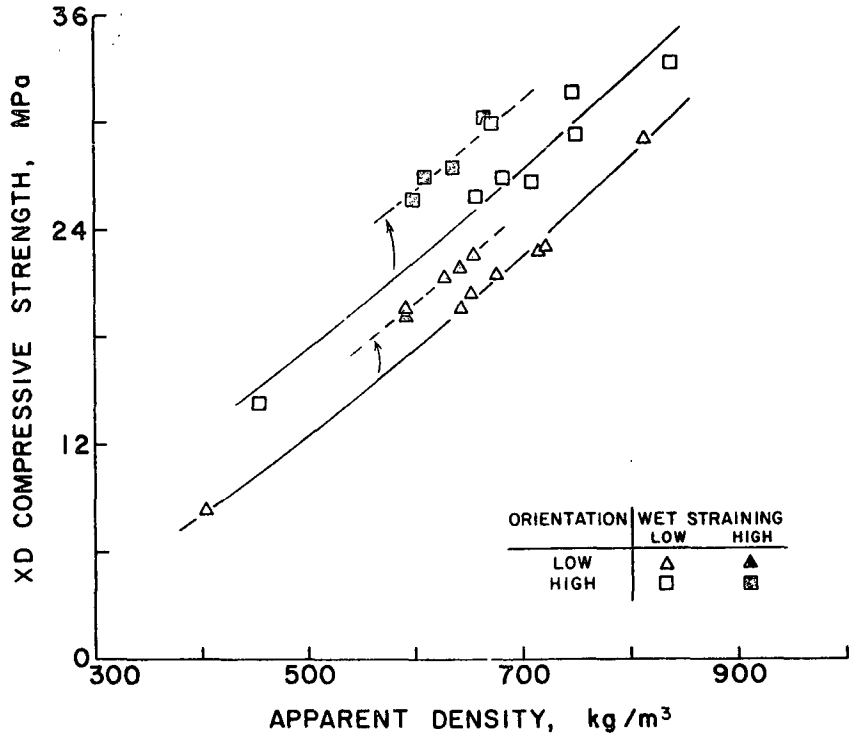

Figure 12. The compressive strength measured in the x-direction.

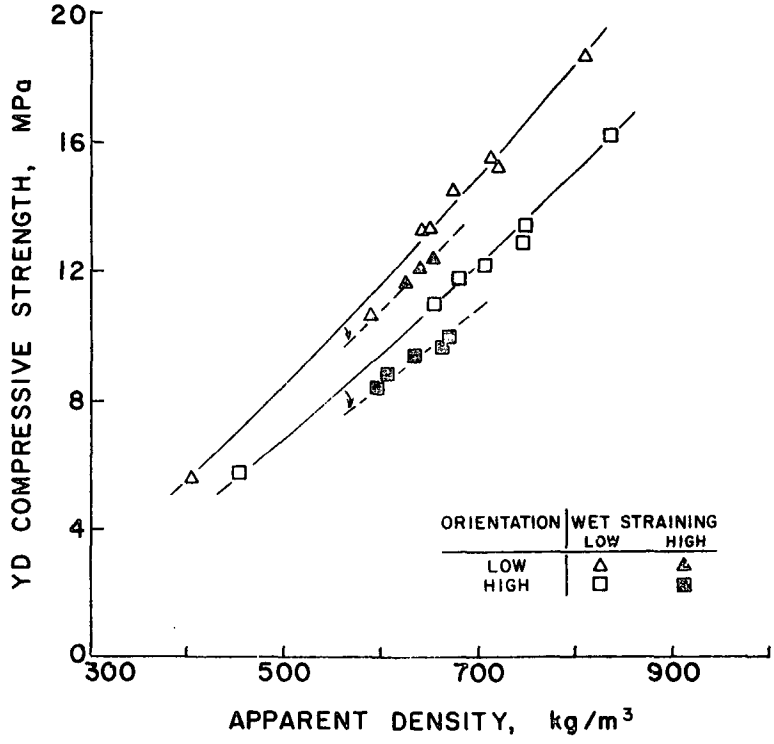

Figure 13. The compressive strength measured in the y-direction.

The similarity between the dependence of the tensile strength and compressive strength on apparent density, fiber orientation, and wet straining allows one to plot one value vs. the other as is done in Fig. 14. Both the x- and y-direction measurements were plotted for the fiber orientation levels random, low, and high at all wet strain levels. Although there is some scatter, there is an approximately linear relationship between the compressive strength and the tensile strength, with the former being about 30% of the latter.

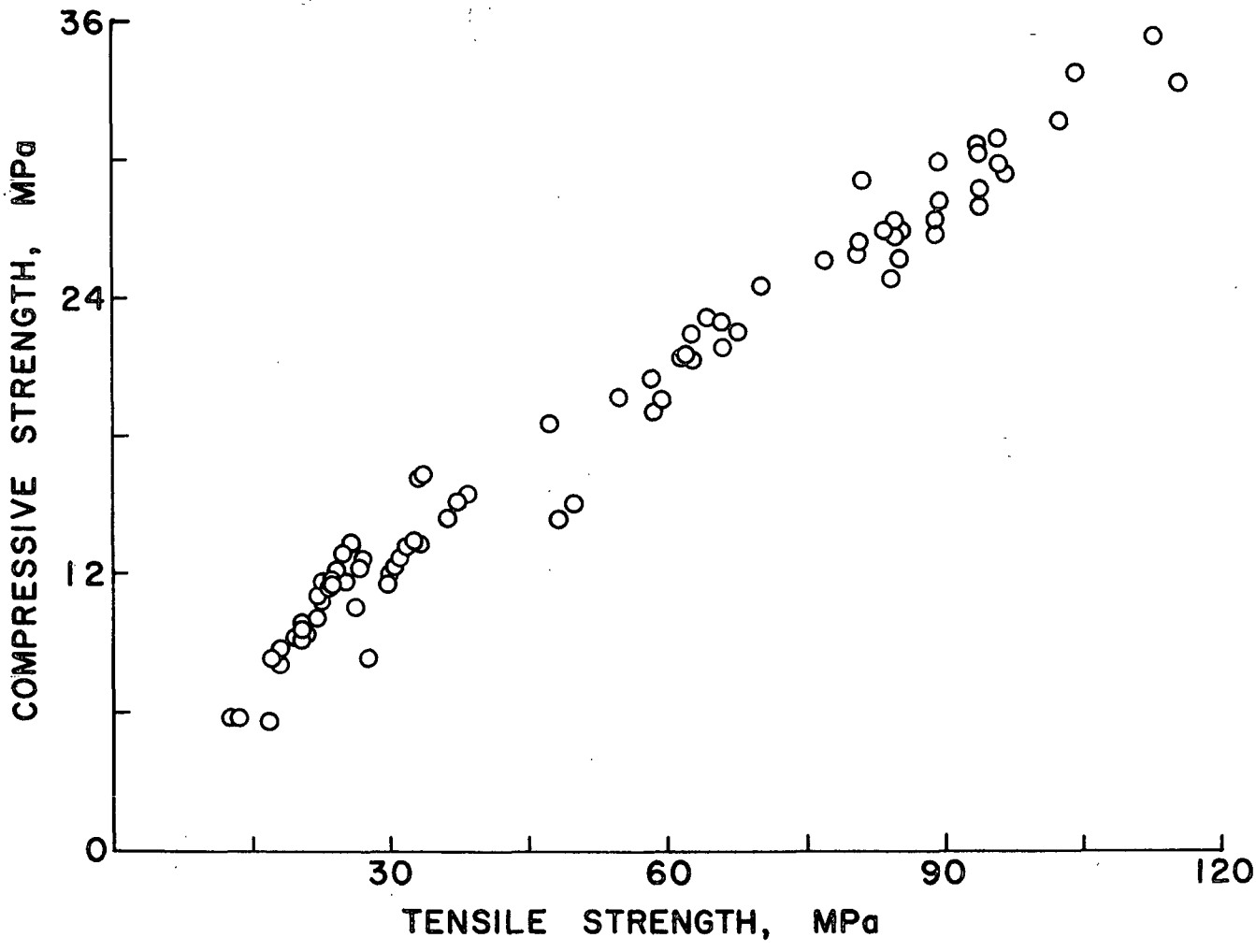

Figure 14. The relationship between the measured compressive strength and tensile strength.

Z-DIRECTION ELASTIC AND STRENGTH PROPERTIES

Perhaps the most interesting results of the mechanical measurements on the sheets was the dependence of the z-direction properties on the degree of wet straining in the plane of the sheet. The stiffness coefficient C_{33} was measured using ultrasonic pulse propagation techniques. The results of these measurements are illustrated in Fig. 15. Because the levels of wet straining were slightly different for the random sheets than for the oriented sheets, only values measured on the oriented sheets are plotted in the figure; C_{33} is seen to depend strongly on the apparent density as indicated in the figure. What is more surprising, however, is the strong dependence on the degree of wet straining induced in the plane of the sheet. The stiffness was only slightly affected by the fiber orientation, but in going from zero to 2.4% induced wet strain in the x-direction, the stiffness C_{33} was reduced by half at the average apparent density.

It is interesting to compare these measured values for the z-direction stiffness with other published literature values. Van Liew (24) measured the z-direction modulus mechanically, as noted earlier. Using a bleached softwood sulfite pulp, Van Liew formed thick sheets. These sheets were dried under pressure in stages between dry blotters. The final sheets had apparent densities ranging from about 800 to 900 kg/m^3. The values for the z-direction modulus reported by Van Liew ranged from about 0.2 to 0.5 GPa.

Mann (1), using ultrasonic techniques, obtained a value of 0.041 GPa for C_{33} measured on a machine-made milk carton board sample. The apparent density of the board was 775 kg/m^3. It is likely that the machine-made board was wet strained perhaps about 3% and calendered after drying. It is thus possible that the difference observed between the values reported by Van Liew and by Mann may be attributed to the differences in sheet density and wet straining only and is not necessarily due to the different measuring techniques.

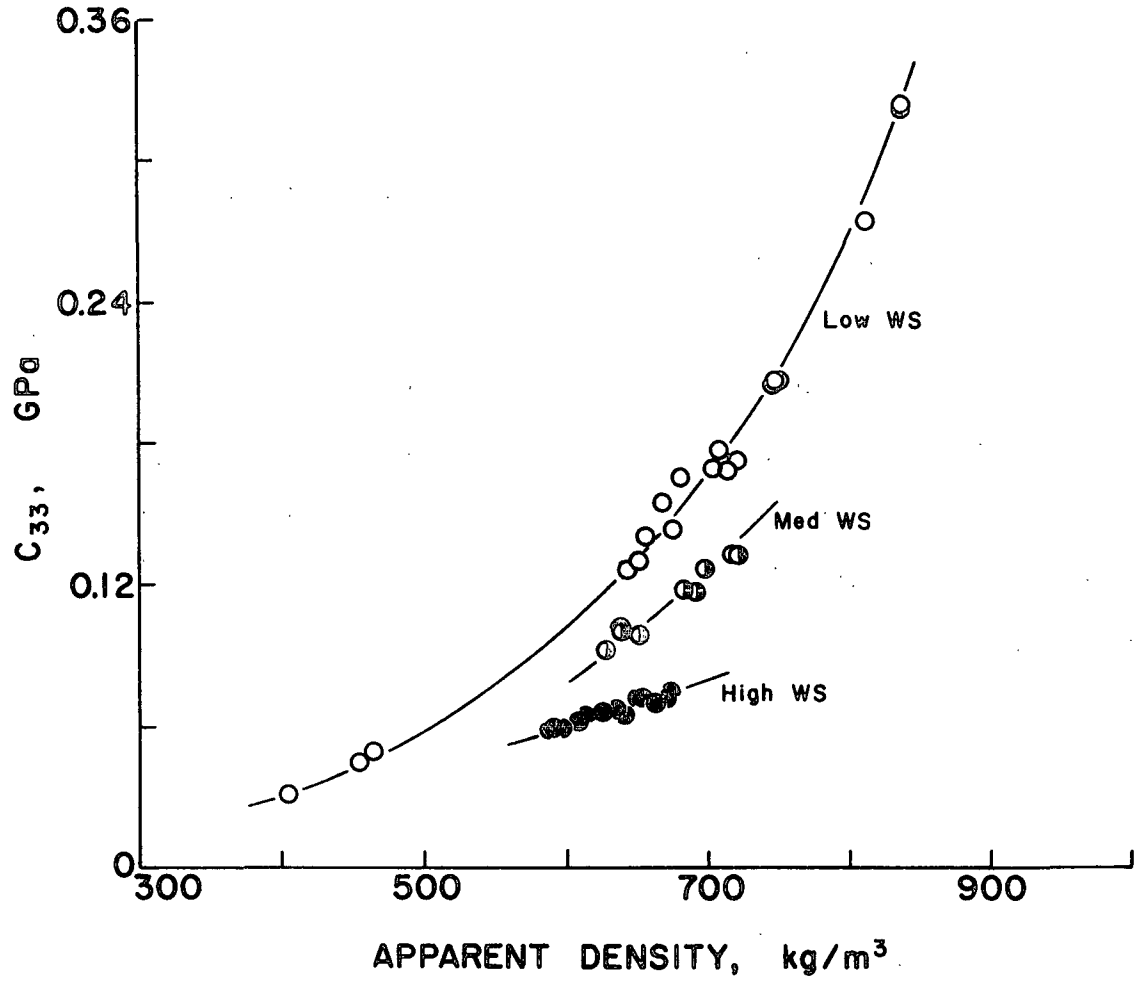

Figure 15. The dependence of C_{33} on apparent density and wet straining for oriented sheets.

The z-direction tensile strength was also determined for these sheets. As noted by Schulz (7) and Parsons (11), the z-direction strength tends to decrease when the sheet is wet strained in the plane of the sheet. In fact, an approximately linear relationship was observed between the z-direction tensile strength and the measured stiffness C_{33} as indicated in Fig. 16.

The out-of-plane shear stiffnesses C_{44} and C_{55} were also measured. Unfortunately, the values are less accurate and show more scatter than the value obtained for C_{33}. Some statistically significant results were obtained, however. C_{55} is the stiffness of the material to a x-z shear strain. One could thus, perhaps, expect it to increase

with wet straining; however, this was not observed to be the case. As indicated in Table IV, C_{55} does increase quite a bit as the fibers become more oriented in the x-direction but decreases somewhat when the sheet is wet strained in this direction. Evidently the reduction in z-direction stiffness with wet straining overwhelms the increase in x-direction stiffness, resulting in a net reduction in C_{55} when the sheet is wet strained.

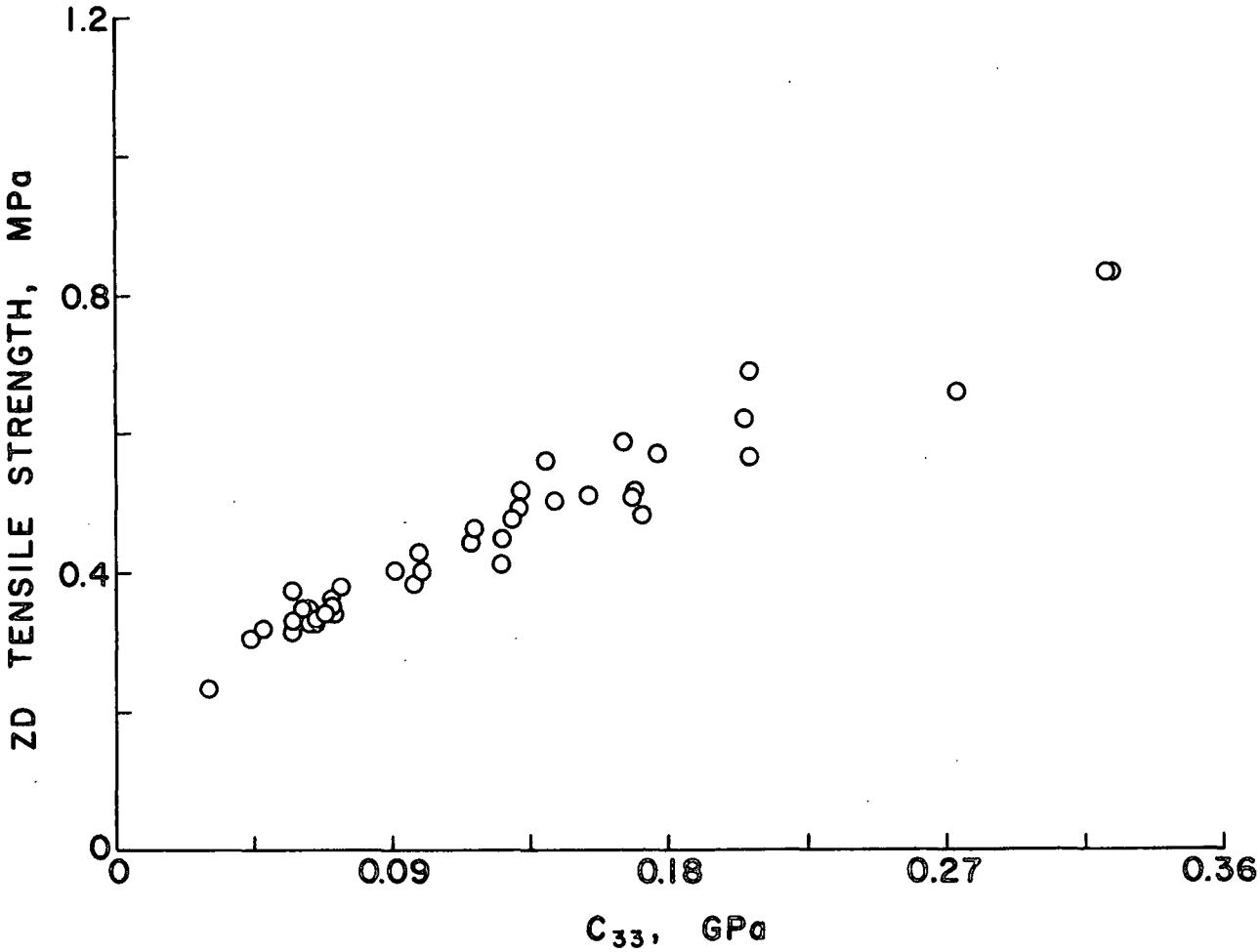

Figure 16. The relationship between the z-direction tensile strength and the stiffness coefficient C_{33}.

The shear stiffness (C_{44}) also decreases with wet straining; however, it is interesting to examine the ratio C_{55}/C_{44}. This is the anisotropy between the stiffness of the material to a x-z shear strain to the stiffness of the material to a y-z

shear strain. As indicated in Table V, this ratio increases with fiber orientation but is quite constant, increasing only slightly, with wet straining.

TABLE IV

THE DEPENDENCE OF C_{55}[a] ON FIBER ORIENTATION AND WET STRAINING IN THE X-DIRECTION

Wet Strain	Fiber Orientation		
	Random	Low	High
Low	0.227	0.266	0.331
Medium	0.213	0.245	0.301
High	0.199	0.225	0.270

[a]Values have units of GPa.

TABLE V

THE DEPENDENCE OF THE RATIO C_{55}/C_{44} ON FIBER ORIENTATION AND WET STRAINING IN THE X-DIRECTION

Wet Strain	Fiber Orientation		
	Random	Low	High
Low	0.97	1.25	1.70
Medium	0.99	1.27	1.73
High	1.00	1.28	1.76

SUMMARY

The in-plane elastic and strength results are consistent with previously published literature. In the range of variables investigated, both wet straining and fiber orientation tend to increase the measured property in the x-direction while reducing the value in the y-direction at a given apparent density.

By examining the proportional increase in the properties measured in the x-direction at a constant apparent density, an estimate of the relative effect of

fiber orientation and wet straining may be obtained. For the Young's modulus, fiber orientation had about twice the effect of wet straining in the range of variables investigated. For the tensile strength, the relative effect was about 4.5:1.

It is difficult to interpret the results observed for the dependence of G_{xy} and C_{12} on fiber orientation and wet straining. What is evident, however, is that the interrelationship between the stresses and strains in the two principal in-plane directions are reduced substantially at the highest level of fiber orientation and wet straining.

Perhaps the greatest effect of wet straining in the x-direction occurred in the z-direction of the sheet. The stiffness C_{33} was a very strong function of apparent density, but at the average apparent density it was reduced by half as a result of only a moderate 2.4% induced wet strain in the x-direction. The z-direction tensile strength was also reduced by wet straining.

The shear stiffness C_{55} increased as the fibers were more oriented in the x-direction but decreased when the sheet was wet strained in this direction. The ratio C_{55}/C_{44} depended almost exclusively on the fiber orientation but did increase slightly with wet straining.

DIELECTRIC PROPERTIES

The complex dielectric constants measured in all three principal directions of paper were strong functions of the apparent density of the sheet. In the figures presented here, the constants are plotted as a function of apparent density using different symbols to indicate the effects of fiber orientation and wet straining. (Recall that the IPC apparent density is used here; see Appendix IV.) To understand the dependence of the dielectric constant on apparent density and to compare the dielectric constants measured in different directions of the sheet, the results are

discussed with reference to the mixture theory relationships presented earlier. To use these relationships, however, a value for the dielectric constant of the solid fiber fraction is required. This value was estimated from the measured in-plane dielectric constants for the randomly oriented sheets using Eq. (12).

For each of the nine sheets with random fiber orientation, the values of the measured in-plane dielectric constants ε_x^* and ε_y^* were averaged. Then from each average value and the measured apparent density for the sheet, a value of ε_f was calculated using Eq. (12). The density of the solid fiber was assumed to be 1550 kg/m^3, and the dielectric constant of air was assumed to be 1.0. Because the measured values of ε_x^* and ε_y^* were complex, the calculated values of ε_f were complex also. The nine values of ε_f were very similar. The average was calculated to be 4.854-j 0.8491 with a standard deviation of 0.047 for the real part and 0.027 for the imaginary part.

All of the dielectric measurements were made in a controlled environment at 23°C and 50% R.H. using a frequency of 9.6 GHz. The moisture content of the sheets at these conditions was measured and found to be 6.8%. This estimate, then, represents the dielectric constant of a solid moist fiber at these conditions. The value would, of course, be different at a different moisture content, temperature, or frequency.

The four mixture theory relationships presented earlier in Fig. 4 are drawn in each of the figures shown here using the calculated value for the dielectric constant of the fiber. The top and bottom lines correspond to the upper and lower bounds possible for the dielectric constant, assuming the solid fiber to be isotropic. The second and third lines from the top are the approximate relations derived by Davies (36) for the in-plane and z-direction dielectric constant of a mixture of long, thin rods randomly oriented in a plane.

In Fig. 17-19 the real components of the complex dielectric constants measured in each of the three principal directions of the sheets are presented as a function of apparent density over the entire range in which the apparent density may vary. For clarity, only the values measured on the random and high levels of orientation are plotted. The open and solid symbols indicate whether or not the sheets were wet strained. Also included in Fig. 17 and 19 are values measured on three very high density sheets. These sheets were formed similarly to the random handsheets but were wet pressed at high pressures and dried between dry filter papers while in a press.

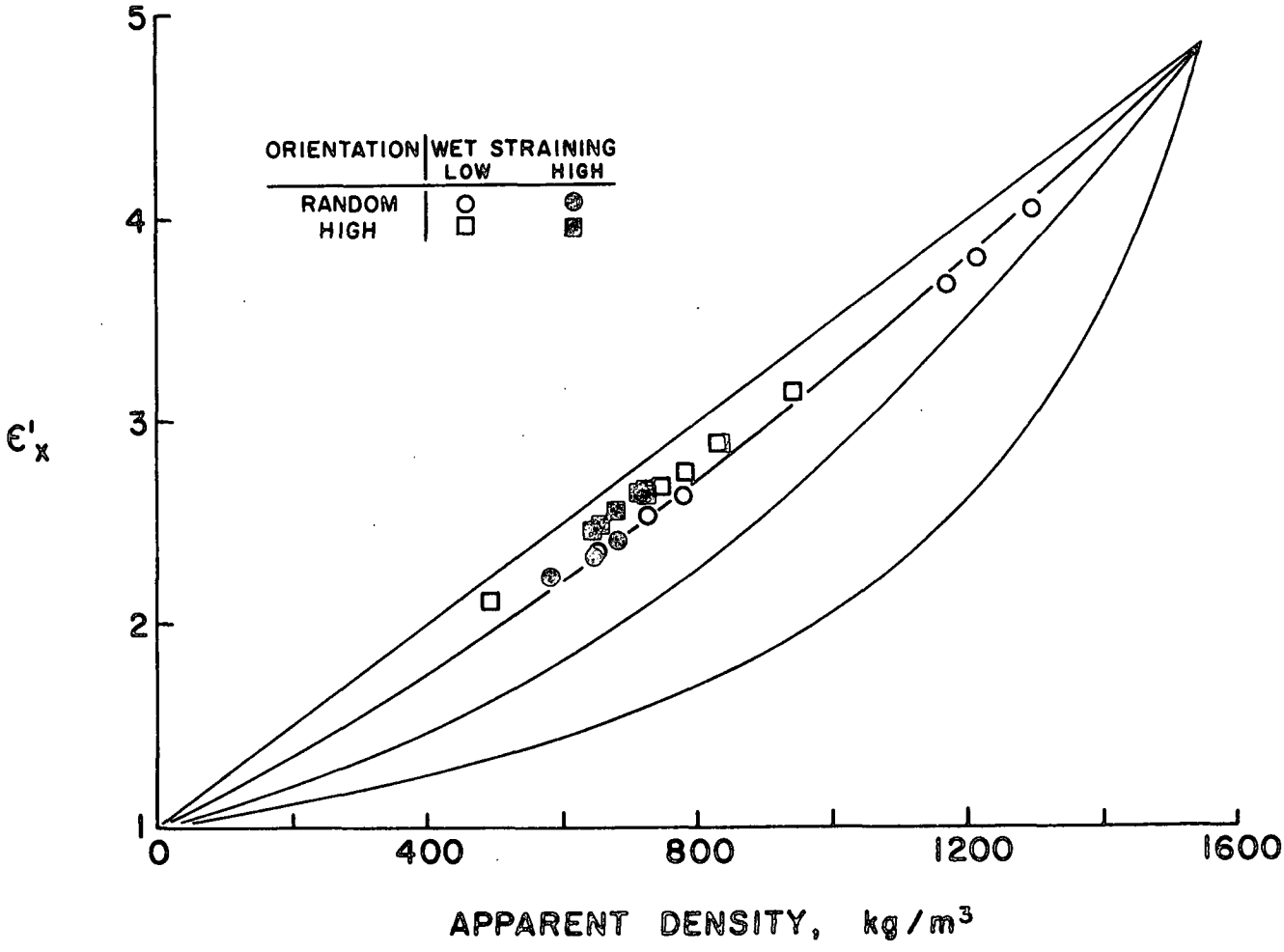

Figure 17. The real component of the complex dielectric constant measured in the x-direction.

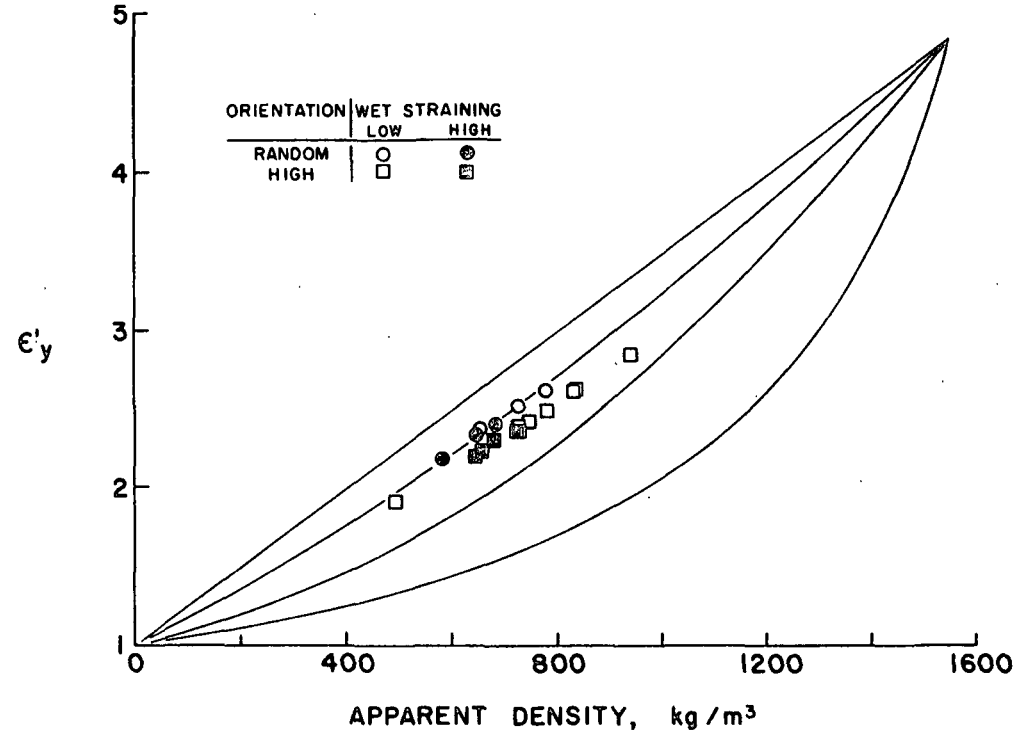

Figure 18. The real component of the complex dielectric constant measured in the y-direction.

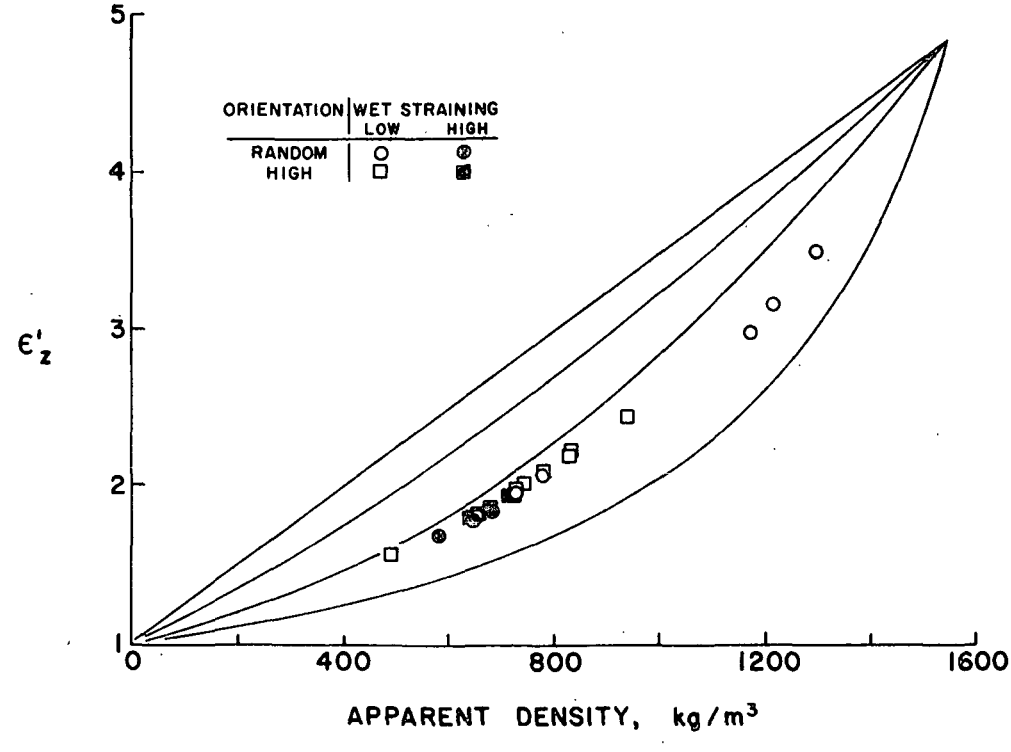

Figure 19. The real component of the complex dielectric constant measured in the z-direction.

Although it must again be pointed out that the theoretical mixture relationships were all drawn assuming a value for the dielectric constant of the solid fiber material calculated from Davies' relationship, a few interesting and important observations may be made concerning how the data lie with respect to these curves. Davies' relationship is seen to explain the dependence of the in-plane dielectric constant on apparent density fairly well. Although the final point at an apparent density of 1550 kg/m^3 was adjusted to fit the data, no adjustment can be made to change the curvature of the line given that it must pass through one at an apparent density of zero. Furthermore, the dielectric constant of the fiber was not calculated using the values measured for the three very high density sheets. Yet even these points are seen to lie along Davies' in-plane mixture theory curve.

In the z-direction, however, all of the measured values lie well below Davies' prediction for the z-direction dielectric constant of a mixture of fibers oriented in a plane. This observation is probably not due to measurement errors. The major error in the measurement of the z-direction dielectric constant is associated with the correction for the air gaps between sheet layers. The correction procedure used, however, slightly overestimates the z-direction dielectric constant (see Appendix V). The lower-than-expected result in the z-direction could be due to anisotropy in the dielectric constant of the fiber or to the fact that the mixture theory relationship represents the dielectric constant of fibers having an almost circular cross section (see footnote on page 19, however). In actuality, wood pulp fibers tend to resemble flattened ribbons in paper rather than circular cylinders. As the fiber becomes more flattened, simple mixture theory would predict that the z-direction dielectric constant of the sheet would be reduced. In the limit, the fiber would exist as sheets separated by air layers. Of course, this geometry is simply the lower bound drawn in the figure. Because no data points fall below this lower bound, the possibility exists that the low z-direction dielectric constant of

paper is the result of fiber geometry alone without having to assume that the fiber itself is anisotropic.

In Fig. 20-22 the real components of the complex dielectric constants are replotted using an expanded scale to better illustrate the effect of fiber orientation and wet straining on the dielectric anisotropy. The orientation of fibers in the x-direction results in an increase in the dielectric constant in that direction. The dielectric constant does not increase beyond the upper bound for a mixture of components with isotropic dielectric constants, however. In the y-direction, the dielectric constant is correspondingly reduced, but not below Davies' relationship for the z-direction dielectric constant. In both cases, wet straining has a very small effect, if any, in relation to fiber orientation.

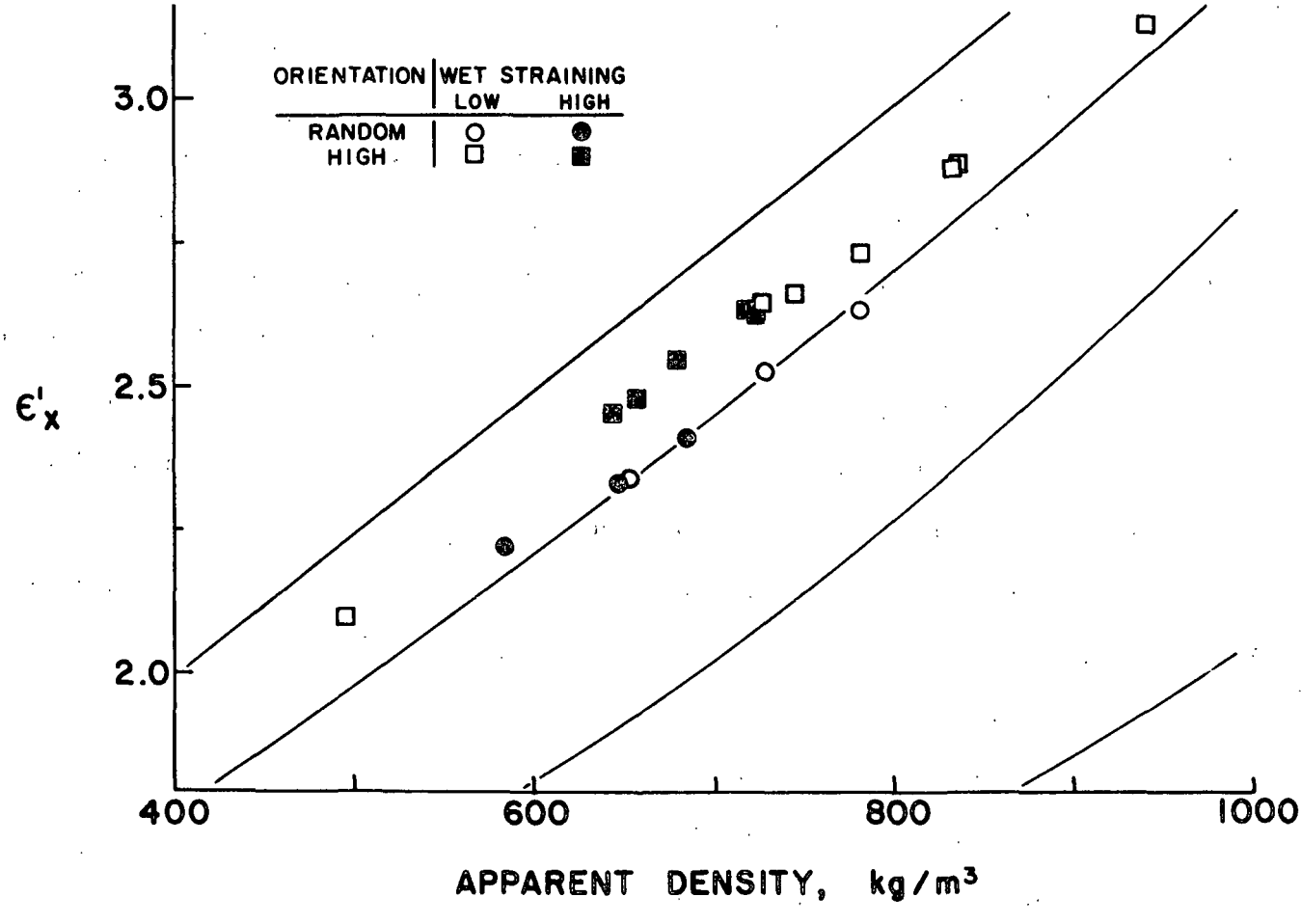

Figure 20. The real component of the complex dielectric constant measured in the x-direction, expanded scale.

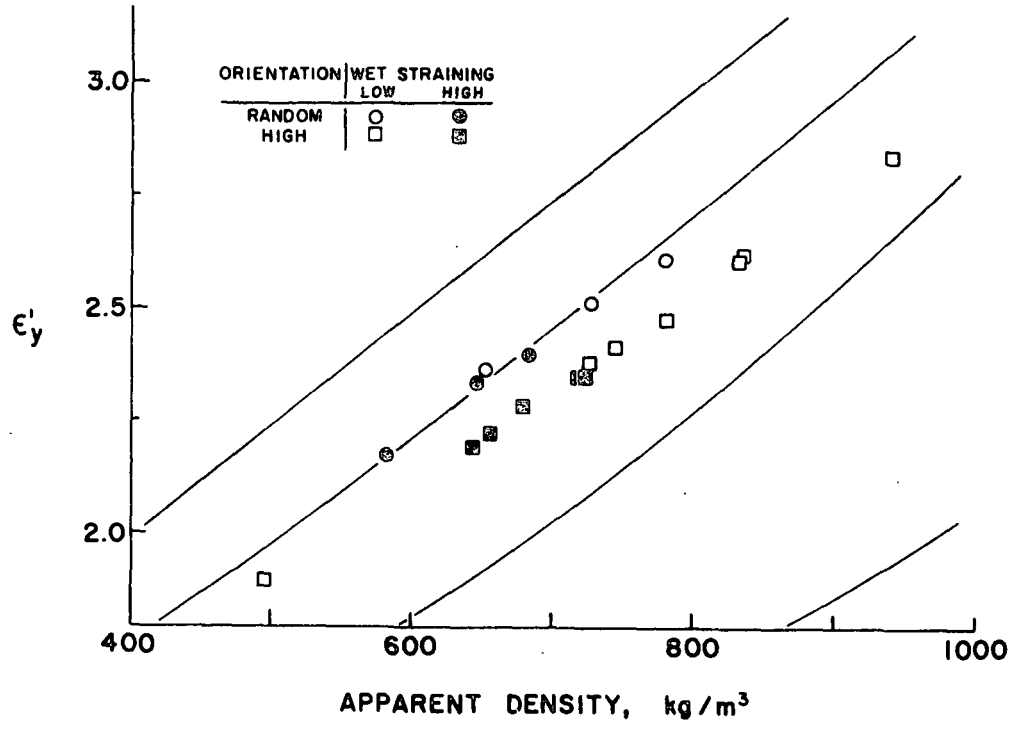

Figure 21. The real component of the complex dielectric constant measured in the y-direction, expanded scale.

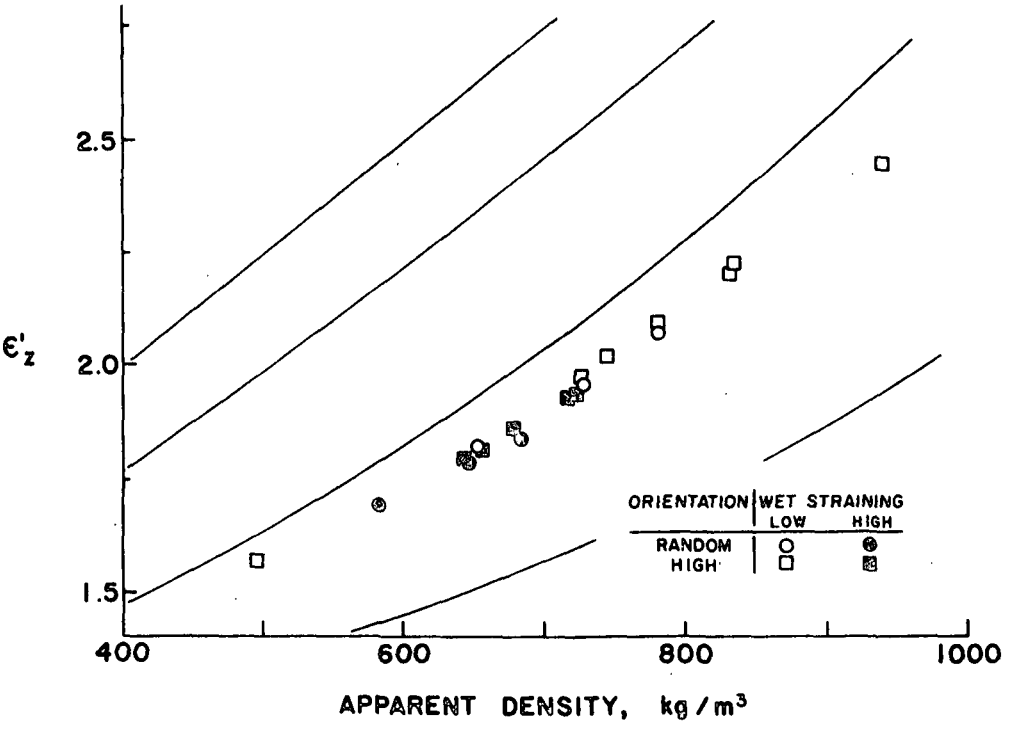

Figure 22. The real component of the complex dielectric constant measured in the z-direction, expanded scale.

The effect of fiber orientation compared with the effect of wet straining on the dielectric constant in the plane of the sheet is best evaluated by examining the ratio $(\varepsilon_x' - 1)/(\varepsilon_y' - 1)$. By using all of the measured in-plane dielectric constants Table VI was prepared. The numbers in the table are values for the anisotropy calculated from a multiple linear regression analysis of the data at an apparent density of 700 kg/m^3.

From the table it is evident that although wet straining has a statistically significant effect on the dielectric anisotropy, it is small compared with the effect of fiber orientation. The relative effect of fiber orientation compared with the effect of wet straining in the range of the variables investigated is about 10:1.

In the z-direction, as indicated in Fig. 22, the dielectric constant does not vary much with either fiber orientation or wet straining in the plane of the sheet. From a regression analysis of the data it was found that both fiber orientation and wet straining have statistically significant effects on the z-direction dielectric constant, given the linear model used in the regression. But in the range of variables investigated, the effect attributable to these two variables is small, being less than 3% of the measured value.

The imaginary components of the complex dielectric constants measured in the three principal directions of the sheets are plotted in Fig. 23-25. These values depended on apparent density, fiber orientation, and wet straining in a manner similar to the real components of the complex dielectric constant. In the plane of the sheet, however, the dependence of these values on apparent density is not explained as well by the mixture theory relations as was the case for the real components. In particular, the data would suggest that the intercept at zero apparent density would be at a value somewhat larger than zero. This may indicate that the measured values of the imaginary components of the dielectric constants are in error perhaps by some constant value. In any case, such an error would not affect the conclusions

about the relative effect of fiber orientation and wet straining on these constants. Indicated in Table VII is the effect of fiber orientation and wet straining on the anisotropy of the imaginary components of the complex dielectric constants measured in the plane of the sheet. The effects of fiber orientation and wet straining on the in-plane anisotropy of the imaginary components of the complex dielectric constants is somewhat greater than the effects on the anisotropy of the real components. But the relative effect of wet straining is still small compared with the effect of fiber orientation.

TABLE VI

THE DEPENDENCE OF THE IN-PLANE DIELECTRIC ANISOTROPY RATIO $(\varepsilon_x' - 1)/(\varepsilon_y' - 1)$ ON FIBER ORIENTATION AND WET STRAINING

Wet Strain	Fiber Orientation		
	Random	Low	High
Low	1.00	1.09	1.19
Medium	1.00	1.09	1.20
High	1.01	1.10	1.21

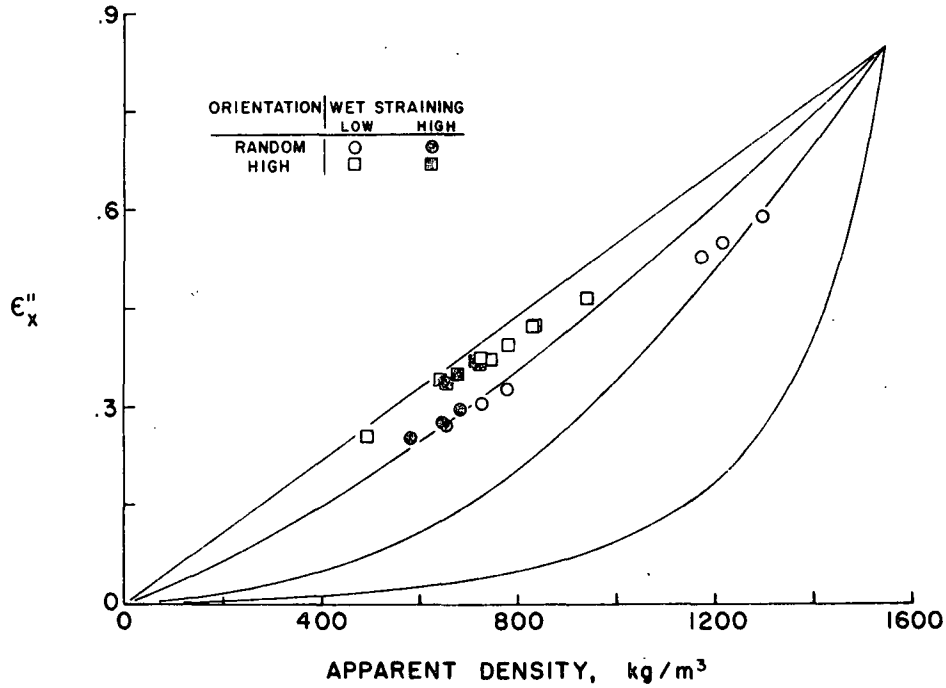

Figure 23. The imaginary component of complex dielectric constant measured in the x-direction.

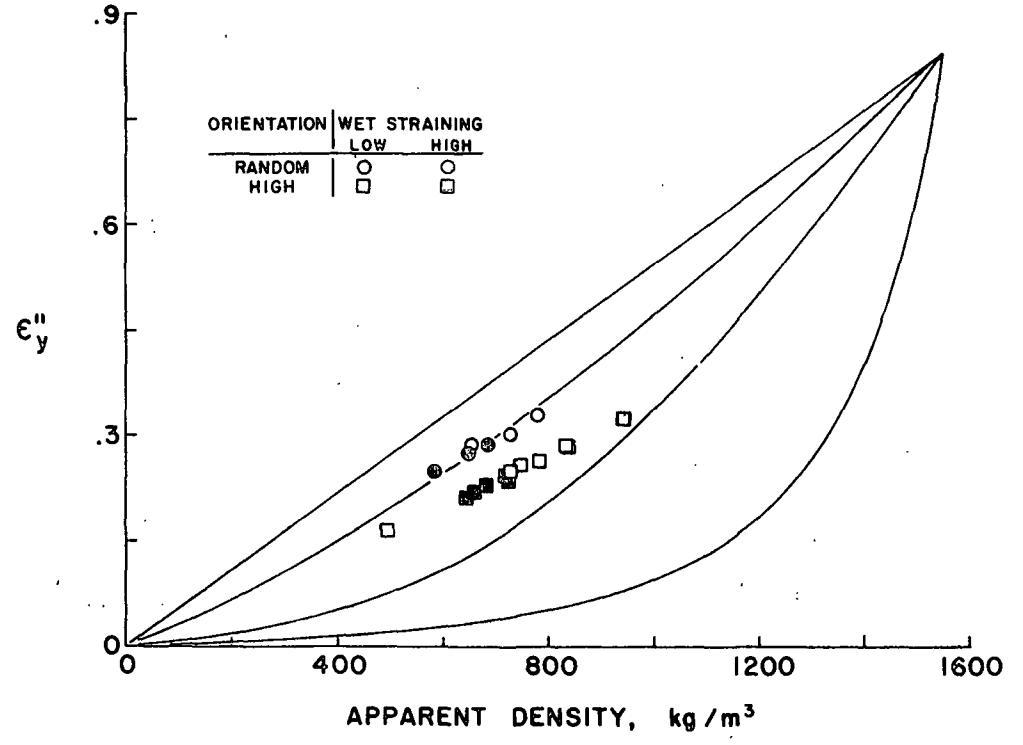

Figure 24. The imaginary component of the complex dielectric constant measured in the y-direction.

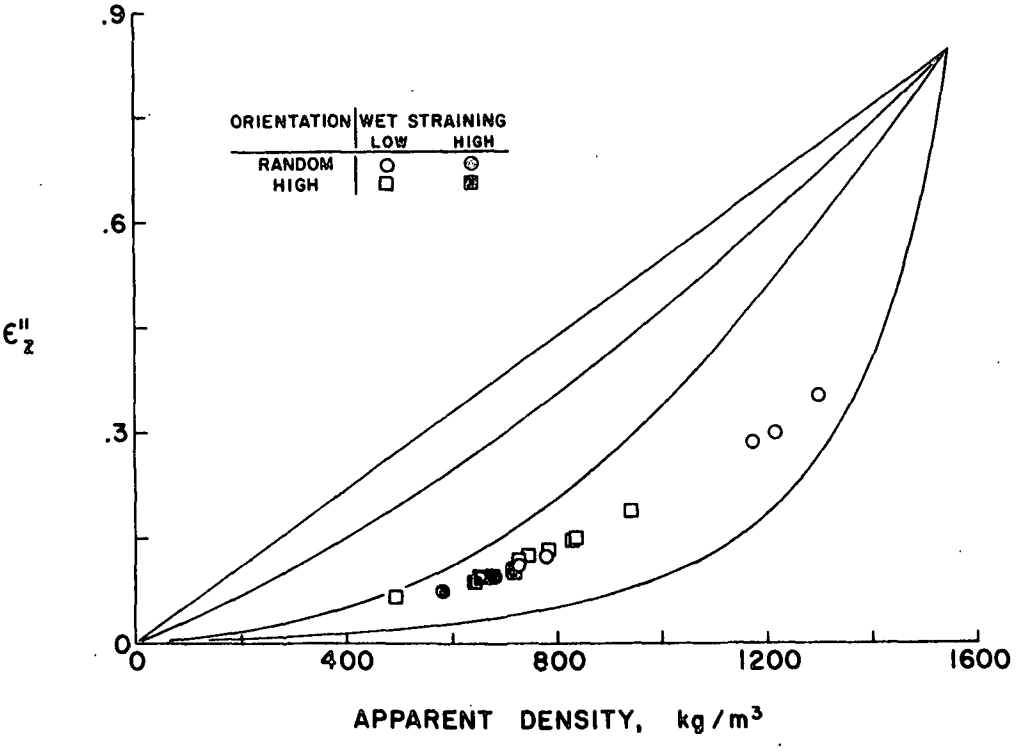

Figure 25. The imaginary component of the complex dielectric constant measured in the z-direction.

TABLE VII

THE DEPENDENCE OF THE IN-PLANE DIELECTRIC ANISOTROPY RATIO ($\varepsilon_x''/\varepsilon_y''$) ON FIBER ORIENTATION AND WET STRAINING

Wet Strain	Fiber Orientation		
	Random	Low	High
Low	1.00	1.19	1.50
Medium	1.02	1.21	1.54
High	1.04	1.24	1.58

THEORETICAL ANISOTROPY PREDICTED FROM A MIXTURE THEORY

The anisotropy observed in the dielectric constant as a result of fiber orientation could be due to two effects. If the fiber itself is anisotropic, and if it has a larger dielectric constant along the fiber, then alignment of the fiber would result in a larger dielectric constant in the direction of alignment without regard to the shape of the fiber. On the other hand, mixture theory relationships predict that since the fiber is long and slender, a certain amount of anisotropy would be predicted as a function of fiber orientation even if the fiber itself were completely isotropic.

Davies (36) presented equations explicitly predicting the dielectric constant of a mixture of isotropic rods randomly oriented in a plane. These equations were given earlier. The derivation, however, was performed for a general case without assuming any orientation distribution for the fibers in the mixture. In particular, the solution was obtained in a coordinate system aligned with the fiber at an arbitrary angle from the coordinate system of the final mixture.

The goal is to obtain a value for the average electric field in the fiber $\langle E_i \rangle_f$. Then from Eq. (11) one can calculate the effective dielectric constant of the sheet. Equation (11) is reproduced here for both principal in-plane directions.

$$\varepsilon_x^* = \varepsilon_a + P(\varepsilon_f - \varepsilon_a)\ \langle E_x\rangle_f / E_x^\circ$$

$$\varepsilon_y^* = \varepsilon_a + P(\varepsilon_f - \varepsilon_a)\ \langle E_y\rangle_f / E_y^\circ \qquad (11)$$

Here the quantities $\langle E_x\rangle$ and $\langle E_y\rangle$ have been replaced by the applied fields E_x° and E_y°, assuming the sample to be large compared with the spacial variations of the dielectric constant.

Using Davies' general solution for an individual fiber segment (his equation 2.16) for the special case of the fiber segment oriented in the x-y plane at an angle α from the x-axis, the solution reduces to (see Appendix VIII for details)

$$\frac{\langle E_x\rangle_f}{E_x^\circ} = \frac{1 + \cos^2 \alpha'\ A^y}{1 + \sin^2 \alpha'\ A^x + \cos^2 \alpha'\ A^y}$$

$$\frac{\langle E_y\rangle_f}{E_y^\circ} = \frac{1 + \sin^2 \alpha'\ A^x}{1 + \sin^2 \alpha'\ A^x + \cos^2 \alpha'\ A^y} \qquad (14)$$

where

$$A^x = (\varepsilon_f - \varepsilon_x^*)/2\varepsilon_x^*$$

$$A^y = (\varepsilon_f - \varepsilon_y^*)/2\varepsilon_y^*$$

$$\cos^2 \alpha' = \varepsilon_y^* \cos^2 \alpha/(\varepsilon_y^* \cos^2 \alpha + \varepsilon_x^* \sin^2 \alpha)$$

$$\sin^2 \alpha' = \varepsilon_x^* \sin^2 \alpha/(\varepsilon_y^* \cos^2 \alpha + \varepsilon_x^* \sin^2 \alpha)$$

The average value of the electric field in an average fiber segment is obtained from Eq. (14) by integrating over the angles α for a particular fiber segment orientation distribution.

Unfortunately Eq. (14) contains both ε_x^* and ε_y^*; thus, Eq. (11) and (14) are coupled. A solution for ε_x^* and ε_y^* was obtained by an iterative process using a computer. First, values for ε_x^* and ε_y^* were guessed. Then using the segment length weighted angular orientation distribution measured on the oriented sheets (see

Appendix VII), values of $\langle E_x \rangle_f / E_x^\circ$ and $\langle E_y \rangle_f / E_y^\circ$ for an average segment were calculated using Eq. (14). Then from Eq. (11) better estimates for ε_x^* and ε_y^* were calculated. The procedure was repeated until the estimates of ε_x^* and ε_y^* did not change appreciably over one iteration.

Using the estimate of the dielectric constant of the fiber calculated earlier, at an apparent density of 700 kg/m^3, the anisotropy predicted by Davies' relationship is compared with the actual measured anisotropy in Table VIII. The measured anisotropy is taken from Tables VI and VII for sheets with no wet straining.

TABLE VIII

A COMPARISON OF THE MEASURED IN-PLANE ANISOTROPY WITH THAT PREDICTED BY DAVIES' (36) MIXTURE RELATIONSHIP

	Fiber Orientation		
$(\varepsilon_x' - 1)/(\varepsilon_y' - 1)$	Random	Low	High
measured	1.00	1.09	1.19
predicted	1.00	1.08	1.17
$\varepsilon_x''/\varepsilon_y''$			
measured	1.00	1.19	1.50
predicted	1.00	1.12	1.28

There is good agreement between the measured and predicted anisotropy of the real component, but for the imaginary component the agreement is only approximate. The predicted anisotropy is relatively insensitive to the actual value assumed for the dielectric constant of the fiber. Thus, if a different value for the density of the solid fiber fraction had been assumed, it would result in a slightly different value for ε_f, but the anisotropy due to the fiber orientation would be little affected.

The results of this calculation indicate that the observed in-plane dielectric anisotropy measured on these sheets can be largely explained on the basis of the geometric arrangement of the fiber segments alone. It is not necessary to assume that the fiber itself has an anisotropic dielectric constant.

SUMMARY

The dielectric constant measured in all three principal directions of the sheet is a strong function of the apparent density. In the x-y plane the dependence of the constants on apparent density is explained reasonably well in terms of a simple mixture theory.

As the fibers are more aligned in the x-direction, the measured dielectric constant increases in that direction and decreases in the y-direction. The effect of wet straining is about 1/10 the effect of fiber orientation in the range of variables investigated. The observed anisotropy in the plane of the sheet can be explained as being the result of the orientation of the fiber segments alone, without having to assume that the fiber has an anisotropic dielectric constant.

The z-direction dielectric constant was lower than would be expected from the measured in-plane constants assuming the fiber to be isotropic with an approximately circular cross section. It is unlikely that this discrepancy is due to measurement errors. The z-direction dielectric constant was not so low as to require the difference to be explained by anisotropy in the dielectric constant of the fiber. Both fiber orientation and wet straining in the plane of the sheet had little effect on the z-direction dielectric constant.

CONCERNING THE MECHANISM FOR THE INCREASE IN ANISOTROPY DUE TO WET STRAINING

When a sheet is wet strained in the x-direction, it contracts in the y-direction. After drying in the restrained condition, the sheet will have a lower apparent density

than if it had not been wet strained. When compared with an unstrained sheet at the same final apparent density, the wet strained sheet is stiffer, stronger, and ruptures at a lower strain in the x-direction and is more elastic, weaker, and ruptures at a larger strain in the y-direction. These observations have been recorded by many earlier investigators.

There have been several mechanisms proposed for the effect of increased drying restraint on sheet properties. The mechanisms, by and large, have as their basis the idea that drying a sheet under restraint effects a plastic deformation resulting in a redistribution of stresses among the load-bearing elements in the sheet. The various ideas differ, however, on where this redistribution of stresses occurs.

Jentzen (21) suggests that this stress redistribution may occur within the free fiber segments between bonds. In these segments the crystallites and fibrils may become more aligned in the longitudinal direction of the fiber, and any dislocations or stress concentrations in the fiber may be reduced due to drying under stress.

The stress redistribution could also occur in the bonded fiber segments. There is considerable evidence that the tendency for paper to shrink as it dries is due not so much to the contraction in the longitudinal direction of the fibers, but rather due to the contraction in the transverse direction (6,42-44). When paper dries, the free water between fibers is removed first. Little or no shrinkage is observed in the fibers or in the sheet. Then when water is evaporated from the fiber cell wall, the fiber starts to shrink. A free fiber shrinks most in the thickness direction (20-40%), considerably in the width direction (10-20%), but only a small amount in the longitudinal direction (1-2%) (6,42). At fiber crossing, however, the fiber-to-fiber bonds are of sufficient strength such that when the fibers start to contract, the transverse shrinkage of one fiber can effect a longitudinal shortening in the other fiber. The net result is that, if unrestrained, a

well-bonded, randomly oriented piece of paper will shrink about 10% in the plane of the sheet during drying. In the final dry sheet, the compressed regions of the fibers in the bonded segments are viewed as stress concentration sites. It is believed that the fiber exhibits a lower modulus in these regions and that failure would be more likely to initiate here. When paper is restrained from shrinkage during drying, it is conceivable that the extent and severity of these compressed regions ("microcompressions" as they are called) are reduced. In this case, drying restraint does not necessarily effect a favorable stress redistribution; rather it prevents an unfavorable stress redistribution from occurring naturally.

The third possibility is that stress redistribution may occur on a much larger scale. As suggested by Van den Akker (45) over thirty years ago, the stresses may become more equalized among the fibers themselves. Because fibers are never perfectly straight, there will always exist a certain amount of curl in the fibers. Increasing the drying restraint could reduce the amount of curl in the fibers oriented in the direction of the applied restraint. The net result would be that a greater number of fiber segments would be supporting a more even load, resulting in the sheet being both stiffer and stronger. Although dyed fibers have not been observed to change their shape much in the plane of the sheet (20), increased drying restraint has been observed to reduce the undulation of fibers in the z-direction (2).

It is reasonable to expect that the stress redistribution occurs at all of these levels in varying degrees when paper is dried under restraint. For the sheets investigated in this study, however, it is possible that the stress redistribution due to wet straining occurs mainly between the fibers and only to a lesser extent (if at all) within the free or bonded fiber segments.

It is unlikely that the free fiber segments between bonds were affected much by wet straining in this investigation. First of all, it must be noted that appreciable

stress does not develop in a wet sheet until it is quite dry, having a dry solids content of about 70-90% (46,47). Furthermore, before the fiber begins to shrink, causing internal stresses to develop, the bond between crossing fibers has to be strong enough to transmit that load. If this is the case, then the bonds within the free fiber segments would be expected to have appreciable strength also. Specifically, the fiber is probably not in a sufficiently plastic state to allow stress redistributions to occur. It should be noted that in the studies performed investigating the effect of drying restraint on individual fiber properties, the load was applied before drying commenced and was maintained at that level throughout the drying process (21-23). Finally, in this investigation the sheets were formed using a once-dried kraft pulp. Although the pulp was beaten lightly before forming the sheets, Kim (23) observed that once-dried kraft fibers showed no increase in strength even when dried under very large stresses.

Regarding the possibility that increased drying restraint reduces the microcompressions induced in the bonded fiber segments, it should be recalled that in this investigation only positive values of wet strain were applied to the sheet. It is reasonable to expect that if shrinkage of the sheet is reduced (by restraint), the extent and severity of microcompressions in the bonded fiber segments would be reduced. But for this mechanism, drying restraint only prevents an unfavorable stress redistribution from occurring. It is somewhat difficult to imagine how stretching a sheet when it is wet could reduce these microcompressions before they should even have formed.

The simplest and most likely mechanism for the effect of wet straining on the sheets studied in this investigation is that suggested by Van den Akker (45). The act of stretching a wet sheet probably tends to straighten curled fibers in the direction of stretching. The fibers, dried in this condition, would more equally support an applied load, resulting in a stiffer and stronger sheet. Viewing a typical

fiber as a long, curled, flattened ribbon, it is reasonable to expect that most straightening of the fiber would occur in the z-direction. In the plane of the sheet, there would be considerable resistance to change in position relative to the other fibers because the fibers are well bonded to other fibers all along their length. If curled in the z-direction, however, the fiber would be freer to straighten with increased wet straining.

Simultaneous with the straightening of fiber segments in the z-direction, one could expect a partial or complete bond breakage between some fibers. This would help explain the large reduction in the z-direction modulus measured on the wet-strained sheets. Because of the Poisson effect when the sheet is wet strained, the fibers oriented in the y-direction may become more curled. But because a negative strain has been allowed in this direction, microcompressions could also be induced in the bonded segments of these fibers. Both of these mechanisms would reduce the y-direction mechanical properties. The results of the dielectric constant measurements are also consistent with this mechanism.

CONCLUSIONS

The increases observed in the mechanical properties in the x-direction as a result of wet straining are most likely due to small structural changes in the geometry of the fibers in the sheet. Specifically, the fibers oriented in the direction of wet straining are probably somewhat straightened, such that upon later application of a load, the fibers respond more equally, resulting in a stiffer and stronger sheet in that direction. The straightening of the fibers probably occurs almost entirely in the z-direction; that is, the amount of fiber undulation in the z-direction is reduced.

Concurrent with a small straightening of the fibers with wet straining is a general disruption of the sheet. The decrease in final sheet apparent density and the marked decrease in z-direction stiffness and strength at a given apparent density suggest that some fiber-to-fiber bonds are being broken or, perhaps more accurately, fewer bonds are permitted to form when the sheet is wet strained. Thus the advantages of the increase in mechanical properties in the x-direction with wet straining may very well be offset by the significant reduction of these properties in the other two directions, particularly in the z-direction.

The dielectric constants measured at microwave frequencies depended on apparent density and fiber orientation in a manner consistent with simple mixture theories. The dependence of the dielectric constant on fiber orientation could be described largely on the basis of the fiber geometry alone without having to assume that the fiber itself has an anisotropic dielectric constant. Wet straining had a small effect on the dielectric anisotropy, compared with fiber orientation. On the basis of these results, together with the results obtained from the elastic measurements, one may conclude that the mechanism by which wet straining enhances the elastic anisotropy does not involve a large fiber reorientation. The small effect of wet

straining on the dielectric anisotropy is consistent with the mechanism thought to be occurring when the sheet is wet strained.

The results of this study have a practical significance. On the basis of this work, it appears that the dielectric constant anisotropy, when measured at microwave frequencies, could provide a measure of the fiber orientation in the sheet that is quite independent of the stresses induced during drying. This could be useful both in the laboratory or on the paper machine. In the laboratory, it could provide a measure of fiber orientation without having to count dyed fibers in the sheet. On the paper machine, it might provide valuable information relating to the control of the jet-to-wire speed ratio, for example.

LIST OF SYMBOLS

English Symbols

A = Cross-sectional area

a.d. = Air dry

C = Capacitance

C_{ij} = Elastic stiffness coefficients

d = Distance from minimum in the wave guide

Δd = Distance between equal dB points about a minimum in the wave guide

D = Dissipation factor, $\varepsilon''/\varepsilon'$

D_i = Displacement vector field

D_x = Distance between 3dB points in the wave guide

D_p = Position of minimum in wave guide

D' = Error to add to D_p

e_{ij} = Strain tensor

E_i = Electric vector field

E_i° = Electric field applied to sample

E_x, E_y = Young's moduli in the x- or y-direction

exp ( ) = Natural number e raised to the power ( )

f = Frequency

f_c = Cross-over frequency for measuring bulk velocities

f_r = Molecular dielectric relaxation frequency

F = Tensile force

F_r = Tensile strength

G_{ii} = Engineering elastic shear moduli

G_{xy} = Shear modulus in the x-y plane

ΔH = Activation energy per mole

I = Current

I_c = Charging current

I_L = Loss current

j = $\sqrt{-1}$

L = Sample length

M = SWR meter reading

M' = Ideal SWR meter reading

o.d. = Oven dry

P = Volume fraction of fiber

P_r = Power

Q = Charge stored on parallel plate capacitor

R = Ideal gas constant

R.H. = Relative humidity

S_{ij} = Elastic compliance coefficients

SWR = Standing Wave Ratio

t = Time

t_d = Delay time with no sample between transducers

T = Absolute temperature

T_g = Calculated air gap thickness between sample and wave guide

T_p = Thickness of paper

U = Energy per unit volume due to accumulated charges

$\vec{u}$ = Displacement vector field for deformed body

V = Voltage

V_x, V_y = Longitudinal Morgan velocities in x- or y-directions

V_{Sxy} = Shear Morgan velocity in x- or y-directions

V_{S45} = Shear Morgan velocity at 45° from x- or y-direction

V_{Lx}, V_{Ly}, V_{Lz} = Longitudinal bulk velocity in x-, y-, or z-directions

VSWR = Voltage Standing Wave Ratio

x, y, z = Principal directions in a rectangular Cartesian coordinate system oriented with the paper specimen

Greek Symbols

α = Angle of fiber segment from x-direction in (x, y, z) coordinate system

α' = Transformed angle α in (χ, η, ξ) coordinate system

δ = Loss angle, arctan ($\varepsilon''/\varepsilon'$)

ε^* = Complex dielectric constant of paper or a mixture in general

ε' = Real component of ε^*

ε'' = Imaginary component of ε^*

ε_a = Dielectric constant of air

ε_f = Isotropic dielectric constant of solid fiber

ε_m^* = Measured complex dielectric constant of paper in z-direction

λ_{ms} = Wavelength in movable short wave guide section

λ_{ss} = Wavelength in slotted wave guide section

ρ = Density

σ_{ij} = Stress tensor

υ_{ij} = Poisson ratios

ω = Angular frequency

χ, η, ξ = Principal directions in a transformed coordinate system

χ'', η'', ξ'' = Principal directions in a rotated, transformed coordinate system

ACKNOWLEDGMENTS

Far from being an individual undertaking, a Ph.D. thesis is, perhaps by its very nature, a culmination of the efforts of many people. The guidance, advice, and teaching of the members of my advisory committee, Dr. Gary Baum (Chairman), Dr. Chuck Habeger, and Dr. Douglas Wahren, are sincerely appreciated.

At one time or another, every member of the Institute faculty and staff has made a contribution, directly or indirectly, to this work. I wish to thank everyone for making this part of my life so enjoyable and worthwhile.

The financial support of the Institute and its member companies is deeply appreciated.

The patience and love of my wife, Debbie, has proved to be invaluable. Indeed, without the help of Debbie and even my son, Scott, it is doubtful that this thesis would have become a reality.

LITERATURE CITED

1. Mann, R. W. Elastic wave propagation in paper. Doctoral Dissertation. Appleton, Wis., The Institute of Paper Chemistry, 1978. 176 p.

2. Page, D. H., Sargent, J. W., and Nelson, R. Structure of paper in cross section. In: F. Bolam's Consolidation of the paper web, Vol. 1. p. 313-49. London, Tech. Sect. of the British Paper and Board Makers' Assoc., Inc, 1966.

3. Van den Akker, J. A., Tappi 53(3):388-400(March, 1970).

4. Habeger, C. C. and Baum, G. A. The interaction of microwave radiation with paper-water systems, Progress Report One, Project 3322. Appleton, Wis., The Institute of Paper Chemistry, 1978. 64 p.

5. Edge, S. R. H., Proc. Tech. Sect., Paper Makers' Assoc. Gt. Brit. Ireland 26:425(1945).

6. Page, D. H. and Tydeman, P. A. A new theory of the shrinkage, structure, and properties of paper. In: F. Bolam's The formation and structure of paper, Vol. 1. p. 397-421. London, Tech. Sect. of the British Paper and Board Makers' Assoc., Inc., 1962.

7. Schulz, J. H., Tappi 44(10):736-44(Oct., 1961).

8. Setterholm, V. C. and Chilson, W. A., U.S. Forest Service Research Paper, FPL-11:26 p. (April, 1964).

9. Setterholm, V. C. and Chilson, W. A., Tappi 48(11):634-40(Nov., 1965).

10. Meyers, G. C., Tappi 50(3):97-100(March, 1967).

11. Parsons, S. R., Tappi 55(10):1516-21(Oct., 1972).

12. Matolesy, G., CPPA Ann. Mtg. (Montreal) 60, Preprints Book B: 19-29 (1974).

13. Cowan, W. F., Tappi 56(2):40(Feb., 1973).

14. Prud'homme, R. E. and Robertson, A. A., Tappi 59(1):145-8(Jan., 1976).

15. Prusas, Z. C., Tappi 46(5):325-30(May, 1963).

16. Gates, E. R. and Kenworthy, E. C., Paper Technol. 4(5):485-94(1963).

17. Sauret, G., Chleq, J. P., and Lafabure, G., Techniques et Recherches Papetieres (6):30-40(1965).

18. Craver, J. K. and Taylor, D. L., Tappi 48(3):142-7(March, 1965).

19. Taylor, D. L. and Craver, J. K. Anisotropic elasticity of paper from sonic velocity measurements. In: F. Bolam's Consolidation of the paper web, Vol. 2. p. 852-72. London, Tech. Sect. of the British Paper and Board Makers' Assoc., Inc., 1966.

20. Setterholm, V. and Kuenzi, E. W., Tappi 53(10):1915-20(Oct., 1970).

21. Jentzen, C. A., Tappi 47(7):412-8(July, 1964).

22. Spiegelberg, H. L., Tappi 49(9):388-96(Sept., 1966).

23. Kim, C. Y., Page, D. H., El-Hosseiny, F., and Lancaster, A. P. S., J. Appl. Polymer Sci. 19:1549-61(1975).

24. Van Liew, G. P., Tappi 57(11):121-4(Nov., 1974).

25. M'Baye, K. and Pellisier, J. P., ATIP Rev. 29(2):51-4(1975).

26. Dusoiu, N., Rev. Roum. Chim. 21(4):563-70(April, 1976).

27. Driscoll, J. L., Paper Technol. 17(2):71-5(T42-46)(April, 1976).

28. McCrum, N. G., Reed, B. E., and Williams, G. Anelastic and dielectric effects in polymeric solids. London, John Wiley and Sons, Ltd., 1967. 617 p.

29. Hill, N. E., Vaughan, W. E., Price, A. H., and Davies, M. Dielectric properties and molecular behaviour. London, Van Nostrand Reinhold Co., 1969. 480 p.

30. Algie, J. E. Dielectric Properties of Keratin and Cellulose. In: F. Happey's Applied Fibre Science, Vol. 2. p. 169-203. London, Academic Press, Inc., 1979.

31. Klason, C. and Kubat, J., Svensk Papperstid. 79(15):494-500(1976).

32. Hasted, J. B. Aqueous dielectrics. London, Chapman and Hall, Ltd., 1973. 302 p.

33. Hearle, J. W. S. and Peters, R. H., eds. Fibre structure. Manchester, The Textile Institute and Butterworths, 1963. 667 p.

34. Atalla, R. H. Molecular orientation in native fibers. Paper presented at the 1979 Intern. Paper Physics Conf., Harrison Hot Springs, B. C. p. 171.

35. Beran, M. J. Statistical continuum theories. Vol. 9, (in a series of) Monographs in Statistical Physics and Thermodynamics, I. Prigogine, ed. New York, N.Y., Interscience, 1968. 424 p.

36. Davies, W. E. A., J. Phys. (D. Appl. Phys.) 7:120-30(1974).

37. Habeger, C. C. Personal communication, 1981.

38. Sauret, G., Bull. ATIP 16(6):446-54(1962).

39. Centre Technique de l'Industrie des Papiers, Cartons, et Celluloses, French patent 2,030,715 (Nov. 13, 1970).

40. Htun, M., Carlsson, L., and Fellers, C. The invariant mechanical properties of oriented handsheets. Paper presented at the 1981 TAPPI Annual Meeting, Chicago, Ill. p. 59-66.

41. Cavlin, S. and Fellers, C., Svensk Papperstid. 78(9):329-32(May 30, 1975).

42. Tydeman, P. A., Wembridge, D. R., and Page, D. H. Transverse shrinkage of individual fibres by micro-radiography. In: F. Bolam's Consolidation of the paper web, Vol. 1. p. 119-44. London, Tech. Sect. of the British Paper and Board Makers' Assoc., Inc., 1966.

43. Page, D. H. and Tydeman, P. A. Physical processes occurring during the drying phase. In: F. Bolam's Consolidation of the paper web, Vol. 1. p. 371-96. London, Tech. Sect. of the British Paper and Board Makers' Assoc., Inc., 1966.

44. Tarnawski, Z., Przeglad Papier. 28(3):73-80(1972).

45. Van den Akker, J. A., Tappi 33(8):398-402(Aug., 1950).

46. Htun, M. and de Ruvo, A., Tappi 61(6):75-7(June, 1978).

47. Kijima, T. and Yamakawa, I., Japan Tappi 32(11):654-9(Nov., 1978).

48. Von Hippel, A. R. Dielectrics and Waves. New York, N.Y., John Wiley and Sons, Inc., 1954. 284 p.

49. Gander, J. W. and McKee, R. C. A study of the biaxial stress-strain behavior of sack paper. Part 1. Theoretical considerations and descriptions of a static biaxial stress-strain tester, Progress Report Ten, Project 2033. Appleton, Wis., The Institute of Paper Chemistry, 1959. 45 p.

50. Baum, G. A. and Bornhoeft, L. R., Tappi 62(5):87-90(May, 1979).

51. Hardacker, K. W. The IPC thickness gage, Report Two, Project No. 2959-8. Appleton, Wis., The Institute of Paper Chemistry, 1974. 7 p.

52. Wink, W. A., Hardacker, K. W., and Van Eperen, R. H., Tappi 47(1):13-15(1963).

53. Van den Akker, J. A., Wink, W. A., and Van Eperen, R. H., Tappi 50(9):466(1967).

54. Wink, W. A. and Van Eperen, R. H., Tappi 50(8):393-400(Aug., 1967).

55. Deschamps, G. A., J. Appl. Phys. 24(8):1046-50(Aug., 1953).

56. Felsen, L. B. Representation and measurement of reciprocal discontinuity structures in single-mode waveguide. In: M. Sucher and J. Fox's Handbook of microwave measurements, Third Ed. p. 227-310. New York, N.Y., Interscience, 1963.

57. Giordano, A. B. Measurement of standing wave ratio. In: M. Sucher and J. Fox's Handbook of microwave measurements, Third Ed. p. 73-133. New York, N.Y., Interscience, 1963.

APPENDIX I

DEFINITION OF THE ELASTIC CONSTANTS

When a force is applied to the surface of a given body, that body is seen to deform. The force per unit area of an infinitesimally small volume element of the body is defined as the stress. The stresses are usually expressed as a tensor of second rank, σ_{ij}, where the first subscript is the direction normal to the plane on which the stress acts and the second subscript indicates the direction of the force. The subscripts 1, 2, and 3 correspond to the coordinate directions x, y, and z, respectively. It can be shown that the stress tensor is symmetric, thus $\sigma_{ij} = \sigma_{ji}$.

The deformation of a body can be expressed in terms of a displacement vector field, $\vec{u}(x, y, z)$. The vector $\vec{u}$ is the difference between a particle's location after deformation of the solid and its original location with respect to a fixed coordinate system. The strain in a body at a point can also be expressed as a second rank tensor when defined in terms of the displacement vector field as follows:

$$e_{11} = \frac{\partial u_x}{\partial x}, \quad e_{12} = e_{21} = \frac{\partial u_x}{\partial y} + \frac{\partial u_y}{\partial x}$$

$$e_{22} = \frac{\partial u_y}{\partial y}, \quad e_{13} = e_{31} = \frac{\partial u_x}{\partial z} + \frac{\partial u_z}{\partial x} \tag{15}$$

$$e_{33} = \frac{\partial u_z}{\partial z}, \quad e_{23} = e_{32} = \frac{\partial u_y}{\partial z} + \frac{\partial u_z}{\partial y}$$

And, of course, the strain tensor is also symmetric, $e_{ij} = e_{ji}$.

A given strain, e_{ij}, is in general linearly related to the stresses for small strains. To express this relationship in matrix form it is convenient to redefine the stress tensor as follows:

$$\sigma_{11} = \sigma_1, \quad \sigma_{23} = \sigma_4$$
$$\sigma_{22} = \sigma_2, \quad \sigma_{13} = \sigma_5 \tag{16}$$
$$\sigma_{33} = \sigma_3, \quad \sigma_{12} = \sigma_6$$

The strains are also similarly redefined. The linear relationship between the stresses and the strains can then be expressed in matrix form. For an orthotropic medium with the elastic planes of symmetry coinciding with the planes formed by the coordinate axes, the matrix relationship is

$$\begin{bmatrix} e_1 \\ e_2 \\ e_3 \\ e_4 \\ e_5 \\ e_6 \end{bmatrix} = \begin{bmatrix} S_{11} & S_{12} & S_{13} & 0 & 0 & 0 \\ S_{21} & S_{22} & S_{23} & 0 & 0 & 0 \\ S_{31} & S_{32} & S_{33} & 0 & 0 & 0 \\ 0 & 0 & 0 & S_{44} & 0 & 0 \\ 0 & 0 & 0 & 0 & S_{55} & 0 \\ 0 & 0 & 0 & 0 & 0 & S_{66} \end{bmatrix} \begin{bmatrix} \sigma_1 \\ \sigma_2 \\ \sigma_3 \\ \sigma_4 \\ \sigma_5 \\ \sigma_6 \end{bmatrix} \tag{17}$$

where (S_{ij}) is termed the compliance matrix. It can be shown that this matrix is symmetric, thus $(S_{ij}) = (S_{ji})$. Thus, there are nine independent elastic constants required to describe the deformation of an orthotropic body in terms of the applied stresses. The components of the compliance matrix can be expressed in terms of the more familiar engineering constants as follows:

$$S_{11} = \frac{1}{E_1}, \quad S_{22} = \frac{1}{E_2}, \quad S_{33} = \frac{1}{E_3}$$
$$S_{44} = \frac{1}{G_{44}}, \quad S_{55} = \frac{1}{G_{55}}, \quad S_{66} = \frac{1}{G_{66}} \tag{18}$$

$$S_{12} = \frac{-\upsilon_{12}}{E_2}, \quad S_{21} = \frac{-\upsilon_{21}}{E_1}, \quad S_{13} = \frac{-\upsilon_{13}}{E_3}$$
$$S_{31} = \frac{-\upsilon_{31}}{E_1}, \quad S_{23} = \frac{-\upsilon_{23}}{E_3}, \quad S_{32} = \frac{-\upsilon_{32}}{E_2} \tag{19}$$

where E_i are the Young's moduli, G_{ii} are the shear moduli, and υ_{ij} are the Poisson ratios. In this case the Poisson ratio υ_{ij} is defined in terms of the strains resulting from an applied stress σ_j as $\upsilon_{ij} = -e_i/e_j$ (i = 1 to 3).

The stresses can be expressed as linear combinations of the strains by the following matrix equation:

$$(\sigma_i) = (C_{ij})\ (e_j) \tag{20}$$

where (C_{ij}) is the stiffness matrix. Of course the stiffness matrix is simply the inverse of the compliance matrix, $(C_{ij}) = (S_{ij})^{-1}$, and since (S_{ij}) is symmetrical, it follows that (C_{ij}) is also symmetrical. When dealing with wave propagation in elastic media, it turns out that the velocity of the wave is more easily related to the elements of the stiffness matrix (C_{ij}) than to the elements of the compliance matrix (S_{ij}).

APPENDIX II

DEFINITION OF THE DIELECTRIC CONSTANT

The following discussion is taken largely from Reference (48).

Consider a parallel plate capacitor connected to a sinusoidal voltage source. The voltage may be expressed as

$$V = V_o \exp(j\omega t) \tag{21}$$

where V_o = voltage amplitude

$j = \sqrt{-1}$

ω = angular frequency = $2 \pi f$

t = time

The amount of charge, Q, that will be stored on the capacitor plates separated by a vacuum is proportional to the applied voltage.

$$Q = C_o V \tag{22}$$

where C_o is the vacuum capacitance of the condenser. If, instead of a vacuum, there is a substance between the plates, the electric field will induce dipoles in that substance with the result that more charge can be stored on the plates at a given potential. The capacitance is thus increased to

$$C = \varepsilon' C_o \tag{23}$$

where ε' is the relative permittivity or dielectric constant of the material (unitless).

In the case of a circuit containing an ideal capacitor whose plates are separated by a vacuum, the charging current I_C is given by

$$I_C = \frac{dQ}{dt} = j\omega C_o V \tag{24}$$

Since $j = \exp(j\ \pi/2)$,

$$I_c = \omega\ C_o V_o\ \exp\ (j(\omega t + \pi/2)) \tag{25}$$

or

$$I_C = I_o\ \exp(j(\omega t + \pi/2)) \tag{26}$$

The current thus leads the voltage by a phase angle of 90°.

In general, for capacitors whose plates are separated by a dielectric material, there will be energy losses due to processes such as the migration of charge carriers between the plates or the friction accompanying the orientation of dipoles within the dielectric. It is customary to introduce a complex dielectric constant, ε^*, defined as

$$\varepsilon^* = \varepsilon' - j\ \varepsilon'' \tag{27}$$

The total current, $I = \frac{dQ}{dt}$, is then

$$I = j\omega\varepsilon' C_o V + \omega\varepsilon''\ C_o V \tag{28}$$

Upon comparison with Eq. (24), one may write

$$I = I_C + I_L \tag{29}$$

where I_C and I_L are the charging current and the loss current, respectively. The charging current leads the voltage by a phase angle of 90°, whereas the loss current is in phase with the voltage. The ratio of the loss current to the charging current is defined as the dissipation factor D, or the loss tangent, tan δ. Thus from Eq. (28) and (29)

$$D = \tan\ \delta = \frac{\varepsilon''}{\varepsilon'} \tag{30}$$

The interpretation of the dielectric constant given above is valid for situations in which the time required for electromagnetic disturbances to propagate through the system is small compared with the period of oscillation. At high frequencies, such as in the microwave range, Maxwell's equations must be applied, and the dielectric constant is defined in terms of the electric and displacement fields (48).

In the case of orthotropic dielectric materials, there will be three independent values of the complex dielectric constant. These three values correspond to situations in which the electric field is applied parallel to each of the three principal axes in the material, respectively.

APPENDIX III

DETAILED PROCEDURES FOR MAKING SHEETS

METHOD USED TO DYE BLACK FIBERS

The random handsheets were made without any black fibers; however, for fiber orientation measurements, all of the oriented sheets had black-dyed fibers dispersed throughout the sheet. The fibers were from the same pulp used to make the random sheets and were dyed using Chlorazol Black E, obtainable from Matheson Coleman and Bell. The fibers were dyed just prior to taking the trip to Washington to make the oriented sheets.

A quantity of the unbeaten dry lap pulp was soaked in deionized water overnight. The next day it was diluted to 6.7% consistency and mixed with a Williams Stirrer until the big chunks were dispersed. Deionized water was heated on a stove until it boiled. The pulp mixture was added to the boiling water, resulting in a pulp mixture at about 80°C and 2% consistency.

An amount of dye equal to 2% of the dry fiber weight was dispersed in hot water and mixed with the hot pulp suspension. The suspension was gently mixed for 10 minutes with a spoon. An amount of sodium chloride equal to 20% of the dry fiber weight was then added, and the mixture was allowed to cool overnight.

The next day the fibers were washed in 10-g batches using a 100 mesh stainless steel wire in an 8-inch-square sheet mold. The 10-g sheets were couched together to form a thick pad at about 20% consistency. The pad was placed in a polyethylene bag and kept cool until used.

HANDSHEET FORMING METHOD

Random Handsheets

A Douglas-fir bleached kraft pulp (Weyerhaeuser Regular Kraft) was obtained in dry lap form at the beginning of the thesis research. A fiber analysis had been performed. The pulp was essentially 100% softwood, at least 75% Douglas-fir. The other softwood fibers included spruce and/or hemlock, with a trace of southern and/or jack pine. There was a trace of hardwood, including birch and/or alder, and maple and/or basswood. The fibers exhibited little or no cutting or fibrillation.

The pulp was refined in a standard laboratory Valley beater for 25 minutes following TAPPI standard procedure T200 os-70. After beating, the pulp had a freeness of about 470 mL CSF. It was then dewatered using a laundry centrifuge-type dewatering device with the pulp contained in a nylon laundry bag. After spinning for 10 minutes, the pulp had a consistency of about 27%. It was then removed from the bag and stored in a cold room until needed to form the sheets. Deionized water was used throughout the pulp preparation process, and no additives of any kind were added to the whole pulp. Cold room storage time did not exceed two months.

Just prior to forming the sheet, the required amount of pulp was weighed and soaked in water for 30 minutes, then dispersed in a standard British disintegrator for 10 minutes. The sheets were formed on a 100 mesh stainless steel wire using an 8-inch-square sheet mold. To achieve the desired basis weight, 6 sheets of about 0.065 a.d. kg/m^2 were couched one on top of another to form the final sheet of about 0.400 a.d. kg/m^2. Successive layers were couched perpendicular to each other. After couching, red-dyed hemp fibers were carefully placed on the wire side of the sheet for measuring strain. The fibers were placed in the shape of a cross at predetermined locations in the sheet. The handsheet was then pressed at the desired pressure for five minutes after attaining the pressure in equal increments over a

period of one minute. Sheets were pressed in a square platen-type press with several dry blotters on either side.

After removal from the press, the sheet was taken to the lab for drying. All but one of the blotters (the one on the felt side of the sheet) were removed, and the sheet was supported by an aluminum plate. The sheet, blotter, and aluminum plate were covered with Saran Wrap, and the distances between the crossed dyed fibers on the wire side of the sheet were measured. The sheet was then clamped in the drying frame.

Oriented Sheets

The oriented sheets were made at Weyerhaeuser's Research Center in Tacoma, Washington. They were formed on a Formette Dynamique sheet machine. The device has been described in the literature (38,39).

The sheets were made using a fresh bale of Weyerhaeuser's Regular Kraft pulp. A fiber analysis performed on this pulp indicated that it consisted of 97% softwood and 74% Douglas-fir. The other softwood fibers were mostly hemlock, including some Engelman spruce and true fir, with a trace of red cedar. The hardwood fibers included red alder, with some bigleaf maple.

The pulp was first soaked in deionized water overnight. The next day it was defibered and then beaten in a standard Valley beater for 18 minutes following TAPPI standard procedures. After beating, the pulp had a freeness of about 500 mL CSF, with individual batches ranging from 480 to 525 mL CSF. The pulp was then diluted with deionized water to a consistency of about 0.17% for sheet formation. One batch of pulp was made each day and was used the same day to make two sheets on the Formette.

A quantity of dyed fibers corresponding to 1-2% of the beaten pulp on a dry fiber weight basis was weighed. The black fibers were washed in a British handsheet mold and then were dispersed for two minutes in deionized water using a standard British disintegrator. The fibers were then added to the beaten pulp, and the stock was mixed in the supply tank for 30 minutes prior to sheet formation.

A commercial Fourdrinier linerboard fabric was cut to fit the inside of the drum on the Formette. The fabric mesh was 40 in the cross-machine direction and 56 in the machine direction. The nozzle used to spray the stock on the wire was a VEE JET H $\frac{1}{4}$ U 2510 type obtainable from Spraying Systems Inc. The nozzle was positioned in a manner such that the stock jet traveled about 33 mm before impinging on the water wall of the rotating drum at an angle of about 25-30°. The nozzle had an elliptical opening, and the stock jet was flattened and about 10 mm wide when it contacted the water wall. The forming fabric, nozzle type, and nozzle configuration were kept constant for all of the oriented sheets.

With the forming consistency and the nozzle configuration constant, there are only two variables that can be adjusted on the Formette to achieve different levels of fiber orientation. These include the pressure of the stock in the flow to the nozzle, which varies the velocity of the stock leaving the nozzle, and the speed of the rotating drum and water wall. From approximate calculations of the jet-to-wire ratio, a set of three standard conditions for forming the oriented sheets was established as indicated in Table IX. The tachometer monitoring the drum speed was checked using a strobe light and found to be accurate.

Single-layer sheets were formed on the Formette having basis weights of about 0.400 a.d. kg/m^2. After formation, the wire and sheet were carefully removed from the drum and set, wire side down, on an aluminum plate. Dry blotters and another aluminum plate were placed on top of the sheet. The blotters-sheet-wire sandwich

supported by the aluminum plates on either side was turned over, and the wire was removed without any couching. The Formette sheet was of sufficient size to make three handsheets 7 1/2 inches square. The handsheets were cut to the required size using a razor blade. Red-dyed hemp fibers were placed on the wire side of the sheet for strain measurements. The sheets were then pressed between several dry blotters in a platen-type press at the required pressure for five minutes.

TABLE IX

STANDARD SETTINGS FOR FORMING ORIENTED SHEETS ON THE FORMETTE

Fiber Orientation	Drum (rpm)	Pressure (bar)	Forming Time (minutes)
Low	1050	1.6	19
Medium	1400	1.3	22
High	1800	0.6	34

The distance between crossed dyed fibers was then measured in a manner similar to that used for the random sheets.

HANDSHEET DRYING METHOD

The sheets were dried under restraint in a frame that had originally been designed and built to be a biaxial tester. The frame in its original state has been described in an unpublished report (49). The frame was modified somewhat for this study, and pictures of the modified device are presented in Fig. 26-28.

Referring to the figures, the frame consists of four six-inch clamps (A) which are fastened to the edges of a 7 1/2-inch-square paper sheet. Each clamp is connected to a movable post (B) through a narrowed steel tension arm (C). Strain gages (D) mounted on the tension arm can be calibrated to record the force imposed on the clamp. Clamp posts positioned opposite one another are connected by a fine thread

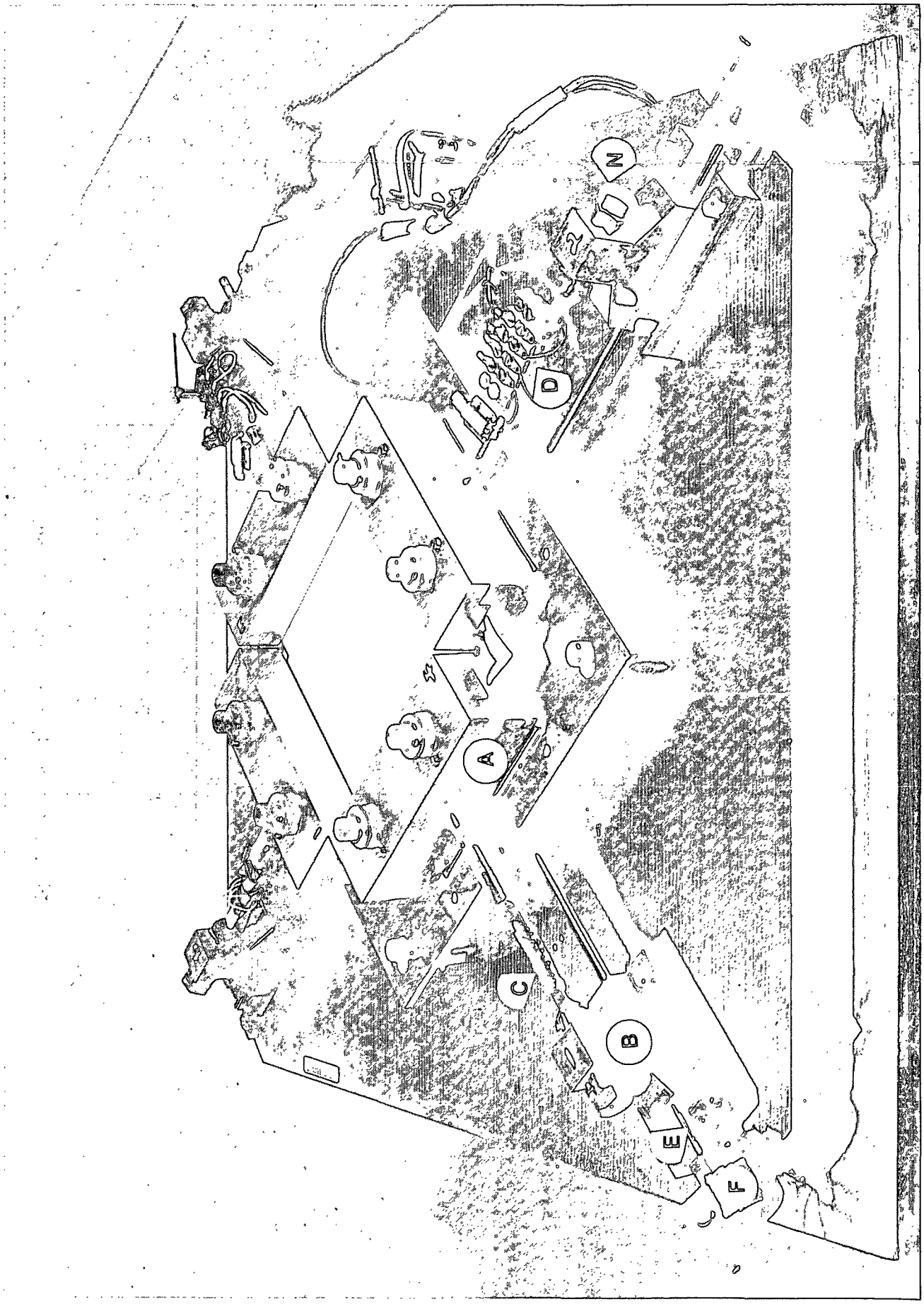

Figure 26. Drying frame.

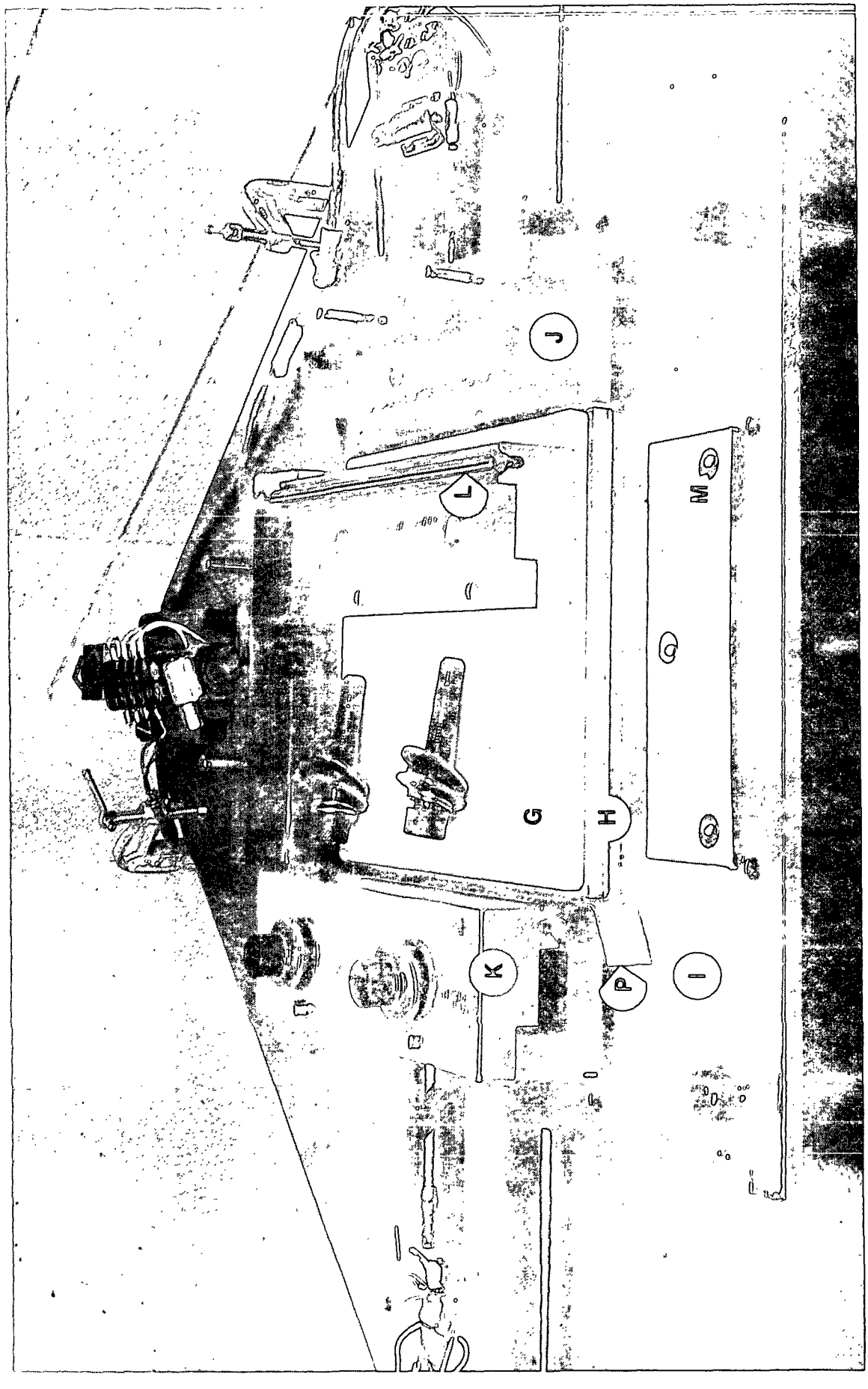

Figure 27. Drying frame showing clamp and support plate detail.

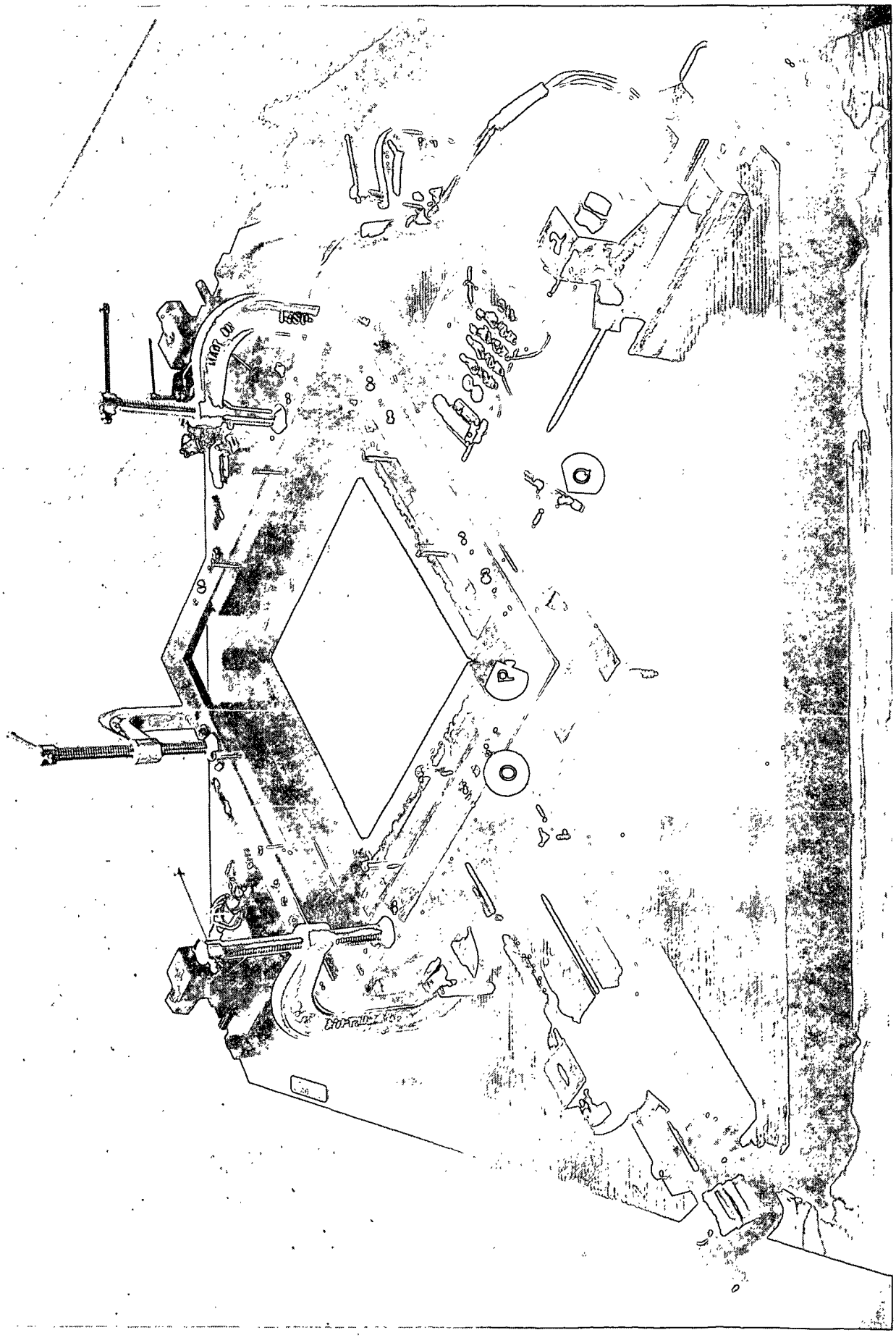

Figure 28. Drying frame with clamp restraining device attached.

screw (E). The opposing posts are moved outward from each other by turning a handwheel attached to the end of the screw (F).

The sheet rests on a 1/2-inch-thick Delrin (E. I. Dupont) plate (G) which in turn rests on two metal backup plates (H). The metal backup plates were carefully machined to be square, 6 inches by 6 inches, and are rigidly attached to the table plate (I) by screws.

The clamps consist of two parts. The lower part (J) is flat and is attached to the tension arm. The upper part (K) is aligned with the lower part by two rods and is bolted to it by two screws. The upper part of the clamp contacts the sheet by means of a 1/4-inch stainless steel rod (L), thus producing a line-type clamp. The area behind the rod is quite open, allowing air to circulate and dry the clamped edges as the sheet dries. Using these specially designed clamps, a sheet could be effectively clamped in the wet state without having to first dry the edges as some researchers have done (8-10,12,20).

The clamps rest on three steel balls (M) which ride on the table plate. The clamp tension arm is not rigidly attached to the clamp posts. Thus the clamps can move from side-to-side and forward and back with little resistance. A locked nut (N) at the end of the tension arm prevents movement beyond a certain point when tension is applied to the clamps.

Before clamping the sheet, the clamps had to be held stationary. This was accomplished using a special clamp-restraining device (O) and four 1/16-inch-thick shims (P). The shims were placed between each clamp and the backup plate. The restraining device was clamped to the table plate, and the clamps were forced against the shim and backup plate by tightening thumbscrews (Q). Care was taken to align the clamps square and flush against the shims and backup plate and to make

sure the clamps rested squarely on the supporting steel balls on the table plate. The handwheels were then turned to produce a small prestress in the clamp arms.

The sheet to be dried was taken from the Saran-wrapped aluminum plate support and gently laid on the Delrin support plate and lower part of the clamps. The upper part of the clamps was put on and bolted down evenly. The sheet was protected during the clamping procedure by a metal plate resting on top of the clamps. The clamp-restraining device was then released and carefully removed. After the shims were removed from between the backup plate and the clamps, the clamps were in a "free" state to record the force induced by the sheet in both principal directions as it dried.

If the sheet was to be wet strained, no shims were placed between the backup plate and the opposite clamps in the direction of straining. The clamp restraining device was then used as before to secure the clamps against the backup plate. The sheet was laid on the lower part of the clamps, and only two of the four clamps were tightened. The thumbscrews on the clamp-restraining device were then released for these two clamps. The sheet was stretched by manually turning the handwheel for these two clamps at a rate of one revolution per 30 seconds while watching a stopwatch. This corresponds to an approximate strain rate of 0.77% per minute. After checking to make sure that the clamps moved away from the backup plate evenly on both sides, the other two clamps were tightened. The clamp-restraining device was released and removed, and the two shims for the y-direction clamps were removed.

The sheets were dried in the drying frame by blowing warm air directly onto the sheet. The air was taken from a controlled environment at 23°C and 50% R.H. and heated by passing over a 1000-watt heating element. A 4 1/4-inch-diameter fan supported 6 1/2 inches above the sheet blew the warm air directly on the sheet. After impinging on the sheet, the air was allowed to escape into the controlled room.

Operation of the drying apparatus did not affect the controlled conditions of the room as indicated by a control monitoring chart.

At steady state, the air blown onto the sheet had a temperature of about 47°C and therefore a relative humidity of about 13%. The wet bulb temperature at these conditions is 23°C, and thus the approximate temperature of the sheet as it dried was 23°C, or about room temperature. As the water evaporates and the sheet approaches dryness, the temperature of the sheet would rise eventually to 47°C. Assuming all the heat supplied by the element is used to warm the incoming air, one can calculate that the fan blew a maximum of 80 ft^3 of warm air per minute onto the sheet.

The strain gages mounted on the tension arms of two clamps allowed the continuous monitoring of the force induced by the sheet in both principal directions as it dried. The strain gages used were type EA-06-270TN-350 obtained from Micro-Measurements, Raleigh, North Carolina. One strain gage consisted of two elements perpendicular to each other. One gage was glued on either side of the narrowed tension arm. The four elements in each tension arm were used as the four resistors in a Wheatstone Bridge circuit for measuring the strain in the tension arm. The voltage imbalance in the circuit was monitored using a two-channel Linear Instrument Recorder in the 0-1 mV operating range. The arms were calibrated by dead weight loading at various temperatures and bridge excitation levels. The response as indicated by the recorder was linear and quite independent of temperature over a range from 23 to 90°C. There was a small zero shift with temperature in this large temperature range, but during drying with warm air blowing on the apparatus no zero shift was observed.

The force induced by the sheet as it dried was recorded continuously. One random sheet was left in the drying apparatus about three hours, and the recorded

drying force as a function of time is reproduced in Fig. 29. As indicated in the figure, the force increased to a maximum and remained constant with time.

It was difficult to obtain accurate values for the moisture content as a function of drying time without an appropriate moisture monitoring system. However, by removing the sheet as quickly as possible from the drying frame and weighing it, moisture contents were estimated at two points along the drying curve. At the point that the sheet develops approximately 50% of the maximum force, the moisture content was about 13%. After drying for 90 minutes, when the drying force curve had just leveled off, the moisture content measured was 4.6% and rising rapidly. Since it took about three minutes to remove the sheet from the drying frame and weigh it, the actual moisture content must have been lower than this measured value. The equilibrium moisture content for the sheets at 50% R.H. is 6.8%. Thus, it was deemed unnecessary to dry the sheets for longer than 90 minutes. All the results presented were obtained from sheets dried 90-100 minutes.

After drying, the heating element was turned off and air at 50% R.H. was blown onto the sheet. This cooled the sheet and apparatus to room temperature and allowed the sheet moisture content to come closer to its equilibrium value before unclamping the sheet. The sheet was not brought to equilibrium before unclamping. For all the sheets presented here, the sheet was removed from the drying frame after 20-30 minutes of cooling. After this amount of time, the force induced by the sheet was about 1/2 of its maximum value. As indicated in the drying curve presented in Fig. 29, the stress would eventually have decayed to about 1/3 of the maximum value if left in the drying frame for a longer time. Some typical drying force curves are reproduced in Fig. 30 and 31.

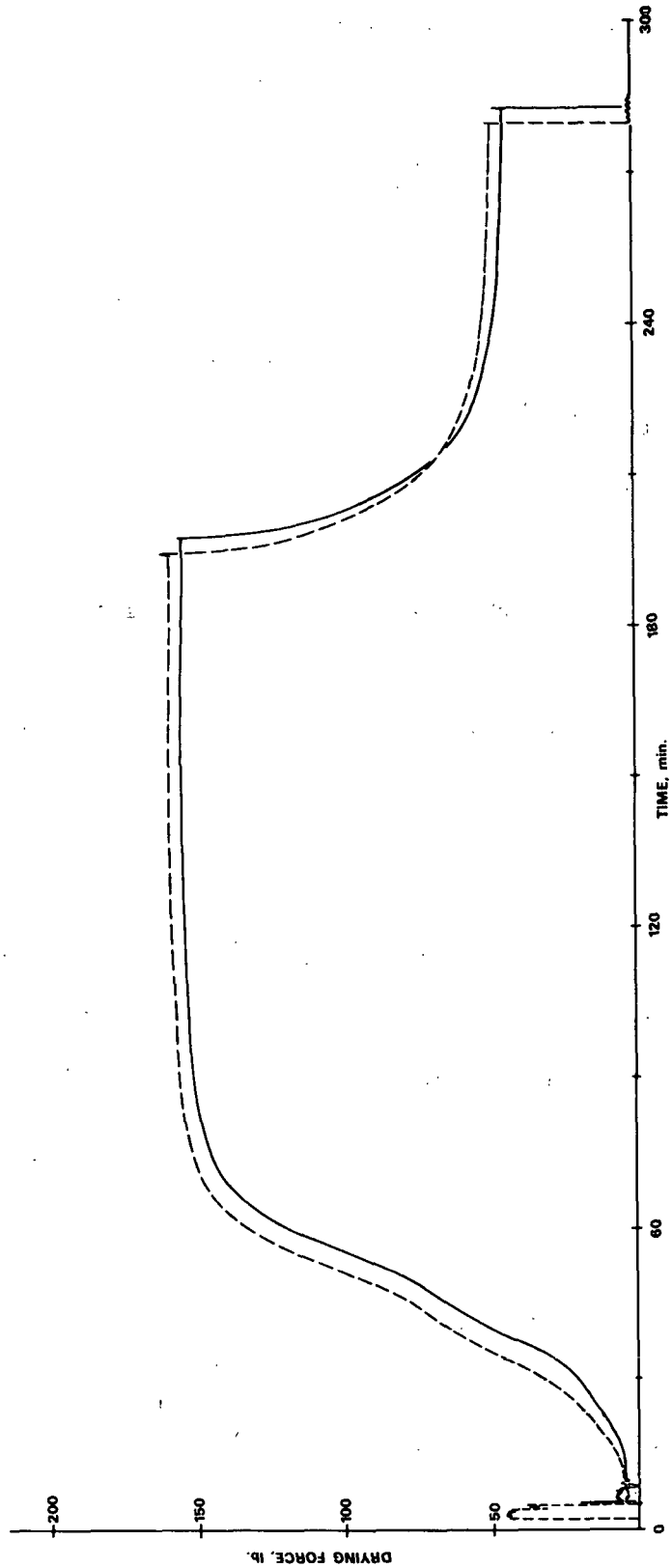

Figure 29. Recorded drying force for one sheet dried for a long period of time. The dotted line is the force recorded in the x-direction and the solid line is the force recorded in the y-direction.

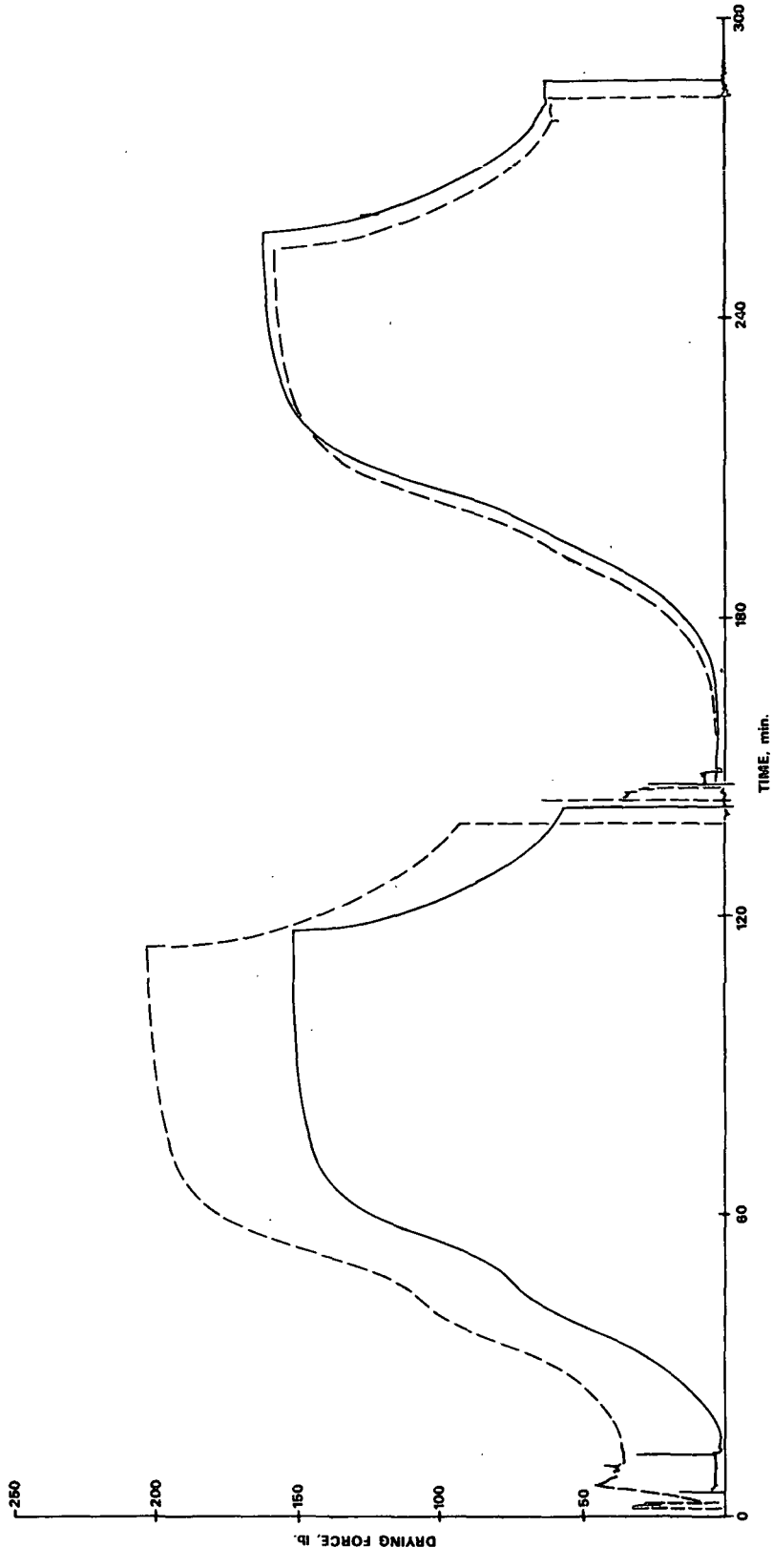

Figure 30. Recorded drying force for two random sheets. The first sheet was strained in the x-direction, whereas the second sheet was not wet strained. The dotted line is the force recorded in the x-direction, and the solid line is the force recorded in the y-direction.

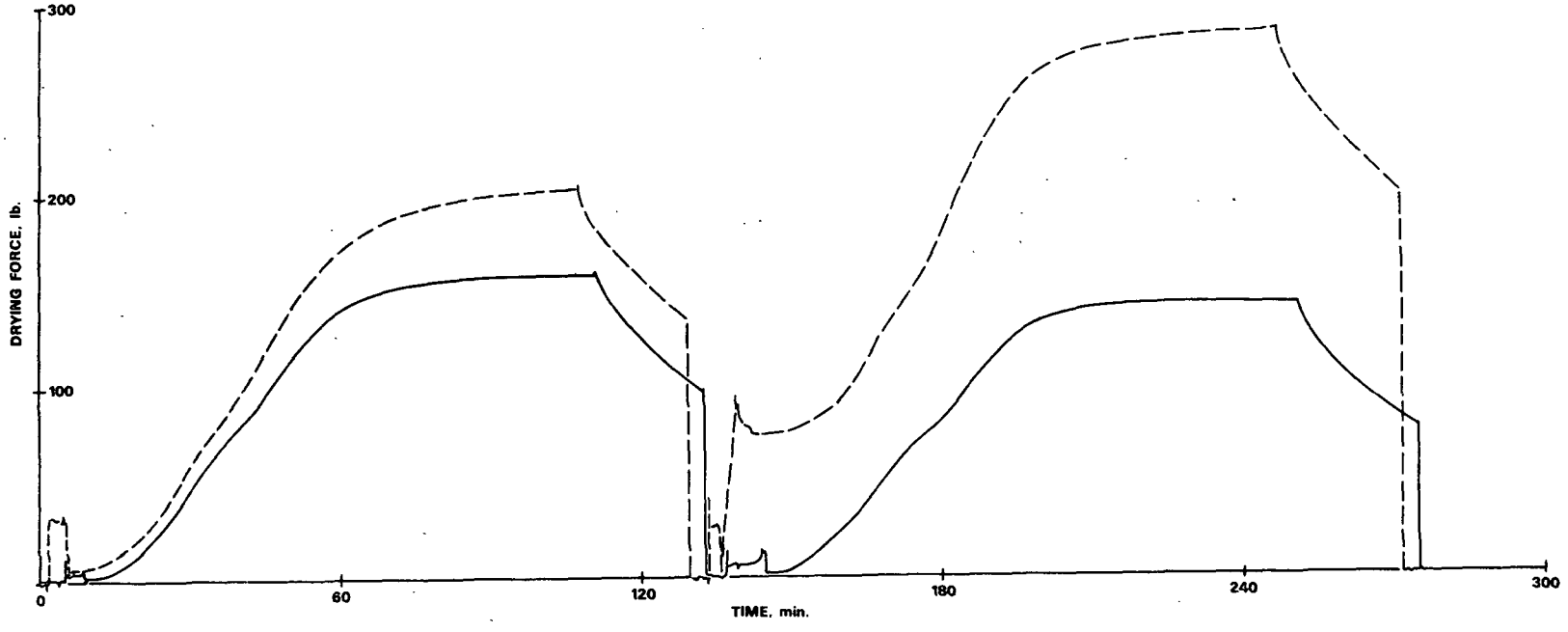

Figure 31. Recorded drying force for two oriented sheets. In this case, the first sheet was not wet strained, whereas the second sheet was wet strained in the x-direction. The dotted line is the force recorded in the x-direction, and the solid line is the force recorded in the y-direction.

After unclamping, the sheet was allowed to come to equilibrium in the controlled environment at 23°C and 50% R.H. All testing was then accomplished at these conditions without any preconditioning at lower relative humidities.

MEASURING THE STRAIN IN THE SHEET

The strain induced in the sheet was determined by measuring the distance between red-dyed hemp fibers placed on the surface of the sheet before the sheet was wet pressed. The fibers were placed on the sheet in the shape of a cross, and the distance was measured to the point where the fibers crossed. For most of the sheets made, the red-dyed fibers were placed at four points on the sheet as indicated by the solid crossed lines in Fig. 32. This arrangement allows the strain to be determined along two lines in each of the two principal directions. For the sheets made to investigate the variation of the strain across the width of the sheet, fibers were placed at four additional points indicated in the figure by the dotted lines, allowing the strain to be determined along three lines in each of the two principal directions.

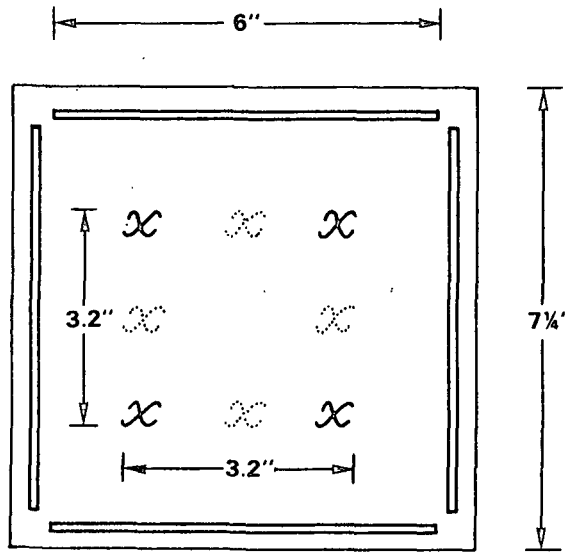

Figure 32. A schematic diagram of the location of the dyed fibers used for strain measurements in the sheets.

The distance between crossed dyed fibers was measured using a microscope with cross hairs in the eyepiece mounted on a precision screw. The screw range was 10 cm graduated in 0.001-cm increments. Individual measurements of distance were reproducible within about 0.005 cm, which corresponds to an accuracy in the strain measurement of about 0.06%. The device was mounted on a table for most measurements, but could be mounted on the drying frame to allow strain measurements to be made with the sheet clamped in the drying frame.

In all cases, the reported strains induced in the sheets were calculated from two distance measurements - one determined prior to clamping the sheet in the drying frame, and the other determined soon after unclamping the dried sheet. For a few sheets, measurements were made at each stage of the sheet drying procedure. The results of these measurements are presented in Table X for three random sheets. The drying procedure apparently allows the control of the strain in the sheets to within about 0.2% strain. The act of clamping does not disturb the sheet much, and the sheet dimensions do not change much during drying. The sheet tends to shrink a little with time after being unclamped, but the effect is small. From measurements made on a few oriented sheets, the amount of shrinkage was only about 0.1% strain after one month.

Variation Across the Width of Randomly Oriented Sheets

A set of 12 randomly oriented sheets was prepared to investigate the variation of mechanical properties across the width of the sheet. All 12 sheets were wet pressed at 50 psi, and 4 sheets were prepared at each of 3 levels of wet straining ranging from zero to +2.8% strain.

The amount of strain induced in each sheet was measured along three lines in both principal in-plane directions of the sheet. The total range of all of the measured strain values is indicated in Fig. 33. When the sheet is stretched in

TABLE X

MEASURED STRAIN IN SHEETS AT VARIOUS STAGES DURING PREPARATION

Sheet Number	Direction	Strain, %[a] After Clamping	After Wet Straining	After Drying	After Unclamping	After a Few Weeks	
158	xa	0.05	No	-0.05	-0.09	-0.17	
	xb	0.02	Wet	-0.07	-0.13	-0.22	
	xc	0.06	Strain	-0.01	-0.06	-0.13	(2 weeks)
	ya	0.05		0.17	0.13	0.07	
	yb	0.04		0.10	0.05	0.02	
	yc	0.06		0.08	0.05	0.00	
169	xa		3.02	2.91	2.79	2.81	
	xb		3.05	2.93	2.88	2.86	
	xc		2.95	2.88	2.80	2.76	(1 week)
	ya		-1.35	-1.23	-1.28	-1.32	
	yb		-2.11	-2.00	-2.07	-2.10	
	yc		-1.28	-1.29	-1.38	-1.40	
187	xa	0.02		0.07	0.00	-0.10	
	xc	0.05	No	0.04	-0.04	-0.07	
	ya	0.01	Wet	0.22	0.14	0.07	(2 weeks)
	yc	0.06	Strain	0.18	0.12	0.05	

[a]All strain values are with respect to the distance measured after wet pressing.

the x-direction, it tends to contract in the y-direction. Although, as indicated in the figure, the positive induced strain is very nearly constant across the width, the negative induced strain in the y-direction varies from zero at the clamped ends to a minimum in the center of the sheet. Furthermore, this negative strain is quite large. At the center of the sheet, the magnitude of the negative strain can be as much as 2/3 of the magnitude of the applied positive strain. The ratio of the negative strain to the positive strain is not constant, but rather appears to increase with increasing positive strain. The strain induced in the sheets is thus somewhat complicated. To have a more uniform strain in the cross direction, the sheet would have to be considerably longer in the direction of applied strain. Fortunately, the strain induced in either direction is quite reproducible.

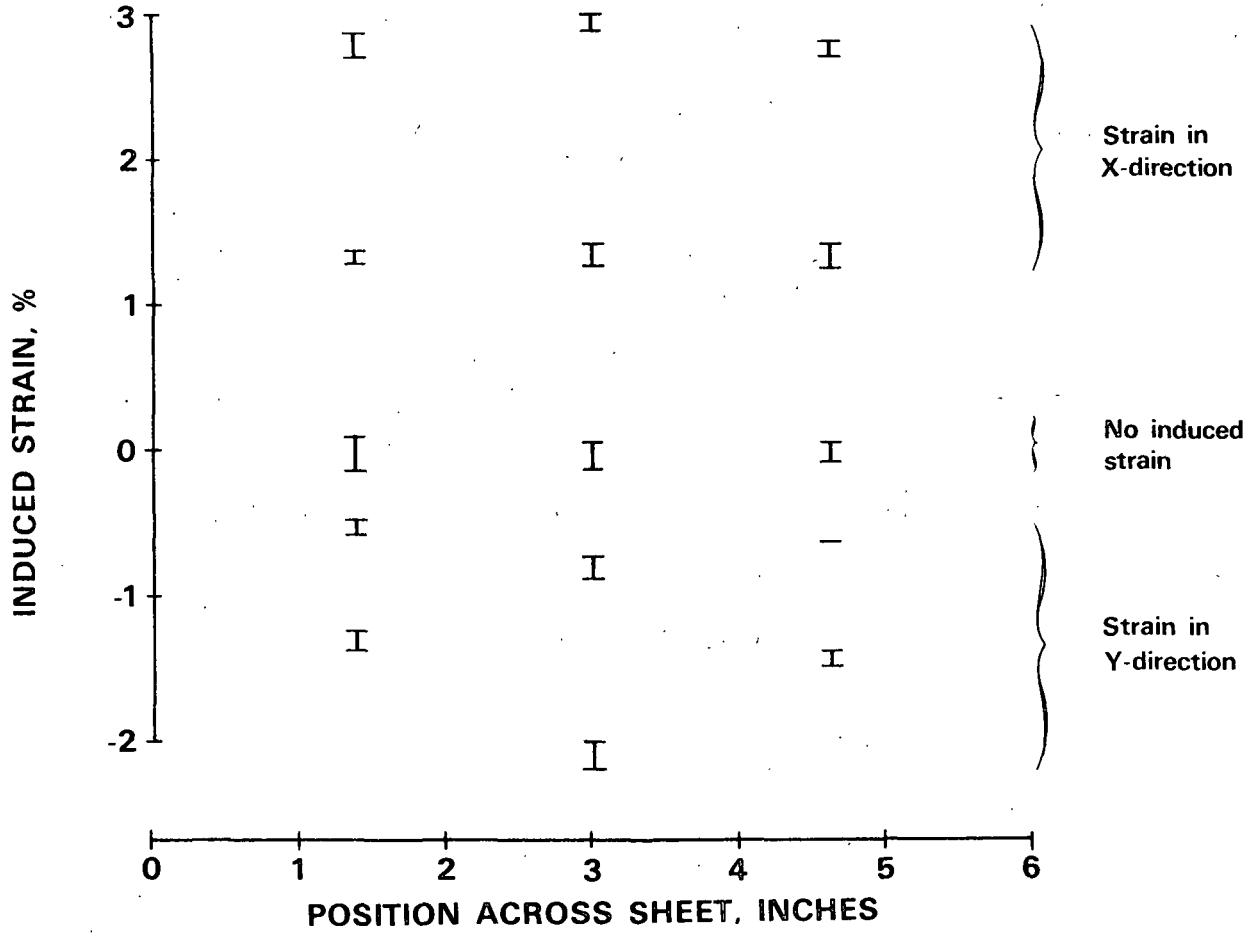

Figure 33. The total range of all strain measurements made on a set of handsheets to determine the variation of properties across the width of the sheet.

The sheets were cut into 12 strips of 1/2-inch widths and tested on the Instron universal testing machine. Two of the four sheets prepared at each strain level were tested in the direction of straining, the x-direction, and the other two sheets were tested in the y-direction. The measured tensile strength and apparent Young's modulus values are plotted as a function of location in the sheet in Fig. 34 and 35. The values are expressed as a percent of the average value measured on unstrained sheets. Both the values measured in the direction of straining and those measured in the cross direction are shown on the same plot.

Although both figures indicate a moderate amount of variability across the width of the sheet, the different levels of wet straining are very distinct (except for the tensile strength at 1.3 and 2.8% strain). The dielectric constant and in-plane wave velocity measurements were all made in the center 3-inch-square area of the sheet as indicated in the figures.

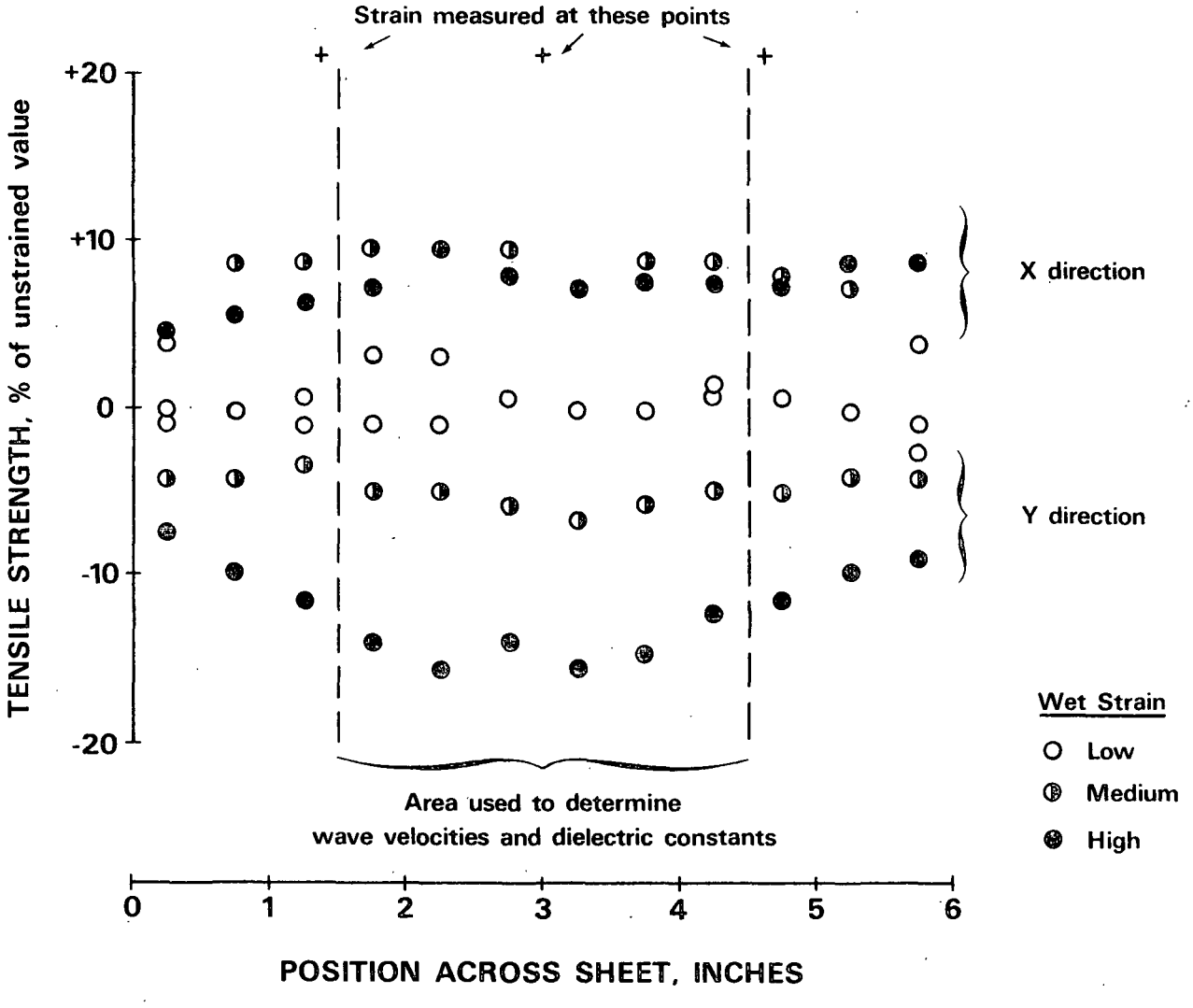

Figure 34. Variation in the measured tensile strength across the width of one set of sheets.

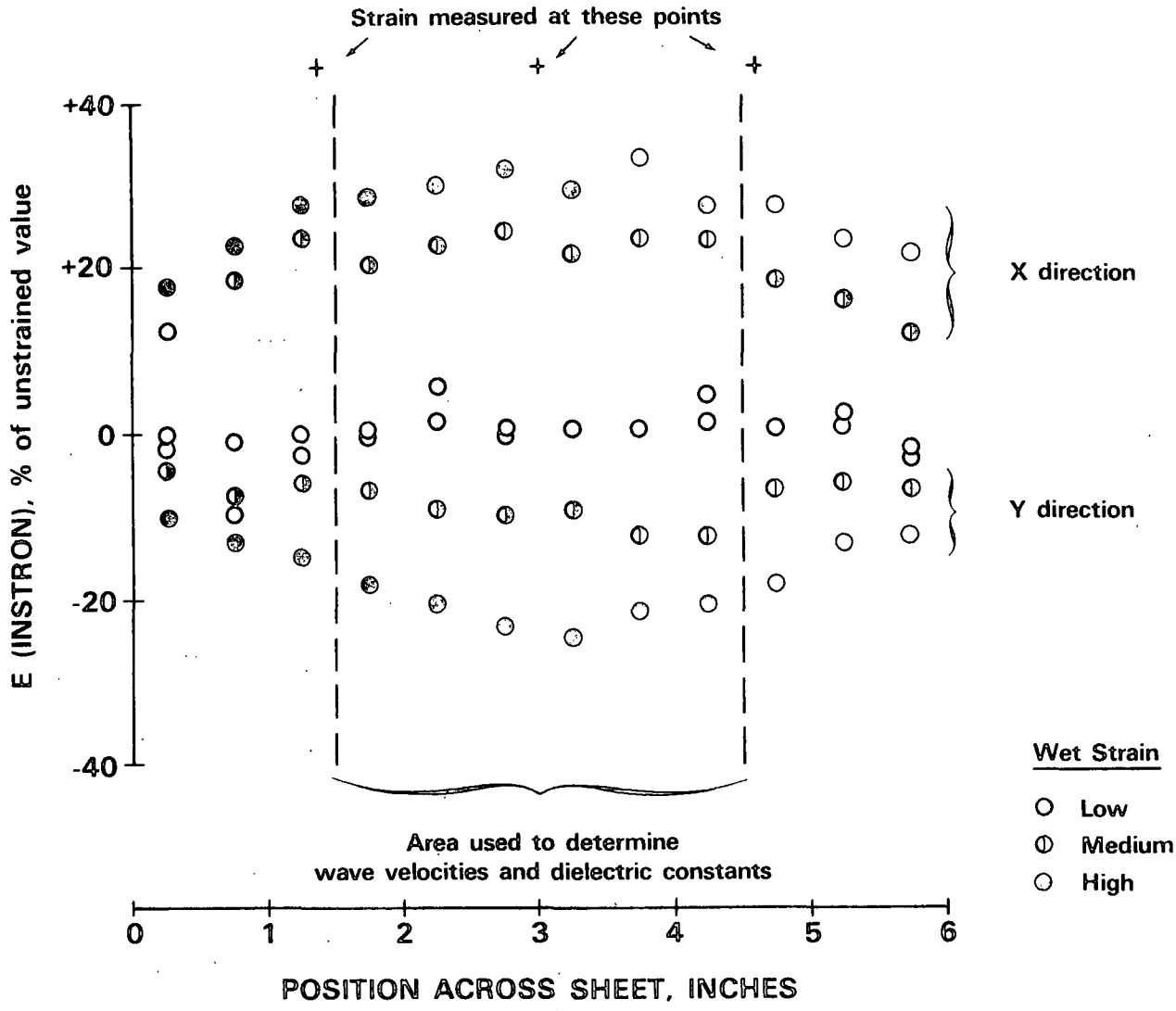

Figure 35. Variation in the measured apparent Young's modulus across the width of one set of sheets.

APPENDIX IV

DETAILED PROCEDURES FOR TESTING SHEETS: MECHANICAL TESTS

MORGAN VELOCITIES

In general, all mechanical wave velocities were determined by measuring the time required for a pulse of sine waves to propagate through the sheet in a given direction. The delay times were determined by measuring the time interval between the triggering of the wave pulse in a frequency generator and the detection of the pulse after it has traveled a measured distance through the sheet. The electrical equipment used to measure these delay times has been described previously (1). Usually the delay times were measured to the first peak in the received wave train. To determine the velocity, delay times were determined as a function of the distance the wave traveled through the sheet.

The velocity of mechanical waves excited in the sheet using point contact transducers sold by the H. M. Morgan Co. are referred to in this thesis as "Morgan velocities." These velocities were measured at a frequency of 60 kHz. By positioning the transducers appropriately, either longitudinal waves or shear waves may be propagated. The longitudinal wave velocity measured in either of the two principal in-plane directions using these transducers at this low frequency are believed to correspond to the velocity of the zeroth order symmetric mode plate wave velocity (1). There was little difference observed between the longitudinal wave velocity measured on the wire side and that measured on the felt side. All Morgan velocities were determined on the wire side of the sheet, with the sheet resting on a one-inch-thick piece of polyurethane foam.

The two Young's moduli (E_x and E_y), the shear modulus (G_{xy}), and the in-plane Poisson ratios (υ_{xy} and υ_{yx}) can be estimated from the Morgan velocities. Assuming

paper to be two-dimensional, four velocities are required to determine these constants (50) - the longitudinal Morgan velocity in the x- and y-directions (V_x and V_y), the shear velocity determined in either of the principal directions (V_{Sxy}), and the shear velocity determined at an angle of 45° from the principal axes (V_{S45}).

For each velocity measurement, the delay time was determined at each of three or four distances ranging from about 30 to 80 mm. At each transducer separation distance, the delay time was measured at 20 to 30 positions in the sheet. These positions were contained within the center 3-inch-square area of the sheet to try to reduce any effects due to the edge of the sheet. The average of the delay times determined at each transducer separation was used to calculate the velocity.

When the transducer separation distance is plotted as a function of delay time, the points should form a straight line, with the slope being the velocity of the propagated wave. For the most part, the data did fit a straight line quite well. The velocity was determined from a least squares fit of a straight line through the points. The correlation coefficient of the fitted line was always greater than 0.999 and often greater than 0.99995.

When the data were examined more closely, however, it was found that the scatter about the regression line was not random. There was a small but distinct curvature in the plot of distance vs. delay time for these sheets. For randomly oriented sheets, the longitudinal Morgan velocities in both the x- and y-directions, V_x and V_y, tended to decrease with increasing transducer separation. The velocity at short separations was about 6% higher than the velocity at the longer separations. Wet straining did not appear to affect the curvature. For oriented sheets, the longitudinal velocities tended to decrease with increasing transducer separation in the x-direction but increase with increasing separation in the y-direction. Again the

curvature was small. In the x-direction the average difference between the velocity at shorter separations and that at longer separations was only 2.5% and quite independent of fiber orientation and wet straining. In the y-direction, the average difference was 7%. The difference tended to increase with wet straining at low fiber orientations but tended to decrease with wet straining at high levels of orientation.

The shear Morgan velocities may be determined by the propagation of a shear wave in either the x- or the y-direction of the sheet. These two shear velocities should be equal. For the oriented sheets, however, the shear velocity measured in the x-direction was greater than the shear velocity measured in the y-direction. As in the case of the longitudinal waves, the plots of distance vs. delay time showed a distinct curvature. In the x-direction the velocity tended to decrease with increasing distance between the transducers, whereas in the y-direction the velocity tended to increase with distance. In the x-direction the curvature tended to get worse with more oriented sheets, and wet straining had a small effect to further increase the curvature. But in the y-direction, the curvature was quite constant independent of both fiber orientation and wet straining. When calculated from the least squares fit of the data points, the difference between the x- and y-direction shear velocities ranged from 1.4 to 5.8%. The difference was approximately independent of fiber orientation but increased slightly with wet straining. The in-plane shear velocity (V_{Sxy}) was taken to be the arithmetic average of the two shear velocities measured in the x- and y-directions for the oriented sheets.

The fourth Morgan velocity determined was the shear velocity at 45° from the two in-plane principal directions (V_{S45}). The plots of distance vs. delay time for this velocity did not show much, if any, significant curvature, with points lying above and below the linear regression line. The correlation coefficient was almost always greater than 0.99995 and often reached as high as 0.999995.

The Young's moduli (E_x and E_y), the shear modulus (G_{xy}), and the Poisson ratios (υ_{xy} and υ_{yx}) were determined from these velocities using equations derived for a two-dimensional material (50). For all of the oriented sheets studied, V_{Sxy} differed from V_{S45} by less than about 2%. (V_{Sxy} was not determined accurately for the random sheets.) Thus, a good estimate of the four elastic constants could be obtained from only three velocities: V_x, V_y, and V_{S45}. This implies that a relationship exists between these four constants. The relationship is quite complex, however, and will not be discussed here. The constants as calculated using three velocities were compared with the constants calculated using all four velocities for the oriented sheets. No significant difference between the two sets of values was observed. Since accurate measurements of V_{Sxy} were not made for all of the random sheets, the values of the in-plane elastic constants presented in the body of the thesis are those calculated from three Morgan velocities. In the tabulated data presented in Appendix VI, however, both sets of values are given.

CUTTING SHEETS

After measuring the Morgan velocities, the sheets were cut into pieces for further tests as indicated by the solid lines in Fig. 36. Also included in the figure are dotted lines which indicate the pieces cut at a later time to determine the dielectric constant of the sheet in each of the three principal directions.

THICKNESS AND APPARENT DENSITY

The thickness, basis weight, and apparent density of the sheets were determined from measurements made on four circular specimens cut from each sheet by using a die. From measurements of the diameter of several die-cut specimens, the area of each specimen was taken to be 2.914 cm^2.

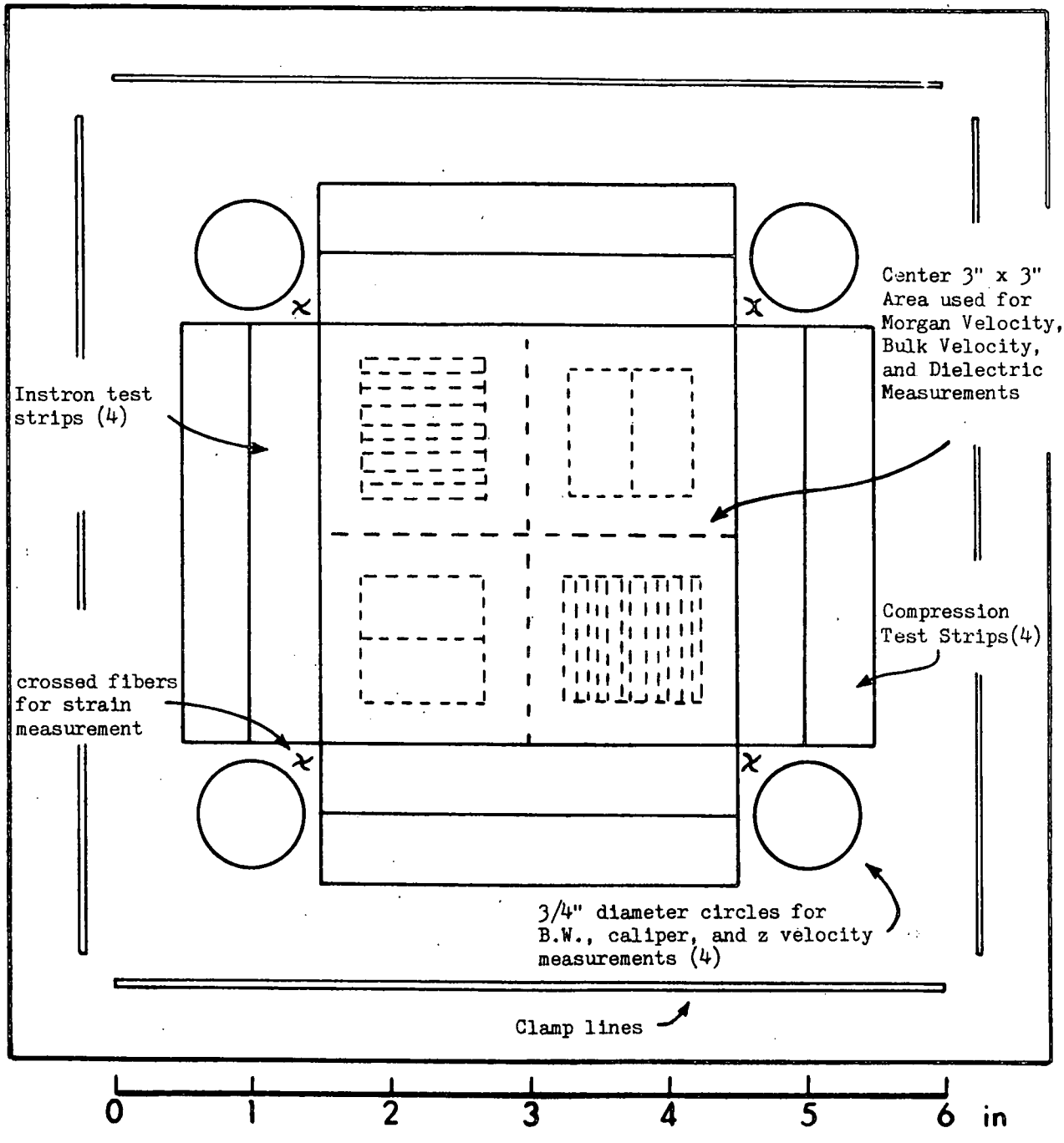

Figure 36. Schematic diagram indicating how the sheets were cut for testing.

Each die-cut specimen was weighed in a 23°C, 50% R.H. controlled environment. The basis weight for each sheet was calculated from the average of the four specimen weights. The thickness and apparent density of each specimen was determined by two different methods.

Using a standard Schopper thickness gage, the thickness was determined for each circular specimen. The Schopper thickness gage measures the thickness between flat metal platens with an area of about 1.70 cm^2 applying a pressure of about 50 kPa. From the thickness and weight of each specimen, an apparent density can be calculated using the area of each specimen given earlier. This apparent density is termed the "Schopper" apparent density. The average apparent density for the four circular specimens was taken as the average apparent density for the sheet. The standard deviation of the measured apparent densities of the four specimens was about 1% of the mean value.

The thickness of each circular specimen was also determined by a different method. The thickness was measured with the specimen placed between two soft rubber sheets. The sheets were each 1/32-inch thick and made of a soft neoprene rubber described as having a 5-10 durometer test result. The thickness of this rubber-paper-rubber sandwich was measured using an instrument manufactured at The Institute of Paper Chemistry. This instrument, referred to here as the "IPC thickness gage," has been described in an unpublished report (51). The upper movable platen of the instrument has an area of about 2.0 cm^2 and the lower stationary platen has an area of 6.4 cm^2.

The measurement was performed by placing a 3/4-inch-diameter circular piece of the sheet rubber on top of the paper specimen and a 1-inch-diameter piece below the specimen. The rubber-specimen-rubber sandwich was placed between the platens of the IPC thickness gage, and weight was applied to adjust the pressure. The thickness was determined at a pressure of 35 kPa after having first increased the pressure to 64 kPa. A flat metal plate was then placed between the two pieces of rubber and the thickness determined using the same procedure. The thickness of the paper specimen was calculated knowing the thickness of the metal plate, assuming the rubber contributed equally to the measured thickness in the two tests.

The metal plate thickness was determined using three independent methods. First, the thickness was determined using the Schopper thickness gage. Next, the thickness was determined using a micrometer from the machine shop. Finally, the thickness was measured using the IPC thickness gage after calibrating the instrument using feeler gages that had been tested by the National Bureau of Standards. The thickness was measured with and without using rubber between the plate and the platens of the IPC thickness gage. The three methods gave essentially the same value for the thickness of the plate within about 2 μm.

From the measurement of the thickness and the weight of each specimen, an apparent density can be calculated as before. This value is called the "IPC apparent density." As in the case with the Schopper apparent density, the average of the measured apparent densities of the four circular specimens was taken as the average apparent density for the sheet.

The thickness of the paper specimens determined by the IPC thickness gage using rubber between the platens and the sample always results in a lower value than that determined using the Schopper gage. This observation is the result of the fact that the rubber tends to conform to the uneven surface of the sheet, whereas the hard metal platens record only the thickness of the higher areas on the surface. This results in the measured IPC apparent density always being greater than the measured Schopper apparent density.

Since all of the sheets studied in this thesis work had similar surface characteristics and were of similar thicknesses, the two values of the apparent density are linearly related as indicated in Fig. 37. The Schopper apparent density is about 10% lower than the IPC apparent density for all of the sheets studied here. Because of this strong linear relationship, and because the two values are not too

dissimilar, it does not matter which value is used in calculating the constants and in the discussion of the results.

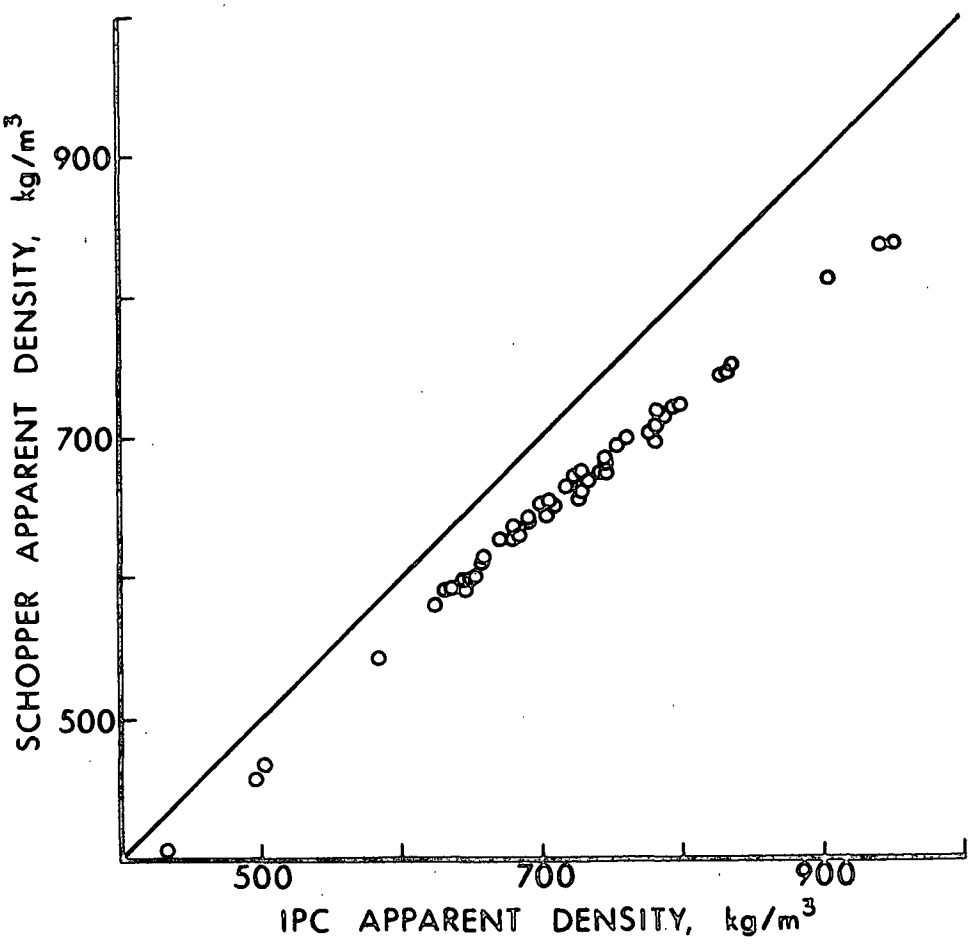

Figure 37. The relationship between the measured Schopper and IPC apparent densities.

For all the mechanical tests, the elastic and strength values are calculated using the Schopper value for thickness and are plotted as a function of Schopper apparent density. This was done to be consistent with literature data in which the TAPPI standard method for determining paper caliper is used. When calculating the dielectric constant of the sheets in the z-direction, it was found that use of the Schopper apparent density would occasionally result in a negative correction for the

wave guide gap. This means that apparently more paper was stacked in the wave guide than should fit, assuming the paper had the measured Schopper thickness. This is very unlikely. Because of this and the belief that the IPC apparent density is a more accurate value for the actual apparent density of the sheet, all of the dielectric data were calculated on the basis of the IPC thickness and plotted as a function of IPC apparent density.

BULK VELOCITIES

Z-Direction Velocities

The longitudinal z-direction velocity (V_{Lz}) was determined using 1 MHz transducers. The transducers were mounted in an apparatus that kept the two transducer faces parallel and directly opposite one another. The pressure applied to the transducers could be adjusted. The same soft neoprene rubber used between the platens of the IPC thickness gage was used to couple the longitudinal transducers to the specimen tested. Two 3/4-inch-diameter circular rubber pieces were put on either side of the specimen and the sandwich placed between the transducers. No grease, tape, or glue was used between the transducers and the rubber or the rubber and the specimen.

The z-direction delay time was measured on each of the four circular specimens cut from each sheet. The same pressure sequence used to measure the thickness with the IPC thickness tester was used in the test for the z-direction delay time. The delay time was determined at 1 MHz measuring to the first peak in the received signal. The delay time was measured with the paper specimen between the rubber and with a piece of cellophane between the rubber. The delay time through the cellophane had been determined earlier to be 0.140 μsec. Using this value, the delay time through the paper specimen could be determined. This method was considered superior to the method by which the delay time is determined with nothing

between the two rubber pieces. It was observed that the two pieces of rubber compress differently at a given pressure when there is something between them than when there is nothing between them.

The velocity (V_{Lz}) was calculated for each specimen from the IPC thickness value and the z-direction delay time. The stiffness coefficient C_{33} was then calculated using the relation $C_{33} = \rho V^2_{Lz}$ where ρ is the Schopper apparent density. The values for each of the four circular specimens were averaged, and the mean value was taken as the average for the sheet. The standard deviation was about 5% of the mean value of the four specimens.

The shear velocities (V_{Sxz} and V_{Syz}) are the velocities of a shear wave propagated in the z-direction polarized in the x- and y-direction, respectively. These velocities were measured at 1 MHz on one of the four circular specimens cut from each sheet using 1MHz shear transducers. The same apparatus was used to keep the transducer faces parallel and directly opposite one another.

The transducers were coupled to the specimen by using a shear couplant material obtained from Panametrics Inc. A small amount of couplant was applied to the center of the face of one transducer, the transducers were brought together, and a pressure of 50 kPa was applied. After the couplant had spread uniformly on the faces of the two transducers, the transducers were separated and the specimen inserted. The delay time was determined with the specimen between the transducers at a pressure of 50 kPa and then with nothing except the couplant between the transducers at the same pressure. The measurement was repeated four times in each of the two directions. The velocity was calculated from the Schopper thickness for the specimen and the difference between the delay times measured with and without the specimen between the transducers. The stiffness coefficients C_{44} and C_{55} were calculated from the equations $C_{44} = \rho V^2_{Syz}$ and $C_{55} = \rho V^2_{Sxz}$.

In-Plane Longitudinal Velocities on Single Thickness Specimens

It is not possible to propagate a bulk wave in the x- or y-directions of a single thickness piece of paper. The interaction of the wave with the surface will result in the propagation of a plate wave. Mann has suggested, however, a method by which the bulk velocity may be determined on single thickness specimens (1). The procedure is the result of the fact that at a certain frequency (f_c) plate waves in paper will progagate at the same velocity as the corresponding longitudinal bulk waves. For measurements in the x-direction, this frequency is given by the relation

$$f_c = \frac{V_{Lz}}{T_p}\left[\frac{1}{1 + \frac{C_{13}\,(C_{13} + 2C_{55})}{C_{11}\,C_{55}}}\right]^{1/2} \qquad (31)$$

where T_p is the thickness of the specimen, V_{Lz} is the bulk longitudinal velocity in the z-direction, and the C_{ij}'s are stiffness coefficients. An analogous equation can be derived giving the frequency required for measurements in the y-direction of paper. For the milk carton stock studied by Mann, the square root term was very nearly equal to unity. It is reasonable to expect that this was true also for the paper sheets studied here. It was originally hoped that by measuring V_{Lz}/T_p one could calculate the frequency (f_c) for measuring the velocity corresponding to the longitudinal bulk velocity in each of the principal in-plane directions using single thickness specimens.

Due to the various process parameters, sheets were made that resulted in values of V_{Lz}/T_p ranging from 280 kHz to 1.2 MHz. However, for all of the sheets tested, the received signal was very weak and the propagated wave apparently very dispersed except in a frequency range from about 250 kHz to 410 kHz. The response as a function of frequency was quite similar for all the sheets, regardless of the theoretically calculated frequency (f_c). The velocity of several sheets, including those corresponding to the extreme theoretical frequencies calculated, was measured

as a function of frequency in the range from 250 to 410 kHz. For all of these sheets, the measured velocity was virtually constant, changing less than 0.5% in the range of frequencies studied. As a result of these curious observations, the velocities were all determined at a single frequency of 330 kHz regardless of the theoretical frequency (f_c) calculated for each sheet.

The velocities were measured using 1 MHz longitudinal transducers, the same transducers used to determine V_{Lz}. A similar apparatus was constructed as for the z-direction measurement, to keep the transducer faces parallel and directly opposite one another. A controlled amount of pressure could be applied to the transducers. The transducers were coupled to the edge of the specimen using the same 1/32-inch-thick circular rubber sheets used in the z-direction measurement. In this case, however, the rubber was attached to the face of each transducer using two-sided tape. Measurements were made on the center 3-inch-square area cut from the sheet as indicated earlier in Fig. 36. Delay times were measured at seven positions across the width in each of the two directions x and y. The measurements were repeated and the delay times averaged for a given position. The 3-inch-square area was then cut in half each way, and delay time through each small square was determined in each direction. From three delay times, one measured with 3 inches of the sheet between the transducers and one measured through each of the halves in a given direction, a value for the delay time with no specimen between the transducers (t_d) can be calculated. Four values for t_d were obtained for each sheet. These values were averaged and used to determine the velocity at each of the seven positions across the width in each direction. These seven velocities were then averaged to obtain V_{Lx} and V_{Ly}. From V_{Lx} and V_{Ly}, C_{11} and C_{22} were calculated using the relations $C_{11} = \rho V_{Lx}^2$ and $C_{22} = \rho V_{Ly}^2$ where ρ is the Schopper apparent density.

Theoretically, the difference between the bulk velocities and the Morgan velocities should provide a measure of the stiffness C_{13} and C_{23} (1). Also, the bulk wave

velocity should always be greater than the Morgan velocity. In the x-direction for all of the oriented sheets, the bulk velocity was usually greater than the Morgan velocity, but not by more than 2%. In the y-direction the bulk velocity was lower than the Morgan velocity by about 1-2% for almost all of the low fiber orientation sheets. For the medium and high fiber orientation sheets, the y-direction bulk velocity was greater than the Morgan velocity and showed a strong dependence on the wet straining level. On average, V_{Ly} was about 6% greater than the Morgan velocity V_y for the highly oriented sheets.

On the basis of these observations, it is evident that accurate estimates of C_{13} and C_{23} cannot be obtained from these data. On the other hand, the close similarity between the longitudinal velocities determined by the two different methods indicates that a fairly good estimate of C_{11} and C_{22} has been obtained for these sheets. Since all of the conclusions in the thesis are the result of comparisons between samples tested in the same manner, either Morgan velocities or the "bulk" velocities as determined on single-thickness specimens could be used to determine the in-plane constants. However, since not as many readings were taken to determine V_{Lx} and V_{Ly} for the randomly oriented sheets, and because all comparisons should be made between sheets tested in a similar manner, the in-plane constants E_x, E_y, υ_{xy}, and υ_{yx} were calculated using Morgan velocities. Values of the bulk velocities V_{Lx} and V_{Ly} as well as the stiffness coefficients C_{11} and C_{22} calculated from these velocities are listed in the tables in Appendix VI.

TENSILE TESTS

In-Plane Tensile Tests

Tensile tests were performed on the random and oriented sheets using the Instron Universal Testing Machine. The tests were performed on each of four 1/2 x 3-inch specimens cut from the sheets as indicated in Fig. 36. The test strips were

individually weighed, and an average thickness for each strip was calculated using the Schopper apparent density measured for each sheet. The strips were tested using a test span of about 2 1/2 inches and a cross head speed of 0.2 inch per minute. This corresponds to a strain rate of 8% per minute.

Three values were determined from each tensile test. The force at rupture was measured, and the tensile strength was calculated in units of force per area using the calculated thickness of each specimen. The apparent Young's modulus was estimated from the initial slope of the load-elongation curve. Correction was made for the strain in the apparatus, and the result was expressed in units of force per area as was the tensile strength. The strain at failure was determined from the load elongation curve and was also corrected for the strain in the apparatus.

For the random sheets, the regular IPC line-type jaws were used (52). However, most of the oriented sheets were too thick to use these clamps. All of the oriented sheets were tested using the jaws manufactured for the IPC in-plane tear test (53). A variable amount of pressure can be exerted by the latter line-type jaws. By trial and error it was found that by applying a torque of 30 inch-pounds to the tightening screw of the jaws satisfactory results could be obtained. The rupture did not occur at the clamp lines, nor was there any evidence of slippage in the clamping area when that area was examined under the microscope.

The amount of apparent apparatus strain was different for the two sets of jaws used. The apparent strain was determined by clamping short pieces of steel in the jaws and measuring the load elongation response in a manner similar to the method used to test the paper specimens. For the regular line-type jaws, the strain error was linear and equal to about 0.0037 inches per 100 pounds force. For the in-plane tear tester jaws, the error was nonlinear. The apparent error was greater at low loads and decreased at higher loads. In the region where the slope of the load

elongation curve was determined for calculating the apparent Young's modulus, the apparent strain error was about 0.010 inch per 100 pounds force. In determining the correction to the measured apparent strain at failure for the in-plane tear tester jaws, the nonlinear nature of the strain error was approximated by a linear relationship. The error was taken to be equal to $0.002 + (0.00006)F_r$ where F_r is the tensile strength in pounds force.

Z-Direction Tensile Tests

The z-direction tensile strength was determined on one of the four circular specimens cut from each sheet. The method used to determine the z-direction tensile strength has been described in the literature (54). The metal cylinders bonded to the surfaces of the specimens had an area of 2.77 cm^2. The specimens were tested using the Instron with the cross head speed set at 0.1 inch/minute.

COMPRESSIVE STRENGTH TESTS

The compressive strength was determined for the oriented sheets only. The test was performed on each of four 1/2 x 3-inch specimens cut from the sheets as indicated in Fig. 36. As for the tensile tests, the test strips were each individually weighed, and an average thickness of each strip was calculated using the Schopper apparent density measured for each sheet. The strips were tested using the STFI compression tester (41). Prior to use, the tester was calibrated using weights suspended from the clamp attached to the load cell.

APPENDIX V

DETAILED PROCEDURES FOR TESTING SHEETS: DIELECTRIC TESTS

The complex dielectric constant was determined for each sheet in each of the three principal directions. The apparatus used was designed and assembled originally by Habeger for a previous study (4). The data collected to determine the dielectric constants of the sheets in this study were analyzed in a manner similar to that used by Habeger. Because the method and apparatus have been described in detail elsewhere, only a brief outline will be given here.

The apparatus consists of a slotted wave guide connected to a movable short of the same internal dimensions as the slotted section. An electromagnetic wave is propagated in the wave guide and is reflected by the short. This reflection results in an almost perfect standing wave being established in the wave guide. The relative power level along the standing wave as well as the physical location of the standing wave minimums with respect to the short position can be measured using a probe inserted in the slot in the wave guide.

The sample is inserted in the wave guide between the slotted section and the movable short. When the sample is inserted, the standing wave minimums are shifted from their original locations. In addition, the incident wave is partially absorbed by the sample, resulting in the reflected wave having a lower amplitude than the incident wave.

With a sample inserted in the wave guide, two measurements were made using the probe at a given short position. The Voltage Standing Wave Ratio (VSWR) is the ratio of the voltage at a maximum in the standing wave to that at a minimum. For the samples tested in this study, an accurate method to determine the VSWR was to measure the distance between two points at a certain power level about the minimum power level. In particular the distance (D_x) between points at a power level of

twice the minimum (3 decibels) was measured using the probe. The VSWR was then calculated using the following relationship

$$VSWR = \left[1 + \frac{1}{\sin^2 \frac{\pi D_x}{\lambda_{ss}}} \right]^{1/2} \qquad (32)$$

where λ_{ss} is the wave length in the slotted section. The position of the minimum relative to the short position, D_p, was also measured. These two measurements, D_x and D_p, were repeated for eight short positions.

The data thus collected were analyzed by a graphical technique outlined by Deschamps (55) and described in detail by Felson (56). A computer program written by Habeger simulates this graphical method. The program, listed in Ref. (4), was used as written except for a minor modification added later by Habeger. A subroutine was added that searched for the best fit of a circle to the transformed data points. The sum of the squares of the distances of the data points from the circle was minimized by this subprogram. From the data collected using the probe in the wave guide together with a measured value of the thickness of the specimen inserted in the wave guide, the computer program calculated the complex dielectric constant for the specimen inserted in the wave guide.

MEASURING CONDITIONS

All dielectric measurements were made on paper specimens in a controlled environment of 23°C and 50% R.H. The same equipment described in Ref. (4) was used to take the data. The measurements were made at a frequency of 9.6 GHz using a power level of OdBm (1 milliwatt) as indicated by the dials on the signal generator. The signal generator output was square wave modulated at about 1 kHz.

The wave guide has internal dimensions of 0.4 by 0.9 inch with the electric field oriented in the direction of the shorter dimension. The slotted section of

the wave guide was cleaned periodically with gauze and ethanol; care was taken not to scratch the surfaces.

The detector probe was inserted about 3.8 mm through the slot into the wave guide. The probe, connected to the Standing Wave Ratio (SWR) meter, was tuned by adjusting the plunger until a maximum response was indicated on the meter. The SWR meter is a tuned radio frequency amplifier that measures the power detected by the probe. The bandwidth on the SWR meter was adjusted to its maximum (about 130 Hz), and the frequency was adjusted for maximum response.

CALIBRATION

Detector Calibration

When there is no sample in the wave guide, the electromagnetic wave is reflected by the short producing an almost perfect standing wave. The detected wave as a function of position in the wave guide is not perfect, however, due to losses in the wave guide, nonlinear effects in the probe detector, and limitations in the amplifying circuits of the SWR meter. The ideal meter response for a perfect wave can be calculated. Ideally, the detector response is proportional to the square of the wave amplitude, which is sinusoidal; thus, the ideal detector response is proportional to $\sin^2 (2\pi d/\lambda_{ss})$ where d is the distance from a minimum, and λ_{ss} is the wave length in the slotted section. The SWR meter is graduated in negative decibels. The ideal meter reading in decibels is thus equal to $-10 \log_{10} (P_r)$ plus a constant, where P_r is the detected power. So, for a perfect standing wave, the ideal meter reading (M') is related to the distance about the minimum measured between two equal meter readings (Δd) by

$$M' = -10 \log_{10} (\sin^2 (\pi \Delta d/\lambda_{ss})) + K \qquad (33)$$

where k is a constant (note that $\Delta d = 2d$ since the wave is symmetrical about the minimum).

Before a calibration was performed, the gain on the SWR meter was adjusted so that the detected power at a minimum was on scale (usually about 65 dB). The SWR meter reading at the minimum was recorded. The probe was then moved to a maximum and the meter reading again recorded. These two readings thus provided a check to determine the validity of a given calibration curve. If settings or conditions changed resulting in different meter readings at the maximum and minimum locations in the standing wave, a new calibration was performed.

The calibration procedure consisted of measuring the distance Δd between equal power level points for several indicated power levels (M). If the power detection system was perfect, then the actual power reading (M) would differ from the ideal meter reading (M') by the constant K for each measured Δd. In the real case, M - M' was constant only in an intermediate power range. At low power levels the SWR meter becomes limited in that the signal is approaching the noise level of the meter. At high power levels the detector response is no longer proportional to the square of the wave amplitude.

After choosing a value for K, Eq. (33) was used to calculate an ideal meter reading (M') for each measured meter reading (M). These values were plotted and a smooth curve drawn between the points. A typical detector calibration curve is indicated in Fig. 38.

The calibration curve was used during data collection when measuring D_x, the distance between two points each 3dB greater than the power at the minimum of the standing wave. First, the actual meter reading (M) was measured at the minimum. From the calibration curve, the ideal meter reading at the minimum (M') was determined. The actual meter reading corresponding to M' - 3dB was then read from

the calibration curve. Using this value, the distance D_x was measured. Usually only two of the eight sets of data points collected for each sample required the use of this calibration curve.

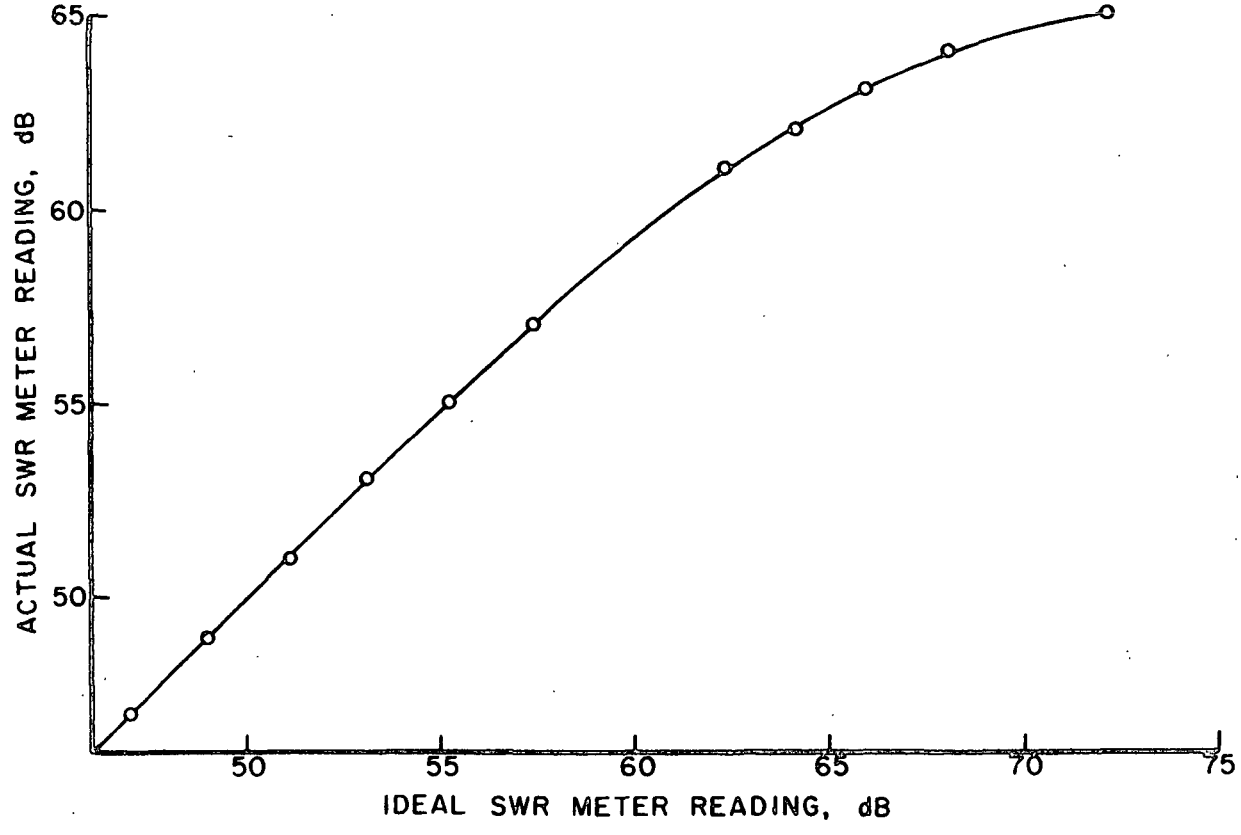

Figure 38. A typical detector calibration curve.

By correcting D_x, this calibration procedure affects the calculated value of the imaginary component of the complex dielectric constant (ε''), leaving the real component (ε') essentially unchanged. If this calibration procedure was not used, the value of ε'' would depend on how much sample was inserted in the wave guide.

Slotted Section Calibration

Whereas the detector calibration procedure corrected values of D_x used to calculate the voltage standing wave ratio, the slotted section calibration corrects the measured probe position of the minimum, D_p, due to errors introduced by the slot. This calibration procedure affects the real component (ε') of the complex dielectric constant, although only to a small degree.

The method for making the calibration is outlined in detail by Giordano (57). With the wave guide empty, the movable short is sequentially set at several positions. The position of the standing wave minimum is then measured in the slotted section for each short position. For each change in the distance of the short ($\Delta S_r/\lambda_{ms}$), there should be an equivalent change in position of the minimum in the slotted section ($\Delta D_r/\lambda_{ss}$). Here ΔS_r and ΔD_r are the change in micrometer settings relative to the initial settings, and λ_{ms} and λ_{ss} are the measured wave lengths in the movable short section and in the slotted section, respectively. A plot of the error $D' = (\Delta S_r/\lambda_{ms} - \Delta D_r/\lambda_{ss}) * \lambda_{ss}$ as a function of probe positions results in a plot similar to that shown in Fig. 39. Each measured value of D_p is then corrected by adding D'. This was done during data collection using a programmable calculator.

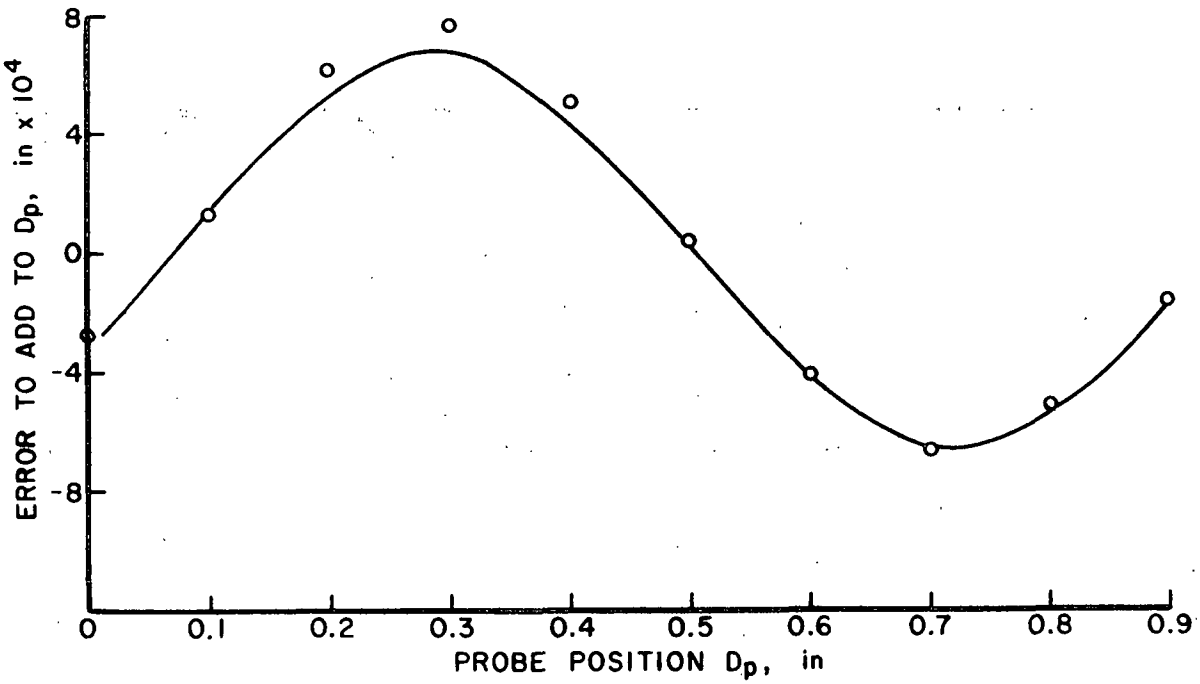

Figure 39. The error to be added to D_p as a function of the probe position, D_p.

When the wave guide is used without "window shims" [as described in Ref. (4)], the correction D' was small and had only a small effect on the final calculated

dielectric constant. In this case, the slotted section calibration affected ε' by less than 0.5%.

SAMPLE PREPARATION

Specimens were cut from the center of the sheets as indicated in Fig. 36; specially made razor dies were used. The dies were constructed by fastening two razor blades parallel to each other on either side of a machined block. Two such dies were required to cut one rectangular specimen.

To determine the dielectric constant in the x- (or y-)direction, two specimens were cut from the sheet, each 0.4 inch by 0.9 inch. The specimens were cut with the shorter dimension in the direction for which the dielectric constant was to be determined. The specimens, which fit snugly in the wave guide, were inserted into the movable short section of the wave guide using the short as a backstop to orient the specimens properly. After connecting the movable short section of the wave guide to the slotted section, the short could be adjusted as required to take the data. The samples were thick enough and fit tightly enough to stand unsupported in the wave guide during data collection.

Before being inserted in the wave guide, the weight of the two die-cut specimens was determined. Knowing the area and weight of the specimens, the total thickness was calculated using the IPC apparent density for each sheet measured earlier. It was this value for the specimen thickness that was used in the computer program to calculate the dielectric constant of the specimens from the collected data.

To determine the dielectric constant in the z-direction, about 15 specimens were cut from the sheet, each 0.1 inch by 0.9 inch. These specimens were stacked in the movable short section of the wave guide, again using the short as a backstop. As many layers as could be stacked in the wave guide were inserted; however, in every

case there was a small gap left between the specimens and the top of the wave guide. More accurately, this gap usually was distributed as many small gaps between each sheet layer. From measurements made on several die-cut specimens, it was found that the actual width of these narrow specimens was about 0.1017 inch, and this value was used for the specimen thickness in the computer program to calculate the dielectric constant of the specimens in the z-direction. The dielectric constant calculated by the computer in this way corresponds to the effective dielectric constant for the paper filled with air gaps between each layer. This dielectric constant thus obviously had to be corrected for these air gaps.

The total air gap thickness was calculated as follows. The total number of layers of paper inserted in the wave guide was weighed. Knowing the two razor die-cut specimen dimensions, the third dimension (the height of the stack of paper) was calculated using the IPC apparent density measured for each sheet. The difference between the wave guide height of 0.4 inch and the calculated height of the paper stack was taken as the total air gap thickness. From visual inspection this calculated air gap thickness value was reasonable when the IPC apparent density value for each sheet was used. If the Schopper apparent density value was used, the calculated air gap thickness was always considerably smaller than visual inspection would indicate, and in some cases (albeit few) the calculated air gap thickness was even negative. For this reason, and because it is believed that the IPC apparent density is more accurate, the latter value was used to calculate the dielectric constant.

Using this calculated air gap thickness (T_g) the measured z-direction dielectric constant was corrected using the relationship

$$\varepsilon_z^* = \frac{1 - T_g/0.4}{\frac{1}{\varepsilon_m^*} + \frac{T_g}{0.4}} \tag{34}$$

where ϵ_z^* is the actual complex dielectric constant of the paper in the z-direction and ϵ_m^* is the measured complex dielectric constant of the paper with air gaps between the layers as measured in the wave guide.

Equation (34) is derived from a series mixture of paper and air and assumes the paper and air layers to be infinite in two dimensions. Theoretically, application of Eq. (34) should result in a slight over correction of ϵ_m^*. From measurements made on layered polymer sheets, this was found to be so, but for air gaps less than about 0.050 inch the overcorrection is less than 5% of the corrected value.

APPENDIX VI

TABULATED DATA

On the following pages the data used to draw the various figures presented in this thesis are tabulated. Included in these tables are measured wave velocities and the elastic constants calculated from these velocities.

KEY:

NUM = Handsheet identification number

FO = Fiber orientation level

WP = Wet pressing level

WS = Wet straining level

VL = Very low (none)

L = Low

M = Medium

H = High

VH = Very high

MEASURED INDUCED STRAIN IN SHEETS

UNITS ARE PERCENT STRAIN
NOTEBOOK 3450 P 17-20, 110-129
VALUES ARE AVERAGES OF TWO NUMBERS

NUM	FO	WP	WS	X	Y
289	L	VL	L	0.08	0.95
259	L	L	L	-0.01	0.05
286	L	L	L	0.01	0.18
246	L	L	M	1.24	-0.43
258	L	L	H	2.46	-1.22
284	L	L	H	2.47	-1.16
248	L	M	L	-0.02	-0.09
255	L	M	M	1.14	-0.49
260	L	M	H	2.39	-1.29
257	L	H	L	-0.07	0.01
287	L	H	L	-0.08	0.04
247	L	H	M	1.10	-0.62
256	L	H	H	2.37	-1.23
285	L	H	H	2.36	-1.20
272	L	VH	L	-0.10	-0.15
273	M	VL	L	0.11	1.33
241	M	L	L	-0.04	0.22
251	M	L	M	1.13	-0.49
242	M	L	H	2.41	-1.37
263	M	M	L	-0.06	0.03
264	M	M	M	1.13	-0.61
265	M	M	H	2.33	-1.37
261	M	H	L	-0.07	-0.11
250	M	H	M	1.10	-0.73
240	M	H	H	2.33	-1.28
275	M	VH	L	-0.06	-0.13
				0.0	0.0
276	H	VL	L	0.16	0.86
245	H	L	L	0.02	0.19
279	H	L	L	-0.07	0.21
243	H	L	M	1.19	-0.54
280	H	L	H	2.40	-1.47
254	H	L	H	2.33	-1.57
268	H	M	L	-0.05	0.13
244	H	M	M	1.12	-0.68
269	H	M	H	2.28	-1.41
253	H	H	L	-0.04	-0.05
281	H	H	L	-0.01	-0.13
252	H	H	M	1.14	-0.59
267	H	H	H	2.32	-1.48
283	H	H	H	2.37	-1.43
278	H	VH	L	-0.09	-0.11
176	R	L	L	0.01	0.09
177	R	M	L	0.05	0.02
178	R	H	L	-0.02	0.08
179	R	L	M	1.43	-0.54
180	R	M	M	1.35	-0.54
181	R	H	M	1.39	-0.53
182	R	L	H	2.84	-1.36
183	R	M	H	2.88	-1.34
184	R	H	H	2.82	-1.24
185	R	M	L	0.03	0.03
186	R	H	H	2.80	-1.33
187	R	L	L	-0.02	0.13

MAXIMUM DRYING STRESS

UNITS ARE MPA BASED ON SCHOPPER PAPER AREA
TAKEN FROM DRYING CURVES

NUM	FO	WP	WS	X	Y
289	L	VL	L	4.00	3.38
259	L	L	L	8.20	7.29
286	L	L	L	7.93	7.03
246	L	L	M	9.09	6.78
258	L	L	H	9.44	5.90
284	L	L	H	9.50	6.11
248	L	M	L	8.82	7.83
255	L	M	M	9.50	7.29
260	L	M	H	10.22	6.55
257	L	H	L	9.52	8.38
287	L	H	L	9.28	8.41
247	L	H	M	10.47	7.84
256	L	H	H	11.03	6.79
285	L	H	H	10.99	6.93
272	L	VH	L	10.72	9.91
273	M	VL	L	5.77	4.03
241	M	L	L	9.26	7.13
251	M	L	M	10.08	6.55
242	M	L	H	11.51	5.92
263	M	M	L	9.86	7.74
264	M	M	M	11.49	7.45
265	M	M	H	12.63	6.47
261	M	H	L	10.53	8.29
250	M	H	M	12.00	7.74
240	M	H	H	13.86	6.77
275	M	VH	L	12.23	10.22
				0.0	0.0

NUM	FO	WP	WS	X	Y
276	H	VL	L	5.73	3.88
245	H	L	L	9.49	7.00
279	H	L	L	9.53	7.26
243	H	L	M	10.56	6.56
280	H	L	H	11.07	5.92
254	H	L	H	11.58	5.85
268	H	M	L	10.15	7.79
244	H	M	M	11.61	7.24
269	H	M	H	12.49	6.31
253	H	H	L	11.30	8.52
281	H	H	L	10.75	8.35
252	H	H	M	12.88	7.88
267	H	H	H	13.75	6.72
283	H	H	H	13.78	6.71
278	H	VH	L	12.28	10.21
176	R	L	L	6.83	7.15
177	R	M	L	8.06	8.24
178	R	H	L	8.70	8.75
179	R	L	M	7.44	6.67
180	R	M	M	8.53	7.59
181	R	H	M	9.53	8.40
182	R	L	H	7.50	5.84
183	R	M	H	8.68	6.68
184	R	H	H	9.56	7.00
185	R	M	L	8.05	8.10
186	R	H	H	9.77	7.25
187	R	L	L	6.92	7.12

BASIS WEIGHT AND APPARENT DENSITY

BW UNITS ARE KG/M2 RHO UNITS ARE KG/M3
NOTEBOOK 3412 P 155,156,160,171
NOTEBOOK 3450 P 40-57,153,186 NOTEBOOK 3433 P 69-73

NUM	FO	WP	WS	BW	SCH	IPC
289	L	VL	L	0.423	405.	433.
259	L	L	L	0.430	651.	708.
286	L	L	L	0.423	643.	703.
246	L	L	M	0.403	628.	682.
258	L	L	H	0.428	590.	631.
284	L	L	H	0.422	591.	635.
248	L	M	L	0.402	675.	741.
255	L	M	M	0.412	651.	708.
260	L	M	H	0.427	626.	670.
257	L	H	L	0.413	714.	787.
287	L	H	L	0.421	721.	793.
247	L	H	M	0.401	692.	753.
256	L	H	H	0.411	641.	691.
285	L	H	H	0.421	654.	705.
272	L	VH	L	0.437	812.	904.
273	M	VL	L	0.422	465.	503.
241	M	L	L	0.414	668.	733.
251	M	L	M	0.422	638.	691.
242	M	L	H	0.415	612.	658.
263	M	M	L	0.421	704.	777.
264	M	M	M	0.432	698.	760.
265	M	M	H	0.433	651.	699.
261	M	H	L	0.427	745.	827.
250	M	H	M	0.422	717.	783.
240	M	H	H	0.418	673.	728.
275	M	VH	L	0.421	838.	951.
				0.0	0.	0.

NUM	FO	WP	WS	BW	SCH	IPC
276	H	VL	L	0.415	455.	496.
245	H	L	L	0.415	656.	726.
279	H	L	L	0.432	681.	745.
243	H	L	M	0.419	639.	690.
280	H	L	H	0.433	608.	657.
254	H	L	H	0.396	597.	644.
268	H	M	L	0.423	708.	781.
244	H	M	M	0.416	683.	744.
269	H	M	H	0.417	635.	680.
253	H	H	L	0.396	747.	832.
281	H	H	L	0.421	750.	835.
252	H	H	M	0.395	721.	798.
267	H	H	H	0.419	663.	717.
283	H	H	H	0.420	671.	723.
278	H	VH	L	0.412	837.	941.
176	R	L	L	0.398	599.	653.
177	R	M	L	0.392	661.	728.
178	R	H	L	0.388	698.	780.
179	R	L	M	0.388	578.	624.
180	R	M	M	0.394	640.	698.
181	R	H	M	0.386	674.	746.
182	R	L	H	0.390	541.	584.
183	R	M	H	0.391	600.	647.
184	R	H	H	0.395	629.	684.
185	R	M	L	0.393	660.	729.
186	R	H	H	0.382	629.	678.
187	R	L	L	0.395	590.	645.
67	R	VH	L	0.391	984.	1173.
69	R	H	L	0.380	757.	813.
70	R	VH	L	0.388	1032.	1217.
118	R	VH	L	0.336	1085.	1298.

MORGAN VELOCITIES

UNITS ARE MM/USEC
NOTEBOOK 3450 P 30,31,34,36-38
NOTEBOOK 3450 P 132-145

NUM	FO	WP	WS	VX	VY	VS45
289	L	VL	L	3.602	2.834	1.906
259	L	L	L	3.855	2.957	2.016
286	L	L	L	3.808	2.980	2.010
246	L	L	M	4.181	2.872	2.036
258	L	L	H	4.284	2.707	1.962
284	L	L	H	4.280	2.735	1.962
248	L	M	L	3.861	3.021	2.061
255	L	M	M	4.160	2.907	2.042
260	L	M	H	4.352	2.746	1.995
257	L	H	L	3.867	2.976	2.089
287	L	H	L	3.888	2.980	2.071
247	L	H	M	4.198	2.889	2.059
256	L	H	H	4.425	2.737	2.000
285	L	H	H	4.363	2.756	2.013
272	L	VH	L	3.940	3.014	2.112
273	M	VL	L	4.248	2.314	1.789
241	M	L	L	4.318	2.413	1.883
251	M	L	M	4.660	2.291	1.859
242	M	L	H	4.897	1.968	1.798
263	M	M	L	4.325	2.451	1.919
264	M	M	M	4.690	2.233	1.871
265	M	M	H	4.902	2.016	1.814
261	M	H	L	4.386	2.465	1.946
250	M	H	M	4.748	2.276	1.899
240	M	H	H	4.967	2.032	1.841
275	M	VH	L	4.456	2.505	1.978
				0.0	0.0	0.0

NUM	FO	WP	WS	VX	VY	VS45
276	H	VL	L	4.252	2.300	1.794
245	H	L	L	4.321	2.374	1.898
279	H	L	L	4.382	2.371	1.893
243	H	L	M	4.600	2.243	1.872
280	H	L	H	4.920	2.023	1.801
254	H	L	H	4.902	1.997	1.784
268	H	M	L	4.386	2.367	1.893
244	H	M	M	4.739	2.202	1.881
269	H	M	H	4.912	2.026	1.799
253	H	H	L	4.413	2.362	1.900
281	H	H	L	4.401	2.395	1.896
252	H	H	M	4.798	2.221	1.897
267	H	H	H	5.020	2.007	1.830
283	H	H	H	5.005	2.041	1.825
278	H	VH	L	4.472	2.478	1.986
176	R	L	L	3.300	3.340	2.040
177	R	M	L	3.400	3.390	2.070
178	R	H	L	3.410	3.400	2.110
179	R	L	M	3.580	3.220	2.080
180	R	M	M	3.630	3.250	2.090
181	R	H	M	3.640	3.300	2.120
182	R	L	H	3.710	3.040	2.010
183	R	M	H	3.740	3.080	2.050
184	R	H	H	3.820	3.080	2.060
185	R	M	L	3.390	3.420	2.050
186	R	H	H	3.890	3.120	2.070
187	R	L	L	3.320	3.320	2.020

BULK LONGITUDINAL VELOCITIES

UNITS ARE MM/USEC
NOTEBOOK 3450 P 44-45,155-185
NOTEBOOK 3433 P 69-73

NUM	FO	WP	WS	VLX	VLY	VLZ	NUM	FO	WP	WS	VLX	VLY	VLZ
289	L	VL	L	3.639	2.798	0.275	276	H	VL	L	4.256	2.345	0.312
259	L	L	L	3.884	2.935	0.446	245	H	L	L	4.376	2.461	0.462
286	L	L	L	3.832	2.930	0.442	279	H	L	L	4.396	2.444	0.492
246	L	L	M	4.159	2.862	0.381	243	H	L	M	4.710	2.384	0.396
258	L	L	H	4.321	2.680	0.313	280	H	L	H	4.867	2.224	0.316
284	L	L	H	4.281	2.687	0.313	254	H	L	H	4.920	2.195	0.311
248	L	M	L	3.910	2.994	0.460	268	H	M	L	4.407	2.470	0.499
255	L	M	M	4.144	2.895	0.386	244	H	M	M	4.774	2.375	0.414
260	L	M	H	4.341	2.730	0.321	269	H	M	H	4.931	2.250	0.321
257	L	H	L	3.916	2.993	0.485	253	H	H	L	4.509	2.456	0.526
287	L	H	L	3.877	2.974	0.488	281	H	H	L	4.439	0.0	0.524
247	L	H	M	4.214	2.896	0.409	252	H	H	M	4.819	2.403	0.427
256	L	H	H	4.385	2.718	0.313	267	H	H	H	5.060	2.253	0.321
285	L	H	H	4.332	2.712	0.331	283	H	H	H	5.014	2.264	0.324
272	L	VH	L	3.991	3.060	0.580	278	H	VH	L	4.510	0.0	0.620
273	M	VL	L	4.324	2.356	0.322	176	R	L	L	0.0	0.0	0.386
241	M	L	L	4.401	0.0	0.480	177	R	M	L	0.0	0.0	0.420
251	M	L	M	4.629	2.395	0.394	178	R	H	L	0.0	0.0	0.443
242	M	L	H	4.965	2.230	0.321	179	R	L	M	0.0	0.0	0.339
263	M	M	L	4.370	2.516	0.490	180	R	M	M	0.0	0.0	0.362
264	M	M	M	4.745	2.413	0.425	181	R	H	M	0.0	0.0	0.379
265	M	M	H	4.944	2.249	0.330	182	R	L	H	0.0	0.0	0.280
261	M	H	L	4.400	2.545	0.523	183	R	M	H	0.0	0.0	0.294
250	M	H	M	4.745	2.434	0.428	184	R	H	H	0.0	0.0	0.293
240	M	H	H	5.048	2.291	0.329	185	R	M	L	0.0	0.0	0.414
275	M	VH	L	4.530	0.0	0.621	186	R	H	H	0.0	0.0	0.300

SHEAR VELOCITIES

UNITS ARE MM/USEC
NOTEBOOK 3450 P 140-151 NOTEBOOK 3242 P 153-160
VSXY IS THE AVERAGE OF VALUES MEASURED IN THE X AND Y DIRECTIONS

NUM	FO	WP	WS	VSYZ	VSXZ	VSXY	NUM	FO	WP	WS	VSYZ	VSXZ	VSXY
289	L	VL	L	0.458	0.530	1.890	276	H	VL	L	0.429	0.593	1.770
259	L	L	L	0.602	0.668	2.000	245	H	L	L	0.569	0.739	1.870
286	L	L	L	0.556	0.633	2.000	279	H	L	L	0.542	0.698	1.860
246	L	L	M	0.575	0.649	2.030	243	H	L	M	0.512	0.676	1.860
258	L	L	H	0.500	0.571	1.990	280	H	L	H	0.460	0.616	1.830
284	L	L	H	0.498	0.572	1.990	254	H	L	H	0.483	0.655	1.810
248	L	M	L	0.628	0.688	2.040	268	H	M	L	0.592	0.778	1.870
255	L	M	M	0.532	0.591	2.040	244	H	M	M	0.504	0.663	1.880
260	L	M	H	0.504	0.571	2.010	269	H	M	H	0.461	0.609	1.850
257	L	H	L	0.615	0.689	2.050	253	H	H	L	0.652	0.833	1.880
287	L	H	L	0.634	0.690	2.030	281	H	H	L	0.569	0.718	1.890
247	L	H	M	0.568	0.638	2.060	252	H	H	M	0.612	0.791	1.900
256	L	H	H	0.551	0.614	2.020	267	H	H	H	0.502	0.666	1.860
285	L	H	H	0.524	0.591	2.010	283	H	H	H	0.458	0.612	1.870
272	L	VH	L	0.689	0.756	2.090	278	H	VH	L	0.596	0.718	1.960
273	M	VL	L	0.444	0.604	1.800	176	R	L	L	0.529	0.531	0.0
241	M	L	L	0.561	0.712	1.880	177	R	M	L	0.575	0.568	0.0
251	M	L	M	0.538	0.681	1.880	178	R	H	L	0.594	0.597	0.0
242	M	L	H	0.469	0.611	1.840	179	R	L	M	0.532	0.533	0.0
263	M	M	L	0.570	0.718	1.910	180	R	M	M	0.557	0.569	0.0
264	M	M	M	0.546	0.682	1.910	181	R	H	M	0.550	0.540	0.0
265	M	M	H	0.489	0.650	1.870	182	R	L	H	0.481	0.489	0.0
261	M	H	L	0.575	0.718	1.930	183	R	M	H	0.518	0.517	0.0
250	M	H	M	0.550	0.695	1.920	184	R	H	H	0.518	0.516	0.0
240	M	H	H	0.474	0.621	1.890	185	R	M	L	0.573	0.561	0.0
275	M	VH	L	0.631	0.755	1.970	186	R	H	H	0.511	0.508	0.0
				0.0	0.0	0.0	187	R	L	L	0.538	0.519	0.0

DIELECTRIC CONSTANTS (REAL COMPONENT)

UNITS ARE DIMENSIONLESS BASED ON IPC THICKNESS
NOTEBOOK 3433 P 114-135
NOTEBOOK 3433 P 138-182

NUM	FO	WP	WS	E'X	E'Y	E'Z
289	L	VL	L	1.897	1.817	1.471
259	L	L	L	2.526	2.398	1.925
286	L	L	L	2.504	2.389	1.918
246	L	L	M	2.424	2.329	1.863
258	L	L	H	2.345	2.232	1.761
284	L	L	H	2.369	2.217	1.780
248	L	M	L	2.595	2.473	1.970
255	L	M	M	2.514	2.408	1.814
260	L	M	H	2.444	2.314	1.823
257	L	H	L	2.706	2.569	2.098
287	L	H	L	2.726	2.592	2.101
247	L	H	M	2.632	2.501	1.994
256	L	H	H	2.504	2.355	1.809
285	L	H	H	2.524	2.396	1.900
272	L	VH	L	2.975	2.844	2.343
273	M	VL	L	2.109	1.900	1.573
241	M	L	L	2.646	2.375	1.969
251	M	L	M	2.550	2.307	1.877
242	M	L	H	2.508	2.234	1.807
263	M	M	L	2.747	2.487	2.070
264	M	M	M	2.718	2.462	2.029
265	M	M	H	2.569	2.310	1.887
261	M	H	L	2.855	2.602	2.189
250	M	H	M	2.768	2.501	2.064
240	M	H	H	2.655	2.380	1.940
275	M	VH	L	3.138	2.830	2.506
				0.0	0.0	0.0

NUM	FO	WP	WS	E'X	E'Y	E'Z
276	H	VL	L	2.099	1.902	1.566
245	H	L	L	2.644	2.380	1.975
279	H	L	L	2.661	2.416	2.017
243	H	L	M	2.558	2.314	1.889
280	H	L	H	2.474	2.222	1.807
254	H	L	H	2.452	2.191	1.785
268	H	M	L	2.731	2.477	2.092
244	H	M	M	2.694	2.410	1.991
269	H	M	H	2.540	2.284	1.852
253	H	H	L	2.878	2.607	2.199
281	H	H	L	2.883	2.620	2.222
252	H	H	M	2.818	2.538	2.112
267	H	H	H	2.625	2.348	1.924
283	H	H	H	2.620	2.349	1.930
278	H	VH	L	3.128	2.839	2.444
176	R	L	L	2.339	2.367	1.820
177	R	M	L	2.524	2.516	1.955
178	R	H	L	2.630	2.612	2.070
179	R	L	M	2.287	2.277	1.763
180	R	M	M	2.459	2.438	1.889
181	R	H	M	2.561	2.572	1.982
182	R	L	H	2.217	2.176	1.686
183	R	M	H	2.330	2.336	1.781
184	R	H	H	2.407	2.400	1.835
185	R	M	L	0.0	0.0	0.0
186	R	H	H	0.0	0.0	0.0
				2.479	2.478	1.945
67	R	VH	L	3.666	0.0	2.970
69	R	H	L	2.720	0.0	2.143
70	R	VH	L	3.795	0.0	3.147
118	R	VH	L	4.031	0.0	3.490

DIELECTRIC CONSTANTS (IMAGINARY COMPONENT)

UNITS ARE DIMENSIONLESS BASED ON IPC THICKNESS
NOTEBOOK 3433 P 114-135
NOTEBOOK 3433 P 138-182

NUM	FO	WP	WS	E''X	E''Y	E''Z
289	L	VL	L	0.197	0.161	0.049
259	L	L	L	0.334	0.262	0.108
286	L	L	L	0.316	0.267	0.105
246	L	L	M	0.294	0.258	0.097
258	L	L	H	0.298	0.242	0.085
284	L	L	H	0.295	0.229	0.084
248	L	M	L	0.346	0.287	0.112
255	L	M	M	0.329	0.277	0.086
260	L	M	H	0.317	0.258	0.089
257	L	H	L	0.370	0.304	0.133
287	L	H	L	0.359	0.297	0.130
247	L	H	M	0.355	0.291	0.113
256	L	H	H	0.325	0.259	0.086
285	L	H	H	0.326	0.262	0.098
272	L	VH	L	0.414	0.346	0.166
273	M	VL	L	0.252	0.165	0.066
241	M	L	L	0.377	0.250	0.115
251	M	L	M	0.353	0.238	0.097
242	M	L	H	0.343	0.218	0.087
263	M	M	L	0.388	0.262	0.127
264	M	M	M	0.387	0.268	0.123
265	M	M	H	0.377	0.238	0.098
261	M	H	L	0.408	0.289	0.149
250	M	H	M	0.407	0.276	0.125
240	M	H	H	0.380	0.234	0.105
275	M	VH	L	0.474	0.321	0.200
				0.0	0.0	0.0

NUM	FO	WP	WS	E''X	E''Y	E''Z
276	H	VL	L	0.256	0.163	0.064
245	H	L	L	0.374	0.251	0.115
279	H	L	L	0.372	0.256	0.123
243	H	L	M	0.357	0.227	0.104
280	H	L	H	0.335	0.215	0.088
254	H	L	H	0.338	0.210	0.083
268	H	M	L	0.393	0.264	0.132
244	H	M	M	0.385	0.249	0.115
269	H	M	H	0.348	0.227	0.091
253	H	H	L	0.422	0.285	0.145
281	H	H	L	0.420	0.284	0.149
252	H	H	M	0.411	0.275	0.133
267	H	H	H	0.368	0.241	0.102
283	H	H	H	0.363	0.234	0.101
278	H	VH	L	0.464	0.322	0.186
176	R	L	L	0.273	0.287	0.093
177	R	M	L	0.305	0.301	0.108
178	R	H	L	0.326	0.329	0.123
179	R	L	M	0.268	0.263	0.084
180	R	M	M	0.301	0.296	0.098
181	R	H	M	0.329	0.313	0.111
182	R	L	H	0.252	0.248	0.071
183	R	M	H	0.276	0.274	0.084
184	R	H	H	0.295	0.285	0.092
185	R	M	L	0.0	0.0	0.0
186	R	H	H	0.0	0.0	0.0
				0.300	0.299	0.106
67	R	VH	L	0.527	0.0	0.284
69	R	H	L	0.350	0.0	0.137
70	R	VH	L	0.547	0.0	0.297
118	R	VH	L	0.588	0.0	0.350

YOUNG'S MODULUS AND SHEAR MODULUS FROM 3 MORGAN VELOCITIES

UNITS ARE GPA BASED ON SCHOPPER PAPER AREA
GXY IS CALCULATED FROM VS45

NUM	FO	WP	WS	EX	EY	GXY
289	L	VL	L	4.86	3.01	1.47
259	L	L	L	8.98	5.29	2.65
286	L	L	L	8.64	5.29	2.60
246	L	L	M	10.17	4.80	2.60
258	L	L	H	9.98	3.98	2.27
284	L	L	H	9.91	4.05	2.28
248	L	M	L	9.41	5.76	2.87
255	L	M	M	10.41	5.08	2.71
260	L	M	H	10.94	4.36	2.49
257	L	H	L	10.16	6.02	3.12
287	L	H	L	10.28	6.04	3.09
247	L	H	M	11.36	5.38	2.93
256	L	H	H	11.58	4.43	2.56
285	L	H	H	11.55	4.61	2.65
272	L	VH	L	11.96	7.00	3.62
273	M	VL	L	7.87	2.33	1.49
241	M	L	L	11.84	3.69	2.37
251	M	L	M	13.23	3.20	2.20
242	M	L	H	14.65	2.37	1.98
263	M	M	L	12.59	4.04	2.59
264	M	M	M	14.93	3.39	2.44
265	M	M	H	15.56	2.63	2.14
261	M	H	L	13.76	4.34	2.82
250	M	H	M	15.69	3.61	2.59
240	M	H	H	16.55	2.77	2.28
275	M	VH	L	15.98	5.04	3.28
				0.0	0.0	0.0

NUM	FO	WP	WS	EX	EY	GXY
276	H	VL	L	7.76	2.27	1.46
245	H	L	L	11.81	3.57	2.36
279	H	L	L	12.56	3.68	2.44
243	H	L	M	13.16	3.13	2.24
280	H	L	H	14.57	2.46	1.97
254	H	L	H	14.22	2.36	1.90
268	H	M	L	13.10	3.82	2.54
244	H	M	M	15.05	3.25	2.42
269	H	M	H	15.16	2.58	2.06
253	H	H	L	14.02	4.02	2.70
281	H	H	L	13.88	4.11	2.70
252	H	H	M	16.27	3.49	2.59
267	H	H	H	16.67	2.67	2.22
283	H	H	H	16.67	2.77	2.23
278	H	VH	L	16.20	4.97	3.30
176	R	L	L	6.13	6.28	2.49
177	R	M	L	7.14	7.10	2.83
178	R	H	L	7.68	7.64	3.11
179	R	L	M	6.96	5.63	2.50
180	R	M	M	7.88	6.32	2.80
181	R	H	M	8.38	6.89	3.03
182	R	L	H	6.89	4.63	2.19
183	R	M	H	7.83	5.31	2.52
184	R	H	H	8.53	5.54	2.67
185	R	M	L	7.01	7.13	2.77
186	R	H	H	8.77	5.64	2.70
187	R	L	L	6.07	6.07	2.41

YOUNG'S MODULUS AND SHEAR MODULUS FROM 4 MORGAN VELOCITIES

UNITS ARE GPA BASED ON SCHOPPER PAPER AREA
GXY IS CALCULATED FROM VSXY

NUM	FO	WP	WS	EX	EY	GXY	NUM	FO	WP	WS	EX	EY	GXY
289	L	VL	L	4.87	3.01	1.45	276	H	VL	L	7.78	2.27	1.43
259	L	L	L	8.99	5.29	2.60	245	H	L	L	11.84	3.58	2.29
286	L	L	L	8.64	5.29	2.57	279	H	L	L	12.60	3.69	2.36
246	L	L	M	10.17	4.80	2.59	243	H	L	M	13.18	3.13	2.21
258	L	L	H	9.96	3.98	2.34	280	H	L	H	14.53	2.46	2.04
284	L	L	H	9.90	4.04	2.34	254	H	L	H	14.18	2.35	1.96
248	L	M	L	9.42	5.76	2.81	268	H	M	L	13.12	3.82	2.48
255	L	M	M	10.42	5.08	2.71	244	H	M	M	15.05	3.25	2.41
260	L	M	H	10.94	4.35	2.53	269	H	M	H	15.06	2.57	2.17
257	L	H	L	10.17	6.02	3.00	253	H	H	L	14.04	4.03	2.64
287	L	H	L	10.29	6.04	2.97	281	H	H	L	13.89	4.12	2.68
247	L	H	M	11.36	5.38	2.94	252	H	H	M	16.27	3.48	2.60
256	L	H	H	11.56	4.42	2.62	267	H	H	H	16.63	2.66	2.29
285	L	H	H	11.55	4.61	2.64	283	H	H	H	16.58	2.76	2.35
272	L	VH	L	11.96	7.00	3.55	278	H	VH	L	16.23	4.98	3.22
273	M	VL	L	7.86	2.33	1.51	176	R	L	L	0.0	0.0	0.0
241	M	L	L	11.84	3.70	2.36	177	R	M	L	0.0	0.0	0.0
251	M	L	M	13.20	3.19	2.25	178	R	H	L	0.0	0.0	0.0
242	M	L	H	14.60	2.36	2.07	179	R	L	M	0.0	0.0	0.0
263	M	M	L	12.59	4.05	2.57	180	R	M	M	0.0	0.0	0.0
264	M	M	M	14.87	3.37	2.55	181	R	H	M	0.0	0.0	0.0
265	M	M	H	15.47	2.62	2.28	182	R	L	H	0.0	0.0	0.0
261	M	H	L	13.78	4.35	2.78	183	R	M	H	0.0	0.0	0.0
250	M	H	M	15.65	3.60	2.64	184	R	H	H	0.0	0.0	0.0
240	M	H	H	16.48	2.76	2.40	185	R	M	L	0.0	0.0	0.0
275	M	VH	L	15.99	5.05	3.25	186	R	H	H	0.0	0.0	0.0

POISSON RATIOS FROM 3 MORGAN VELOCITIES

UNITS ARE DIMENSIONLESS
GMEAN IS THE GEOMETRIC MEAN

NUM	FO	WP	WS	VXY	VYX	GMEAN
289	L	VL	L	0.214	0.346	0.272
259	L	L	L	0.205	0.348	0.267
286	L	L	L	0.212	0.346	0.271
246	L	L	M	0.186	0.394	0.271
258	L	L	H	0.177	0.444	0.280
284	L	L	H	0.186	0.454	0.291
248	L	M	L	0.199	0.345	0.262
255	L	M	M	0.192	0.394	0.275
260	L	M	H	0.175	0.440	0.277
257	L	H	L	0.169	0.286	0.220
287	L	H	L	0.183	0.311	0.239
247	L	H	M	0.180	0.380	0.262
256	L	H	H	0.172	0.451	0.279
285	L	H	H	0.170	0.426	0.269
272	L	VH	L	0.173	0.296	0.226
273	M	VL	L	0.136	0.458	0.250
241	M	L	L	0.124	0.398	0.222
251	M	L	M	0.104	0.432	0.212
242	M	L	H	0.017	0.106	0.042
263	M	M	L	0.119	0.371	0.210
264	M	M	M	0.079	0.349	0.166
265	M	M	H	0.030	0.176	0.073
261	M	H	L	0.112	0.355	0.199
250	M	H	M	0.082	0.358	0.171
240	M	H	H	0.023	0.140	0.057
275	M	VH	L	0.112	0.354	0.199
				0.0	0.0	0.0

NUM	FO	WP	WS	VXY	VYX	GMEAN
276	H	VL	L	0.129	0.440	0.238
245	H	L	L	0.104	0.343	0.189
279	H	L	L	0.107	0.366	0.198
243	H	L	M	0.080	0.335	0.164
280	H	L	H	0.040	0.238	0.098
254	H	L	H	0.038	0.229	0.093
268	H	M	L	0.106	0.364	0.196
244	H	M	M	0.064	0.297	0.138
269	H	M	H	0.042	0.249	0.102
253	H	H	L	0.102	0.355	0.190
281	H	H	L	0.114	0.386	0.210
252	H	H	M	0.065	0.302	0.140
267	H	H	H	0.020	0.125	0.050
283	H	H	H	0.037	0.223	0.091
278	H	VH	L	0.100	0.325	0.180
176	R	L	L	0.248	0.242	0.245
177	R	M	L	0.256	0.257	0.256
178	R	H	L	0.231	0.233	0.232
179	R	L	M	0.221	0.274	0.246
180	R	M	M	0.229	0.286	0.256
181	R	H	M	0.226	0.274	0.249
182	R	L	H	0.223	0.332	0.272
183	R	M	H	0.214	0.315	0.260
184	R	H	H	0.214	0.329	0.265
185	R	M	L	0.277	0.273	0.275
186	R	H	H	0.225	0.350	0.281
187	R	L	L	0.260	0.260	0.260

POISSON RATIOS FROM 4 MORGAN VELOCITIES

UNITS ARE DIMENSIONLESS
GMEAN IS THE GEOMETRIC MEAN

NUM	FO	WP	WS	VXY	VYX	GMEAN
289	L	VL	L	0.214	0.345	0.272
259	L	L	L	0.204	0.347	0.266
286	L	L	L	0.212	0.346	0.271
246	L	L	M	0.186	0.394	0.271
258	L	L	H	0.179	0.448	0.283
284	L	L	H	0.187	0.458	0.293
248	L	M	L	0.198	0.324	0.253
255	L	M	M	0.192	0.394	0.275
260	L	M	H	0.176	0.442	0.279
257	L	H	L	0.168	0.284	0.218
287	L	H	L	0.182	0.309	0.237
247	L	H	M	0.180	0.380	0.262
256	L	H	H	0.174	0.454	0.281
285	L	H	H	0.170	0.425	0.269
272	L	VH	L	0.173	0.295	0.226
273	M	VL	L	0.137	0.462	0.252
241	M	L	L	0.124	0.397	0.222
251	M	L	M	0.107	0.443	0.218
242	M	L	H	0.029	0.177	0.072
263	M	M	L	0.118	0.368	0.208
264	M	M	M	0.085	0.375	0.179
265	M	M	H	0.043	0.254	0.105
261	M	H	L	0.111	0.350	0.197
250	M	H	M	0.085	0.371	0.178
240	M	H	H	0.036	0.213	0.088
275	M	VH	L	0.111	0.352	0.198
276	H	VL	L	0.126	0.432	0.233
245	H	L	L	0.100	0.333	0.182
279	H	L	L	0.103	0.353	0.191
243	H	L	M	0.078	0.328	0.160
280	H	L	H	0.047	0.277	0.114
254	H	L	H	0.044	0.266	0.108
268	H	M	L	0.103	0.354	0.191
244	H	M	M	0.064	0.296	0.138
269	H	M	H	0.054	0.315	0.130
253	H	H	L	0.099	0.347	0.185
281	H	H	L	0.114	0.384	0.209
252	H	H	M	0.065	0.305	0.141
267	H	H	H	0.028	0.175	0.070
283	H	H	H	0.047	0.284	0.116
278	H	VH	L	0.097	0.316	0.175
176	R	L	L	0.0	0.0	0.0
177	R	M	L	0.0	0.0	0.0
178	R	H	L	0.0	0.0	0.0
179	R	L	M	0.0	0.0	0.0
180	R	M	M	0.0	0.0	0.0
181	R	H	M	0.0	0.0	0.0
182	R	L	H	0.0	0.0	0.0
183	R	M	H	0.0	0.0	0.0
184	R	H	H	0.0	0.0	0.0
185	R	M	L	0.0	0.0	0.0
186	R	H	H	0.0	0.0	0.0

STIFFNESS COEFFICIENTS FROM LONGITUDINAL VELOCITIES

UNITS ARE GPA BASED ON SCHOPPER PAPER AREA
C11 AND C22 ARE FROM MORGAN VELOCITIES

NUM	FO	WP	WS	C11	C22	C33
289	L	VL	L	5.25	3.25	.0306
259	L	L	L	9.67	5.69	.1295
286	L	L	L	9.32	5.71	.1256
246	L	L	M	10.98	5.18	.0912
258	L	L	H	10.83	4.32	.0578
284	L	L	H	10.83	4.42	.0579
248	L	M	L	10.06	6.16	.1428
255	L	M	M	11.27	5.50	.0970
260	L	M	H	11.86	4.72	.0645
257	L	H	L	10.68	6.32	.1679
287	L	H	L	10.90	6.40	.1717
247	L	H	M	12.20	5.78	.1158
256	L	H	H	12.55	4.80	.0628
285	L	H	H	12.45	4.97	.0716
272	L	VH	L	12.61	7.38	.2732
273	M	VL	L	8.39	2.49	.0482
241	M	L	L	12.45	3.89	.1539
251	M	L	M	13.85	3.35	.0990
242	M	L	H	14.68	2.37	.0631
263	M	M	L	13.17	4.23	.1690
264	M	M	M	15.35	3.48	.1261
265	M	M	H	15.64	2.65	.0709
261	M	H	L	14.33	4.53	.2038
250	M	H	M	16.16	3.71	.1313
240	M	H	H	16.60	2.78	.0728
275	M	VH	L	16.64	5.26	.3232
				0.0	0.0	.0

NUM	FO	WP	WS	C11	C22	C33
276	H	VL	L	8.23	2.41	.0443
245	H	L	L	12.25	3.70	.1400
279	H	L	L	13.08	3.83	.1648
243	H	L	M	13.52	3.21	.1002
280	H	L	H	14.72	2.49	.0607
254	H	L	H	14.35	2.38	.0577
268	H	M	L	13.62	3.97	.1763
244	H	M	M	15.34	3.31	.1171
269	H	M	H	15.32	2.61	.0654
253	H	H	L	14.55	4.17	.2067
281	H	H	L	14.53	4.30	.2059
252	H	H	M	16.60	3.56	.1315
267	H	H	H	16.71	2.67	.0683
283	H	H	H	16.81	2.80	.0704
278	H	VH	L	16.74	5.14	.3217
176	R	L	L	6.52	6.68	.0892
177	R	M	L	7.64	7.60	.1166
178	R	H	L	8.12	8.07	.1370
179	R	L	M	7.41	5.99	.0664
180	R	M	M	8.43	6.76	.0839
181	R	H	M	8.93	7.34	.0968
182	R	L	H	7.45	5.00	.0424
183	R	M	H	8.39	5.69	.0519
184	R	H	H	9.18	5.97	.0540
185	R	M	L	7.58	7.72	.1131
186	R	H	H	9.52	6.12	.0566
187	R	L	L	6.50	6.50	.0874

STIFFNESS COEFFICIENTS FROM SHEAR VELOCITIES

UNITS ARE GPA BASED ON SCHOPPER PAPER AREA
NOTEBOOK 3242 P 153-160 (FOR C44 AND C55)
C66 CALCULATED FROM VS45

NUM	FO	WP	WS	C44	C55	C66	NUM	FO	WP	WS	C44	C55	C66
289	L	VL	L	0.085	0.114	1.471	276	H	VL	L	0.084	0.160	1.464
259	L	L	L	0.236	0.290	2.646	245	H	L	L	0.212	0.358	2.363
286	L	L	L	0.199	0.258	2.598	279	H	L	L	0.200	0.332	2.440
246	L	L	M	0.208	0.265	2.603	243	H	L	M	0.168	0.292	2.239
258	L	L	H	0.147	0.192	2.271	280	H	L	H	0.129	0.231	1.972
284	L	L	H	0.147	0.193	2.275	254	H	L	H	0.139	0.256	1.900
248	L	M	L	0.266	0.320	2.867	268	H	M	L	0.248	0.429	2.537
255	L	M	M	0.184	0.227	2.715	244	H	M	M	0.173	0.300	2.417
260	L	M	H	0.159	0.204	2.491	269	H	M	H	0.135	0.236	2.055
257	L	H	L	0.270	0.339	3.116	253	H	H	L	0.318	0.518	2.697
287	L	H	L	0.290	0.343	3.092	281	H	H	L	0.243	0.387	2.696
247	L	H	M	0.223	0.282	2.934	252	H	H	M	0.270	0.451	2.595
256	L	H	H	0.195	0.242	2.564	267	H	H	H	0.167	0.294	2.220
285	L	H	H	0.180	0.228	2.650	283	H	H	H	0.141	0.251	2.235
272	L	VH	L	0.385	0.464	3.622	278	H	VH	L	0.297	0.431	3.301
273	M	VL	L	0.092	0.170	1.488	176	R	L	L	0.168	0.169	2.493
241	M	L	L	0.210	0.339	2.369	177	R	M	L	0.219	0.213	2.832
251	M	L	M	0.185	0.296	2.205	178	R	H	L	0.246	0.249	3.108
242	M	L	H	0.135	0.228	1.978	179	R	L	M	0.164	0.164	2.501
263	M	M	L	0.229	0.363	2.593	180	R	M	M	0.199	0.207	2.796
264	M	M	M	0.208	0.325	2.443	181	R	H	M	0.204	0.197	3.029
265	M	M	H	0.156	0.275	2.142	182	R	L	H	0.125	0.129	2.186
261	M	H	L	0.246	0.384	2.821	183	R	M	H	0.161	0.160	2.521
250	M	H	M	0.217	0.346	2.586	184	R	H	H	0.169	0.167	2.669
240	M	H	H	0.151	0.260	2.281	185	R	M	L	0.217	0.208	2.774
275	M	VH	L	0.334	0.478	3.279	186	R	H	H	0.164	0.162	2.695
				0.0	0.0	0.0	187	R	L	L	0.171	0.159	2.407

YOUNG'S MODULUS FROM INSTRON

UNITS ARE GPA BASED ON SCHOPPER PAPER AREA
ESTIMATED FROM THE INITIAL SLOPE OF THE LOAD ELONGATION CURVE

NUM	FO	WP	WS	EX	EY
289	L	VL	L	3.14	1.62
259	L	L	L	6.44	3.37
286	L	L	L	5.88	3.08
246	L	L	M	7.08	3.20
258	L	L	H	8.14	2.56
284	L	L	H	7.72	2.53
248	L	M	L	6.46	3.73
255	L	M	M	7.61	3.39
260	L	M	H	8.22	2.83
257	L	H	L	7.40	3.92
287	L	H	L	7.51	3.69
247	L	H	M	8.44	3.65
256	L	H	H	9.32	2.82
285	L	H	H	9.14	2.78
272	L	VH	L	9.31	4.85
273	M	VL	L	5.55	1.37
241	M	L	L	0.0	2.44
251	M	L	M	9.62	2.12
242	M	L	H	0.0	1.69
263	M	M	L	8.61	2.62
264	M	M	M	10.81	2.29
265	M	M	H	12.25	1.92
261	M	H	L	9.15	2.67
250	M	H	M	12.46	2.44
240	M	H	H	0.0	0.0
275	M	VH	L	12.01	3.30
				0.0	0.0

NUM	FO	WP	WS	EX	EY
276	H	VL	L	4.97	1.26
245	H	L	L	8.19	2.30
279	H	L	L	8.78	2.34
243	H	L	M	10.47	2.04
280	H	L	H	11.48	1.75
254	H	L	H	11.49	1.67
268	H	M	L	9.28	2.49
244	H	M	M	11.69	2.24
269	H	M	H	13.05	1.86
253	H	H	L	10.69	2.66
281	H	H	L	10.05	2.72
252	H	H	M	13.24	2.42
267	H	H	H	13.96	1.95
283	H	H	H	13.84	1.92
278	H	VH	L	12.14	3.33
176	R	L	L	4.16	4.38
177	R	M	L	5.01	5.24
178	R	H	L	5.55	5.26
179	R	L	M	4.81	4.11
180	R	M	M	5.21	4.43
181	R	H	M	6.00	4.87
182	R	L	H	4.88	3.31
183	R	M	H	5.53	3.78
184	R	H	H	6.00	4.08
185	R	M	L	4.94	5.21
186	R	H	H	5.95	4.10
187	R	L	L	4.34	4.45

STRAIN AT FAILURE IN TENSILE TEST

UNITS ARE PERCENT STRAIN
TAKEN FROM THE LOAD ELONGATION CURVE

NUM	FO	WP	WS	X	Y
289	L	VL	L	2.500	2.500
259	L	L	L	3.110	3.610
286	L	L	L	3.160	3.470
246	L	L	M	2.390	3.650
258	L	L	H	1.930	4.020
284	L	L	H	1.950	3.940
248	L	M	L	3.250	3.580
255	L	M	M	2.360	3.570
260	L	M	H	1.960	4.040
257	L	H	L	3.180	3.810
287	L	H	L	3.240	3.670
247	L	H	M	2.410	3.970
256	L	H	H	1.860	3.990
285	L	H	H	1.910	4.240
272	L	VH	L	3.440	3.870
273	M	VL	L	2.520	2.630
241	M	L	L	0.0	3.550
251	M	L	M	2.350	3.860
242	M	L	H	0.0	3.960
263	M	M	L	3.140	3.800
264	M	M	M	2.290	3.900
265	M	M	H	1.770	4.290
261	M	H	L	3.060	4.110
250	M	H	M	2.230	4.110
240	M	H	H	0.0	0.0
275	M	VH	L	3.160	4.320
				0.0	0.0

NUM	FO	WP	WS	X	Y
276	H	VL	L	2.510	2.460
245	H	L	L	3.040	3.540
279	H	L	L	2.980	3.460
243	H	L	M	2.240	3.850
280	H	L	H	1.720	3.860
254	H	L	H	1.820	3.800
268	H	M	L	3.090	3.740
244	H	M	M	2.250	4.020
269	H	M	H	1.750	4.180
253	H	H	L	3.120	3.590
281	H	H	L	3.060	3.750
252	H	H	M	2.240	3.780
267	H	H	H	1.620	4.360
283	H	H	H	1.690	4.130
278	H	VH	L	3.180	4.020
176	R	L	L	3.300	3.080
177	R	M	L	3.190	3.060
178	R	H	L	3.220	3.250
179	R	L	M	2.490	3.330
180	R	M	M	2.390	3.500
181	R	H	M	2.450	3.620
182	R	L	H	2.230	3.810
183	R	M	H	1.960	3.750
184	R	H	H	1.790	3.930
185	R	M	L	3.240	3.130
186	R	H	H	2.150	3.710
187	R	L	L	3.090	3.090

TENSILE STRENGTH

UNITS ARE MPA BASED ON SCHOPPER PAPER AREA
NOTEBOOK 3433 P 78,80-84
NOTEBOOK 3433 P 76-88

NUM	FO	WP	WS	X	Y	Z	NUM	FO	WP	WS	X	Y	Z
289	L	VL	L	27.8	16.9	0.231	276	H	VL	L	48.3	12.9	0.302
259	L	L	L	58.3	33.4	0.472	245	H	L	L	80.5	22.6	0.559
286	L	L	L	54.7	31.8	0.406	279	H	L	L	85.3	23.0	0.586
246	L	L	M	61.5	31.0	0.398	243	H	L	M	84.7	20.5	0.406
258	L	L	H	59.4	26.2	0.315	280	H	L	H	83.5	18.1	0.342
284	L	L	H	58.5	26.4	0.329	254	H	L	H	85.1	17.3	0.374
248	L	M	L	61.9	36.4	0.501	268	H	M	L	89.1	24.1	0.559
255	L	M	M	62.5	32.7	0.374	244	H	M	M	93.9	22.3	0.454
260	L	M	H	62.6	29.6	0.332	269	H	M	H	89.1	19.9	0.318
257	L	H	L	65.8	38.4	0.501	253	H	H	L	102.5	24.9	0.682
287	L	H	L	64.4	37.3	0.472	281	H	H	L	96.6	25.8	0.557
247	L	H	M	70.2	36.3	0.434	252	H	H	M	104.4	23.7	0.498
256	L	H	H	65.9	29.9	0.321	267	H	H	H	93.7	20.6	0.329
285	L	H	H	67.7	30.7	0.345	283	H	H	H	96.0	20.6	0.345
272	L	VH	L	81.1	47.4	0.662	278	H	VH	L	115.7	33.1	0.819
273	M	VL	L	49.9	13.6	0.310	176	R	L	L	37.3	38.4	0.0
241	M	L	L	77.1	23.5	0.506	177	R	M	L	44.9	44.5	0.0
251	M	L	M	80.8	22.1	0.418	178	R	H	L	48.9	48.3	0.0
242	M	L	H	84.3	18.0	0.340	179	R	L	M	40.8	35.8	0.0
263	M	M	L	84.7	26.7	0.514	180	R	M	M	46.6	39.7	0.0
264	M	M	M	93.7	23.9	0.442	181	R	H	M	50.6	44.3	0.0
265	M	M	H	89.5	20.4	0.356	182	R	L	H	38.3	29.2	0.0
261	M	H	L	89.4	27.0	0.612	183	R	M	H	43.9	34.3	0.0
250	M	H	M	95.8	25.1	0.488	184	R	H	H	46.4	37.7	0.0
240	M	H	H	94.0	20.8	0.369	185	R	M	L	43.7	44.8	0.0
275	M	VH	L	113.0	33.6	0.832	186	R	H	H	48.1	37.2	0.0
				0.0	0.0	0.0	187	R	L	L	36.9	37.8	0.0

COMPRESSIVE STRENGTH (STFI)

UNITS ARE MPA BASED ON SCHOPPER PAPER AREA
NOTEBOOK 3433 P 74,75,183,184

NUM	FO	WP	WS	X	Y
289	L	VL	L	8.26	5.51
259	L	L	L	20.48	13.24
286	L	L	L	19.59	13.16
246	L	L	M	21.35	12.64
258	L	L	H	19.59	10.50
284	L	L	H	19.03	10.52
248	L	M	L	21.51	14.40
255	L	M	M	22.35	13.37
260	L	M	H	21.33	11.52
257	L	H	L	22.94	15.42
287	L	H	L	23.12	15.14
247	L	H	M	24.50	14.35
256	L	H	H	21.75	11.97
285	L	H	H	22.50	12.25
272	L	VH	L	29.02	18.57
273	M	VL	L	15.00	5.70
241	M	L	L	25.56	11.36
251	M	L	M	26.37	10.08
242	M	L	H	24.81	8.04
263	M	M	L	27.32	12.25
264	M	M	M	30.57	11.45
265	M	M	H	28.17	9.07
261	M	H	L	29.80	12.62
250	M	H	M	30.88	11.66
240	M	H	H	27.91	9.33
275	M	VH	L	35.25	16.31
276	H	VL	L	14.26	5.70
245	H	L	L	25.85	10.89
279	H	L	L	26.88	11.71
243	H	L	M	26.58	9.93
280	H	L	H	26.79	8.71
254	H	L	H	25.59	8.28
268	H	M	L	26.72	12.13
244	H	M	M	28.69	11.06
269	H	M	H	27.39	9.23
253	H	H	L	31.62	12.85
281	H	H	L	29.35	13.35
252	H	H	M	33.69	11.82
267	H	H	H	30.19	9.55
283	H	H	H	29.75	9.84
278	H	VH	L	33.31	16.18
176	R	L	L	0.0	0.0
177	R	M	L	0.0	0.0
178	R	H	L	0.0	0.0
179	R	L	M	0.0	0.0
180	R	M	M	0.0	0.0
181	R	H	M	0.0	0.0
182	R	L	H	0.0	0.0
183	R	M	H	0.0	0.0
184	R	H	H	0.0	0.0
185	R	M	L	0.0	0.0
186	R	H	H	0.0	0.0

APPENDIX VII

MEASUREMENT OF THE FIBER ORIENTATION DISTRIBUTION FOR THE ORIENTED SHEETS

To measure directly the fiber orientation in the oriented sheets, a small amount (1-2%) of black-dyed fibers was added to the furnish prior to forming these sheets. After the sheets were dry, both the felt and wire sides were photographed onto full size negative films. The negatives were the same size as the sheets. In the center of each negative film, a reference line one inch long oriented in the x-direction was scratched on the surface of the film. An enlarged print, 7.25X, was made of the center 1.9 x 1.5 $inch^2$ area of the sheet.

The fiber orientation distribution was measured with the aid of a graphics tablet and an APPLE minicomputer. Using a penlike probe, one can assign a pair of coordinate values to any point on the graphics tablet. The enlarged photograph of the dyed fibers on the surface of the sheet was placed on the graphics tablet and the fibers were traced with the probe. The computer analyzes the x, y coordinate values inputted by the graphics tablet to calculate the angular orientation distribution of the fibers. The computer program to do this is listed at the end of this appendix.

The program calculates a segment length-weighted angular orientation distribution. When the pen is traced along each fiber, the fiber is divided into a variable number of straight line segments. The length of each segment is calculated with respect to the reference line length, and the angle of each segment is calculated with respect to the reference line also. The distribution is formed by summing the segment length in the appropriate angle interval. The distribution is measured in angle intervals of one degree from -90 to +90 degrees. When printed out, however, the user may specify the angle interval. The total segment lengths measured in each angle interval is then listed along with the total segment length, the total number

of segments counted, and the total number of fibers counted. Also included is a normalized distribution for which the total area under the distribution is normalized to one.

All of the dyed fibers distinguishable on the enlarged photograph of the center 1.9 x 1.5 inch^2 area of the sheets were traced with the pen. Since the reference line length in each photograph was one inch long, all of the segment lengths have the units of inches. In this small area, the total segment length measured was usually about 80-100 inches, and the total number of segments counted was about 3000-5000. The average length per segment was thus about 0.02 inch.

The fiber orientation distribution was determined for seven of the forty-one oriented sheets tested in this study. These seven sheets are described in Table XI.

TABLE XI

DESCRIPTION OF THE SHEETS FOR WHICH THE FIBER ORIENTATION DISTRIBUTION WAS MEASURED

Sheet Number	Fiber Orientation	Wet Pressing	Wet Straining
248	Low	Medium	Low
257	Low	High	Low
260	Low	Medium	High
263	Medium	Medium	Low
268	High	Medium	Low
253	High	High	Low
269	High	Medium	High

The distributions measured on the wire side of the sheet differed from those determined on the felt side of the sheet. This is indicated in Table XII in which the normalized distributions are listed for sheet numbers 248, 263, and 268.

TABLE XII

NORMALIZED DISTRIBUTIONS MEASURED ON THE FELT AND WIRE SIDES OF THREE SHEETS WITH DIFFERENT FIBER ORIENTATIONS

Angle Interval Degrees	Fiber Orientation					
	Low		Medium		High	
	Felt	Wire	Felt	Wire	Felt	Wire
0-10	1.11	1.68	1.72	2.18	1.88	2.29
10-20	1.12	1.53	1.51	1.70	1.61	1.70
20-30	0.94	1.23	1.32	1.28	1.22	1.29
30-40	0.99	1.06	1.03	0.92	0.98	0.95
40-50	0.87	0.88	0.80	0.83	0.85	0.74
50-60	1.01	0.70	0.73	0.63	0.67	0.61
60-70	0.99	0.67	0.64	0.56	0.62	0.50
70-80	1.05	0.59	0.66	0.48	0.59	0.44
80-90	0.92	0.65	0.59	0.43	0.57	0.48

The sum of the felt and wire side distributions was taken as the best estimate of the distribution of the entire sheet. Wet straining had little or no effect on the distribution as indicated in Table XIII for sheet numbers 248, 260, 268, and 269.

The final distributions used for the low, medium, and high fiber orientation levels are given in Fig. 40-42 as printed out by the computer in angle intervals of five degrees. The low and high fiber orientation distributions are each the sum of six distributions, the felt and wire sides of three sheets. The total fiber segment length measured to determine each of these distributions is about 550 inches, and the total number of segments is about 28,000.

TABLE XIII

THE EFFECT OF WET STRAINING ON THE MEASURED NORMALIZED DISTRIBUTIONS

Angle Interval Degrees	Fiber Orientation: Low — Low Wet Strain	Fiber Orientation: Low — High Wet Strain	Fiber Orientation: High — Low Wet Strain	Fiber Orientation: High — High Wet Strain
0-10	1.40	1.51	2.09	2.08
10-20	1.33	1.39	1.66	1.68
20-30	1.08	1.20	1.25	1.25
30-40	1.02	1.02	0.96	0.95
40-50	0.88	0.96	0.80	0.73
50-60	0.85	0.79	0.64	0.67
60-70	0.83	0.72	0.56	0.60
70-80	0.82	0.71	0.52	0.50
80-90	0.78	0.70	0.52	0.54

Following the figures is a listing of the computer program used, written in Applesoft BASIC.

SEGMENT ANGLE DISTRIBUTION FOR
AVG248+AVG257+AVG260

ANGLE INTERVAL	SEGMENT LENGTH	NORMALIZED LENGTH
FROM 0 TO 5	44.2579163	1.44326635
FROM 5 TO 10	44.4622709	1.44993042
FROM 10 TO 15	42.4260346	1.38352803
FROM 15 TO 20	39.2805321	1.28095208
FROM 20 TO 25	35.4319894	1.15544974
FROM 25 TO 30	33.5850374	1.09521998
FROM 30 TO 35	32.2068214	1.05027587
FROM 35 TO 40	30.0566421	0.980157757
FROM 40 TO 45	29.4374528	0.959965774
FROM 45 TO 50	26.5228818	0.864920581
FROM 50 TO 55	26.9436709	0.878642663
FROM 55 TO 60	24.6792566	0.804799311
FROM 60 TO 65	24.8829599	0.811442147
FROM 65 TO 70	23.8478114	0.777685588
FROM 70 TO 75	24.2287941	0.790109567
FROM 75 TO 80	22.7619439	0.742275062
FROM 80 TO 85	24.2772281	0.791689018
FROM 85 TO 90	22.6826745	0.739690058

THE TOTAL SEGMENT LENGTH RELATIVE TO THE
REFERENCE LINE LENGTH IS 551.971918
THE TOTAL NUMBER OF SEGMENTS IS 27142
THE TOTAL NUMBER OF FIBERS IS 4124

Figure 40. The average segment length distribution for three low fiber orientation sheets.

SEGMENT ANGLE DISTRIBUTION FOR
S 263W+263F

ANGLE INTERVAL	SEGMENT LENGTH	NORMALIZED LENGTH
FROM 0 TO 5	22.3985295	2.08975144
FROM 5 TO 10	19.4558837	1.81520672
FROM 10 TO 15	18.2415152	1.70190783
FROM 15 TO 20	16.1623658	1.50792611
FROM 20 TO 25	14.1797357	1.32294949
FROM 25 TO 30	13.673699	1.27573698
FROM 30 TO 35	11.6844884	1.09014641
FROM 35 TO 40	9.15762198	0.854393309
FROM 40 TO 45	9.29849016	0.867536114
FROM 45 TO 50	8.17881628	0.763072109
FROM 50 TO 55	7.81118743	0.728772851
FROM 55 TO 60	6.77921162	0.632490952
FROM 60 TO 65	6.35312422	0.592737595
FROM 65 TO 70	6.48711741	0.605238973
FROM 70 TO 75	6.50933384	0.607311734
FROM 75 TO 80	5.69101667	0.530963887
FROM 80 TO 85	5.21030382	0.486114052
FROM 85 TO 90	5.6564996	0.527743493

THE TOTAL SEGMENT LENGTH RELATIVE TO THE
REFERENCE LINE LENGTH IS 192.92894
THE TOTAL NUMBER OF SEGMENTS IS 11606
THE TOTAL NUMBER OF FIBERS IS 1498

Figure 41. The average segment length distribution for one medium fiber orientation sheets.

SEGMENT ANGLE DISTRIBUTION FOR
AVG253+AVG268+AVG269

ANGLE INTERVAL	SEGMENT LENGTH	NORMALIZED LENGTH
FROM 0 TO 5	66.7577627	2.1839682
FROM 5 TO 10	61.7448874	2.01997289
FROM 10 TO 15	54.6918695	1.78923468
FROM 15 TO 20	47.3904096	1.55036873
FROM 20 TO 25	40.6552766	1.33003007
FROM 25 TO 30	36.5277248	1.19499795
FROM 30 TO 35	31.0331426	1.01524368
FROM 35 TO 40	28.515304	0.932873042
FROM 40 TO 45	25.1128705	0.821563041
FROM 45 TO 50	22.1080279	0.723260158
FROM 50 TO 55	20.7895686	0.680126999
FROM 55 TO 60	18.5652887	0.607360082
FROM 60 TO 65	18.0489196	0.590467159
FROM 65 TO 70	16.1868351	0.529549401
FROM 70 TO 75	15.0739685	0.493142169
FROM 75 TO 80	15.1520975	0.495698146
FROM 80 TO 85	15.1314515	0.495022715
FROM 85 TO 90	16.7239462	0.547120893

THE TOTAL SEGMENT LENGTH RELATIVE TO THE
REFERENCE LINE LENGTH IS 550.209351
THE TOTAL NUMBER OF SEGMENTS IS 29393
THE TOTAL NUMBER OF FIBERS IS 4285

Figure 42. The average segment length distribution for three high fiber orientation sheets.

```
]LIST

10  REM ************************************************************************
20  REM THIS PROGRAM CALCULATES THE ANGULAR ORIENTATION DISTRIBUTION OF LINE
30  REM SEGMENTS COLLECTED FROM A PEN PRESS RELATIVE TO A REFERENCE LINE
40  REM THE DATA IS STORED AS THE TOTAL SEGMENT LENGTH RELATIVE TO THE REFERENCE LINE
50  REM LENGTH IN EACH ANGLE INTERVAL OF 1 DEGREE FROM -90 TO +90 DEGREES
60  REM ************************************************************************
70  ONERR  GOTO 9000
100  DIM A(180),B(180),C(180),LA(180),NB(180)
105  DIM X(50),Y(50)
110 B$ =  CHR$ (7): REM  BELL
120 D$ =  CHR$ (4): REM  CONT D
130 PI = 3.1415926535
140 DR = 180 / PI
145 N9 = 90.9999999
150  REM ----------------------------------------------------------------------
160  REM           INITIALIZE TABLET   PRINT MAIN MENU
170  REM ----------------------------------------------------------------------
180  PRINT D$;"PR#7": PRINT "T1,F,C,Q": PRINT D$;"PR#0"
200  HOME
210  PRINT "MAIN MENU": PRINT : PRINT
220  PRINT "    N:  START NEW DATA SET"
230  PRINT "    A:  ADD TO AN EXISTING DATA SET"
240  PRINT "    S:  SAVE DATA SET"
250  PRINT "    G:  GET DATA SET"
260  PRINT "    P:  PRINT DATA"
270  PRINT "    E:  EXIT"
300  PRINT : PRINT
310  INPUT "ENTER CHOICE-";C$
320  IF C$ = "N" THEN  GOTO 1000
330  IF C$ = "A" THEN  GOTO 2000
340  IF C$ = "S" THEN  GOSUB 3000: GOTO 200
350  IF C$ = "G" THEN  GOSUB 4000: GOTO 200
360  IF C$ = "P" THEN  GOSUB 5000: GOTO 200
370  IF C$ = "E" THEN  END
380  GOTO 200
500  REM ----------------------------------------------------------------------
504  REM             GET A PEN PRESS
508  REM ----------------------------------------------------------------------
510  FOR I = 0 TO 50:X(I) = 0:Y(I) = 0: NEXT
520 M = 0: PRINT "READY";B$
530  PRINT D$;"IN#7": INPUT X,Y,Z: PRINT D$;"IN#0"
540  IF Z < 0 THEN  GOTO 800
550  IF  ABS (Z) >  = 10 THEN  PRINT "THE PEN IS OFF SCALE": INPUT "PRESS RETURN";C$: GOTO 510
560  IF Z = 1 THEN  PRINT B$;B$: RETURN
570  IF Z = 0 THEN  GOTO 600
580  GOTO 530
600  IF M = 0 THEN M = M + 1:X(M) = X:Y(M) = Y: GOTO 530
610  IF RL <  = 0 THEN  GOTO 530
620  IF  SQR ((X - X(M)) ^ 2 + (Y - Y(M)) ^ 2) >  = (RL / 200) THEN  GOTO 640
630  GOTO 530
640 M = M + 1:X(M) = X:Y(M) = Y
650  PRINT M,X(M),Y(M)
655  IF M = 50 THEN  PRINT B$;B$;B$: RETURN
660  GOTO 530
690  RETURN
800  HOME : PRINT "THE KEYBOARD HAS BEEN PRESSED": PRINT
```

```
805  PRINT "PRESS D TO DELETE LAST PEN PRESS,"
807  PRINT "PRESS R TO REDEFINE REFERENCE LINE,"
810  PRINT "PRESS C TO CONTINUE TAKING DATA"
815  PRINT "PRESS S TO STOP TAKING DATA"
840  PRINT : INPUT C$
850  IF C$ = "D" THEN  GOSUB 900: GOTO 500
860  IF C$ = "R" THEN  GOSUB 1500: PRINT "CONTINUE TO COLLECT DATA": GOTO 500
870  IF C$ = "C" THEN  GOTO 500
880  IF C$ = "S" THEN  RETURN
890  GOTO 800
900  REM ------------------------------------------------------------------------
905  REM          DELETE LAST PEN PRESS
910  REM ------------------------------------------------------------------------
915  IF LS <  = 0 THEN  PRINT "NO LAST FIBER": INPUT "PRESS RETURN";C$: RETURN
920  FOR I = 0 TO 180:A(I) = A(I) - LA(I):LA(I) = 0: NEXT
930 NS = NS - LS:TL = TL - LL:NF = NF - 1
935 LS = 0:LL = 0
940  PRINT "LAST FIBER DELETED"
950  RETURN
1000  REM ------------------------------------------------------------------------
1010  REM            START A NEW DATA SET
1020  REM ------------------------------------------------------------------------
1030  HOME : PRINT "WARNING....AM ABOUT TO DESTROY ALL DATA IN MEMORY"
1035  PRINT : PRINT "PRESS G TO CONTINUE"
1040  INPUT C$: IF C$ = "G" THEN  GOTO 1100
1050  GOTO 200
1100  FOR I = 0 TO 180:A(I) = 0:LA(I) = 0: NEXT
1110 N$ = "":TL = 0:NS = 0:NF = 0:LS = 0:LL = 0
1120 XR = 0:YR = 0:RL = 0:TA = 0
1130  HOME : PRINT "ENTER THE NAME OF THE NEW DATA SET"
1140  PRINT : PRINT "THE NAME MUST BEGIN WITH A LETTER"
1150  PRINT : INPUT N$
1160  IF N$ = "" THEN  GOTO 200
1170  GOSUB 1500
1175  IF C$ = "S" THEN  GOTO 200
1180  GOTO 8000
1500  REM ------------------------------------------------------------------------
1510  REM          DEFINE REFERENCE LINE
1520  REM ------------------------------------------------------------------------
1550  PRINT "PRESS PEN AT BEGINNING OF REFERENCE LINE"
1560  GOSUB 500
1565  IF C$ = "S" THEN  RETURN
1570  IF X(1) = 0 THEN  GOTO 1550
1580 X1 = X(1):Y1 = Y(1)
1590  PRINT "PRESS PEN AT END OF REFERENCE LINE"
1600  GOSUB 500
1610  IF X(1) = 0 THEN  GOTO 1590
1620 X2 = X(1):Y2 = Y(1)
1630 XR = (X2 - X1):YR = Y2 - Y1
1634  IF XR = 0 THEN TA = PI / 2: GOTO 1640
1635 TA =  ATN (YR / XR)
1640 RL =  SQR (XR ^ 2 + YR ^ 2)
1650  RETURN
2000  REM ------------------------------------------------------------------------
2010  REM            ADD TO AN EXISTING DATA SET
2020  REM ------------------------------------------------------------------------
2030  IF N$ = "" THEN  GOTO 2500
2040  HOME : PRINT "EXISTING DATA SET IN MEMORY IS"
2050  PRINT N$: PRINT
2060  PRINT "DO YOU WISH TO KEEP IT? Y,N"
2070  INPUT C$
2080  IF C$ = "Y" THEN  GOTO 2100
2090  IF C$ = "N" THEN  GOSUB 4000
2095  GOTO 2000
2100  GOSUB 1500
2105  IF C$ = "S" THEN  GOTO 200
```

```
2110  GOTO 8000
2500  HOME : PRINT "NO EXISTING DATA IN MEMORY": PRINT
2510  PRINT "DO YOU WISH TO GET ONE? Y,N"
2520  INPUT C$
2530  IF C$ = "Y" THEN  GOSUB 4000: GOTO 2000
2540  GOTO 200
3000  REM ------------------------------------------------------------------------
3010  REM            SAVE DATA SET
3020  REM ------------------------------------------------------------------------
3025  IF N$ = "" THEN  PRINT "NO DATA IN MEMORY ": INPUT "PRESS RETURN";C$: RETURN
3030  HOME : PRINT "SAVING DATA SET IN FILE NAME"
3040  PRINT N$
3050  PRINT D$;"OPEN ";N$: PRINT D$;"DELETE ";N$
3060  PRINT D$;"OPEN ";N$
3070  PRINT D$;"WRITE ";N$
3080  PRINT NF: PRINT NS: PRINT TL
3090  FOR I = 0 TO 180: PRINT A(I): NEXT
3100  PRINT D$;"CLOSE ";N$
3110  RETURN
4000  REM ------------------------------------------------------------------------
4010  REM              GET DATA SET
4020  REM ------------------------------------------------------------------------
4030  PRINT "DO YOU WISH TO SEE THE CATALOG? Y,N"
4040  INPUT C$
4050  IF C$ = "Y" THEN  GOTO 4080
4060  IF C$ = "N" THEN  GOTO 4100
4070  RETURN
4080  PRINT D$;"CATALOG": INPUT "<RETURN TO CONTINUE>";C$
4100  PRINT "WHAT FILE DO YOU WANT?"
4110  INPUT N$
4115  IF N$ = "" THEN  RETURN
4120  PRINT D$;"OPEN ";N$
4130  PRINT D$;"READ ";N$
4140  INPUT NF: INPUT NS: INPUT TL
4150  FOR I = 0 TO 180: INPUT A(I): NEXT
4160  PRINT D$;"CLOSE ";N$
4170  RETURN
5000  REM ------------------------------------------------------------------------
5010  REM             PRINT DATA SET
5020  REM ------------------------------------------------------------------------
5030  IF N$ = "" THEN  PRINT "NO DATA IN MEMORY": INPUT "PRESS RETURN";C$: RETURN
5040  PRINT "DO YOU WISH TO PRINT DATA SET ";N$;"?"
5050  INPUT "Y,N ?";C$
5060  IF C$ = "N" THEN  RETURN
5070  IF C$ = "Y" THEN  GOTO 5090
5080  RETURN
5090  PRINT "WHAT ANGLE INTERVAL DO YOU WANT?"
5095  PRINT "    (IN DEGREES)
5100  INPUT IN
5105  FOR I = 0 TO 180:C(I) = A(I):B(I) = 0: NEXT
5110  PRINT "DO YOU WANT THE NEGATIVE ANGLES INCLUDED WITH THE POSITIVE? Y,N"
5120  INPUT C$
5130  IF C$ = "Y" THEN  GOTO 5140
5135  IF C$ = "N" THEN  GOTO 5200
5136  RETURN
5140  FOR I = 1 TO 90
5150 J = 90 + I:K = 90 - I + 1
5155 B(I) = C(J) + C(K)
5160  NEXT
5165  FOR I = 1 TO 90:C(I) = B(I): NEXT
5170 N = 90:VL = 0
5180  GOSUB 5500
5190  RETURN
5200 N = 180:VL =  - 90
5210  GOSUB 5500
5220  RETURN
```

```
5500  PRINT "TURN ON THE PRINTER,": INPUT "THEN HIT RETURN TO START";C$
5505  PRINT D$;"PR#1": PRINT "  ": PRINT : PRINT
5507  PRINT "SEGMENT ANGLE DISTRIBUTION FOR"
5508  PRINT N$: PRINT
5510  PRINT "ANGLE INTERVAL","SEGMENT LENGTH","NORMALIZED LENGTH"
5520  PRINT "---------------","---------------","-----------------"
5521  PRINT
5540  FOR I = 0 TO 180:B(I) = 0: NEXT
5560 NI = N / IN
5570  FOR I = 1 TO NI
5580  FOR J = 1 TO IN
5590 K = (I - 1) * IN + J
5600 B(I) = B(I) + C(K)
5610  NEXT J
5620  NEXT I
5630  FOR I = 1 TO NI
5640 L = VL + (I - 1) * IN:H = L + IN
5650  IF VL = 0 THEN NB(I) = B(I) * 90 / (IN * TL): GOTO 5660
5655  IF VL =  - 90 THEN NB(I) = B(I) * 180 / (IN * TL): GOTO 5660
5659 NB(I) = 0
5660  PRINT "FROM ";L;" TO ";H,B(I),NB(I)
5670  NEXT I
5680  PRINT : PRINT "THE TOTAL SEGMENT LENGTH RELATIVE TO THE "
5685  PRINT "     REFERENCE LINE LENGTH IS ";TL
5690  PRINT "THE TOTAL NUMBER OF SEGMENTS IS ";NS
5700  PRINT "THE TOTAL NUMBER OF FIBERS IS ";NF
5710  PRINT D$;"PR#0": HOME : PRINT "FINISHED PRINTING": RETURN
8000  REM ------------------------------------------------------------------
8010  REM             COLLECT DATA
8020  REM ------------------------------------------------------------------
8030  HOME
8040  PRINT "NOW START COLLECTING DATA": PRINT
8050  PRINT "TRACE THE PEN ALONG EACH FIBER": PRINT "DATA IS COLLECTED WHEN PEN IS DOWN"
8060  PRINT "COLLECT DATA ONLY WHEN THE COMPUTER IS"
8070  GOSUB 500
8075  IF C$ = "S" THEN  GOTO 200
8078  IF M <  = 1 THEN  GOTO 8070
8080  HOME : PRINT "CALCULATING"
8085  FOR I = 0 TO 180:LA(I) = 0: NEXT
8090 LL = 0:LS = N - 1:NS = NS + LS:NF = NF + 1
8100  FOR I = 2 TO N
8105 K = I - 1
8110 XS = X(I) - X(K):YS = Y(I) - Y(K)
8120 SL =  SQR (XS ^ 2 + YS ^ 2) / RL
8125  IF XS = 0 THEN TH = PI / 2:TH = TH - TA: GOTO 8135
8130 TH =  ATN (YS / XS):TH = TH - TA
8135 J =  INT (TH * DR + N9)
8140  IF J <  = 0 THEN J = J + 180: GOTO 8151
8150  IF J > 180 THEN J = J - 180: GOTO 8151
8151  PRINT J,SL
8160 LA(J) = LA(J) + SL
8165 A(J) = A(J) + SL
8170 LL = LL + SL
8180  NEXT
8181  PRINT LL
8310 TL = TL + LL
8330  GOTO 8070
9000  REM ------------------------------------------------------------------
9010  REM             WHEN AN ERROR OCCURS
9020  REM ------------------------------------------------------------------
9030  HOME : PRINT B$;B$;B$;B$;B$;"    THERE HAS BEEN AN ERROR.....": PRINT
9040  INPUT "PRESS RETURN TO GO TO MAIN MENU";C$: GOTO 200
```

APPENDIX VIII

DERIVATION OF EQ. (14) FROM DAVIES' (36) GENERAL SOLUTION

Davies (36) obtained a solution for the average electric field within a fiber segment in a coordinate system aligned with the fiber segment. He started with a rectangular Cartesian coordinate system (x, y, z) aligned with respect to the three principal directions of the mixture. He then defined a new coordinate system $\rightarrow = (\ ,\ ,\ )$ by

$$= \frac{x}{x^*}, \quad = \frac{y}{y^*}, \quad = \frac{z}{z^*} \tag{35}$$

In this coordinate system, the differential equation was solved by an integral method.

A third coordinate system, rotated such that the direction " is aligned along the fiber segment with " in the plane of the sheet, was then defined by

$$\begin{bmatrix} " \\ " \\ " \end{bmatrix} = \begin{bmatrix} \frac{\cos\ '}{\sin\ '} & -\frac{\cos\ '}{\sin\ '} & 0 \\ \frac{\cos\ '\cos\ '}{\sin\ '} & \frac{\cos\ '\cos\ '}{\sin\ '} & -\sin\ ' \\ \cos\ ' & \cos\ ' & \cos\ ' \end{bmatrix} \begin{bmatrix} \\ \\ \end{bmatrix} \tag{36}$$

where cos ', cos ', and cos ' are the direction cosines of the segment in the , , and directions, respectively. In this coordinate system, when averaged over the volume of the segment, the solution was given by Davies as

$$\langle R_{\chi''} \rangle = R_{\chi''}^{\circ} - \frac{1}{2} \langle Q_{\chi''} \rangle$$

$$\langle R_{\eta''} \rangle = R_{\eta''}^{\circ} - \frac{1}{2} \langle Q_{\eta''} \rangle \qquad (37)$$

$$\langle R_{\xi''} \rangle = R_{\xi''}^{\circ}$$

where

$$R_i(\vec{\rho}) = \sqrt{\varepsilon_{(i)}^*}\, E_i(\vec{\rho})$$

$$Q_i(\vec{\rho}) = 2\sqrt{\varepsilon_{(i)}^*}\, A^{(i)}\, E_i(\vec{\rho})$$

$$A^{(i)} = (\varepsilon_f - \varepsilon_{(i)}^*)/2\,\varepsilon_{(i)}^*$$

and E_i° is the applied field. Indices in parentheses are not summed.

For the special case in which the fiber segment is oriented in the χ, η plane at an angle α' from the χ axis, Eq. (36) becomes

$$\begin{bmatrix} \chi'' \\ \eta'' \\ \xi'' \end{bmatrix} = \begin{bmatrix} \sin\alpha' & -\cos\alpha' & 0 \\ 0 & 0 & -1 \\ \cos\alpha' & \sin\alpha' & 0 \end{bmatrix} \begin{bmatrix} \chi \\ \eta \\ \xi \end{bmatrix} \qquad (38)$$

One considers separately the cases in which the applied field is aligned in each of the three principal directions. For $E_{\chi}^{\circ} \neq 0$, $E_{\eta}^{\circ} = E_{\xi}^{\circ} = 0$, writing Eq. (37) in terms of the $\vec{\rho}$ coordinates using Eq. (38) one obtains

$$\langle \sin\alpha' \sqrt{\varepsilon_x^*}\, E_{\chi} - \cos\alpha' \sqrt{\varepsilon_y^*}\, E_{\eta} \rangle =$$

$$\sin\alpha' \sqrt{\varepsilon_x^*}\, E_{\chi}^{\circ} - \frac{1}{2} \langle 2 \sin\alpha' \sqrt{\varepsilon_x^*}\, A^x E_{\chi} - 2\cos\alpha' \sqrt{\varepsilon_y^*}\, A^y E_{\eta} \rangle \qquad (39)$$

$$\langle -\sqrt{\varepsilon_z^*}\, E_{\xi} \rangle = \frac{1}{2} \langle 2 \sqrt{\varepsilon_z^*}\, A^z E_{\xi} \rangle$$

$$\langle \cos\alpha' \sqrt{\varepsilon_x^*}\, E_{\chi} + \sin\alpha' \sqrt{\varepsilon_y^*}\, E_{\eta} \rangle = \cos\alpha' \sqrt{\varepsilon_x^*}\, E_{\chi}^{\circ}$$

which reduces to

$$(1 + A^x)\frac{\langle E_\chi\rangle}{E_\chi^\circ} - \frac{\cos\alpha'}{\sin\alpha'}\frac{\sqrt{\epsilon_y^*}}{\sqrt{\epsilon_x^*}}(1 + A^y)\frac{\langle E_\eta\rangle}{E_\chi^\circ} = 1$$

$$\langle E_\xi\rangle = 0 \tag{40}$$

$$\frac{\langle E_\chi\rangle}{E_\chi^\circ} + \frac{\sin\alpha'}{\cos\alpha'}\frac{\sqrt{\epsilon_y^*}}{\sqrt{\epsilon_x^*}}\frac{\langle E_\eta\rangle}{E_\chi^\circ} = 1$$

solving for $\langle E_\chi\rangle/E_\chi^\circ$ one obtains

$$\frac{\langle E_\chi\rangle}{E_\chi^\circ} = \frac{1 + \cos^2\alpha'\ A^y}{1 + \sin^2\alpha'\ A^x + \cos^2\alpha'\ A^y} \tag{41}$$

Considering similarly the cases in which $E_\eta^\circ \neq 0$ and $E_\xi^\circ \neq 0$ one obtains

$$\frac{\langle E_\eta\rangle}{E_\eta^\circ} = \frac{1 + \sin^2\alpha'\ A^x}{1 + \sin^2\alpha'\ A^x + \cos^2\alpha'\ A^y} \tag{42}$$

and

$$\frac{\langle E_\xi\rangle}{E_\xi^\circ} = \frac{1}{(1 + A^z)} \tag{43}$$

Note that $\langle E_\xi\rangle/E_\xi^\circ$ does not depend on the fiber segment angle in the χ, η plane.

Equations (41)-(43) are written in the $\vec{\rho} = (\chi, \eta, \xi)$ coordinates. It may be noted that

$$\frac{\langle E_x\rangle}{E_x^\circ} = \frac{\langle E_\chi\rangle}{E_\chi^\circ}$$

$$\frac{\langle E_y\rangle}{E_y^\circ} = \frac{\langle E_\eta\rangle}{E_\eta^\circ} \tag{44}$$

$$\frac{\langle E_z\rangle}{E_z^\circ} = \frac{\langle E_\xi\rangle}{E_\xi^\circ}$$

However, the transformed angle α' in the $\vec{\rho}$ coordinates is not equal to the fiber segment angle α in the (x, y, z) coordinates. From Eq. (35) it follows that

$$\cos^2\alpha' = \varepsilon_y^* \cos^2\alpha/(\varepsilon_y^* \cos^2\alpha + \varepsilon_x^* \sin^2\alpha)$$

$$\sin^2\alpha' = \varepsilon_x^* \sin^2\alpha/(\varepsilon_y^* \cos^2\alpha + \varepsilon_x^* \sin^2\alpha) \qquad (45)$$